Satan's skeleton revealed: a tomographic and comparative osteology of *Satan eurystomus*, the subterranean Widemouth Blindcat (Siluriformes, Ictaluridae)

Author(s): John G. Lundberg, Dean A. Hendrickson, Kyle R. Luckenbill, Mariangeles Arce H.
Source: Proceedings of the Academy of Natural Sciences of Philadelphia, 165():117-173.
Published By: The Academy of Natural Sciences of Philadelphia
https://doi.org/10.1635/053.165.0108
URL: http://www.bioone.org/doi/full/10.1635/053.165.0108

ISSN 0097-3157

PROCEEDINGS OF THE ACADEMY OF NATURAL SCIENCES OF PHILADELPHIA 165: 117-173 2017

Satan's skeleton revealed: a tomographic and comparative osteology of *Satan eurystomus*, the subterranean Widemouth Blindcat (Siluriformes, Ictaluridae)

JOHN G. LUNDBERG

Department of Ichthyology, The Academy of Natural Sciences, 1900 Benjamin Franklin Parkway, 19103-1195 Philadelphia, PA, USA.
E-mail: lundberg@ansp.org

DEAN A. HENDRICKSON

University of Texas Austin, Department of Integrative Biology, Biodiversity Collections (Texas Natural History Collections), 10100 Burnet Rd., PRC176 EAST/R4000, Austin, Texas 78758-4445 USA.
E-mail: deanhend@austin.utexas.edu

KYLE R. LUCKENBILL

Department of Ichthyology, The Academy of Natural Sciences, 1900 Benjamin Franklin Parkway, 19103-1195 Philadelphia, PA, USA.
E-mail: luckenbill@drexel.edu

MARIANGELES ARCE H.

Department of Ichthyology, The Academy of Natural Sciences, 1900 Benjamin Franklin Parkway, 19103-1195 Philadelphia, PA, USA.
E-mail: m.arce@drexel.edu

ABSTRACT.—The Widemouth Blindcat, *Satan eurystomus* Hubbs and Bailey 1947, was the second of four stygobitic species of Ictaluridae discovered in the subterranean waters of southern Texas and northeastern Mexico. The skeletal anatomy of *Satan* has been scarcely known from a few, dated radiographs. Using additional radiographs and high resolution CT-datasets for two well-ossified specimens, we applied high-resolution X-ray computed tomography (HRXCT) to visualize, illustrate and describe the bony skeleton of *Satan*. We also provide an online archive of still and animated tomographic images of the skeletal anatomy of this little-known species.

The skeleton and soft anatomy of *Satan* are distinctive. Twelve skeletal autapomorphies are described that singularly distinguish *Satan* within Ictaluridae and, probably in combination, from all other catfishes. Some of these are reductive losses or simplifications of skull bones (e.g. loss of one infraorbital bone; reduced ornamentation of the pterotic bone) and joint complexity (e.g. simple overlapping frontal-lateral ethmoid articulation; loosely ligamentous interopercle-posterior ceratohyal joint). Some of the autapomorphies are anatomically and perhaps developmentally complex (e.g. a novel series of three midline joints closing a middle span of the posterior cranial fontanel; a deeply excavated temporal fossa and an unusually enlarged interhyal bone). The tiny dorsal-fin spinelet (first lepidotrich) o *Satan* has a novel peaked and twisted shape.

Ten apparent and exclusive synapomorphies within Ictaluridae gathered from this and previous studies suggest that *Satan* and *Pylodictis* are closest relatives. Most of these are functionally related to prey detection and suction feeding: fusion of the symphyseal mandibular sensory pores and increase in the number of preoperculo-mandibular canal pores; depressed, flattened heads and wide transverse mouths; prominent posterior process of the lateral ethmoid alongside and below the frontal bone margin; vertical and blade-like supraoccipital posterior process; unique arrangement of the parasagittal and occipital muscle-attachment crests on the skull roof; large triangular panel of integument within the operculum framed by the opercle, preopercle and interopercle bones; elongated posterior ceratohyal; and, form of the fourth supraneural and loss of its anterior nuchal plate.

In contrast, 15 synapomorphies recovered by Arce-H. et al. 2016, are confirmed suggesting that *Satan* is one of the four stygobitic ictalurids comprising a "Troglobites" subclade within the family: (*Trogloglanis*, *Satan*, *Prietella phreatophila*, *P. lundbergi*). These features include three stygomorphic and reductive apomorphies that are exclusive within Ictaluridae: loss of fully developed eyes and pigmentation, and simplification of the fifth vertebra and its joint with the Weberian apparatus. Twelve other synapomorphies shown by the Troglobites are also apparent homoplasies of character states shared with various other ictalurids. These include reductive characters such as shortened lateral line canal, reduced infraorbitals and underdeveloped or incomplete ossifications of the pterotic, supraoccipital, hyoid arch bones and transcapular ligament. Also, the Troglobites and various other ictalurids have: an adnate adipose-caudal fin, foreshortened anterior cranial fontanelle, reduced ventral wings of the frontal bone, replacement of bone by cartilage in hypohyal joints; incompletely ossified transcapula ligament, and consolidation of some hypural bones.

Completing a full morphological character dataset across the Troglobites has been impeded by incomplete specimen preparations and study of *P. lundbergi* and to a lesser extent, *P. phreatophila* and *Trogloglanis*.

Submitted: 19 May 2017, Accepted: 9 October 2017, Published Online: October 31 2017.

INTRODUCTION

In 1938 ichthyologist Carl Hubbs visited the Witte Memorial Museum in San Antonio, TX where he examined and later received for study two small, pallid and eyeless catfishes. Both were collected from the outflow of an artesian well tapping the deep >400m San Antonio Pool of the Edwards Aquifer. One specimen is *Trogloglanis pattersoni* (Plate I, p. 173), a bizarre toothless species described by Carl Eigenmann in 1919. The second catfish (Fig. 1, Plate I) is an unusual well-toothed specimen that represented an undescribed species. In 1947, following the hiatus during World War II, Hubbs and Reeve Bailey at the University of Michigan Museum of Zoology described and cleverly named this specimen *Satan eurystomus* as a new genus and species in the North American freshwater catfish family Ictaluridae. Hubbs and Bailey also gave this species its common name Widemouth Blindcat.

Ictaluridae currently include many familiar catfishe of surface waters (Page et al., 2013): Channel and Blue catfishes (*Ictalurus*, 10 living and five fossil species), Bullheads (*Ameiurus*, seven living and nine named plus some undescribed fossil species), the Flathead Catfish (*Pylodictis olivaris*, monotypic, Plate I) and Madtoms (*Noturus*, 29 living species). In addition, there are four named subterranean species in the family (Plate I). *Satan eurystomus* (hereafter *Satan*) followed *Trogloglanis pattersoni* Eigenmann as the second-described hypogean ictalurid. Both are known only from the deep waters of the Edwards Aquifer below San Antonio. Later, two more blindcat species were discovered in subsurface waters of northeastern Mexico: *Prietella phreatophila* Carranza (1954) from the State of Coahuila and, remarkably, recently collected north of the Rio Grande in nearby cave waters of Val Verde County, Texas (Hendrickson et al. 2001, 2017), and *P. lundbergi* Walsh and Gilbert (1995) in the State of Tamaulipas.

The subterranean ictalurids are divergent, remote, and specimens of them are rare. They hold the attention of ichthyologists, biospeleologists and conservationists (Taylor, 1969; Hubbs, 1971; Longley and Karnei, 1979a, b; Lundberg, 1982; Hendrickson et al., 2017) yet these species remain little known. All share the common features of stygomorphic fishes (Langecker and Longley, 1993): regression and loss of functional eyes and pigmentation, reduced pineal organ, and some amplification of cutaneous sensory receptors. These are small fishes with relatively weakly developed musculoskeletal systems; three (*Satan*, *Trogloglanis*, *P. lundbergi*) have lost the swimbladder and one or more of the paired Weberian ossicles. Moreover, each species is singularly distinctive. *Trogloglanis* is exceptionally so as a detritivore with a large head, an open, toothless and fleshy mouth, plus strongly spinous dorsal and pectoral fins (Lundberg, 1982, 1992; Arce-H. et al. 2016). *Satan* resembles *Pylodictis* as first reported by Hubbs and Bailey (1947) and noted by subsequent authors (Suttkus, 1961; Taylor, 1969; Lundberg, 1970, 1975, 1982, 1992; Arce-H. et al. 2016). Among the shared features of *Pylodictis* and *Satan* are their wide gape, depressed head, expanded branchiostegal and opercular membranes, and anterior extension of epaxial muscle. The species of *Prietella* resemble epigean *Noturus* (Taylor, 1969), and the two species are distinct from each other in morphological features including fin shapes and presence or absence of the swim bladder (Walsh and Gilbert, 1995) as well as mitochondrial gene sequences (Wilcox et al., 2004). Hypotheses on the interrelationships of the blind ictalurids are based on incomplete morphological data and, for *Prietella* only, scant molecular data. Phylogenetic results run the spectrum from separate ancestries of the four stygobites scattered among the epigean ictalurids (Lundberg, 1982, 1992; Wilcox et al., 2004; Egge and Simons, 2009) to the exclusive monophyly of a subterranean clade within Ictaluridae containing just those species (Arce-H. et al. 2016). More generally, there is lack of agreement among the morphology and molecular based studies of Ictaluridae on the inter- and intra-relationships of the epigean genera and species. Without a more complete and well-supported resolution of ictalurid phylogeny, there are few robust topological constraints on subtrees that include the stygobites.

Satan is uncommon with just 14 preserved individuals known to be in natural history collections. Though Langecker and Longley (1993) reported data from 28 specimens, including 21 specimens (30–114 mm SL) deposited at what is now Texas State University, San Marcos, and previously cited by Longley and Karnei (1979a), our recent inquiries there found only two – both included in the 14 we list herein. One of these is now TNHC 63279 and the other remains in Texas State's uncatalogued teaching collection. The last known specimens of *Satan* were collected over 30 years ago in 1984. During 2008-2010, a biological monitoring effort at wells in the Edwards Aquifer in the San Antonio area obtained several individuals of *Trogloglanis* and many invertebrate species, but *Satan* was not collected (Zara Environmental LLC, 2010, 2014). Most of the known specimens of *Satan* were formalin-preserved before tissue collecting became routine in fish systematics for extraction of proteins, amino and nucleic acids. Tissue was taken in 1984 from specimens of *Satan* at the Biodiversity Research and Teaching Collections of Texas A&M University (TCWC) and used for gel electrophoresis of protein (Kelsch, pers. com.). Unfortunately, there are no published data or results from that work, and the tissue samples have not been located at the TCWC fish collection. There is little hope for molecular sequence data from *Satan* unless a fresh, frozen or alcohol preserved specimen becomes available, or unless there

is a technological breakthrough for obtaining non-degraded nucleic acids from formalin-fixed or eDNA samples. Also, no specimen of *Satan* has been cleared and stained for detailed study of skeletal anatomy; many specimens are now decalcifie and thus likely unsuitable for alizarin staining.

Thus, the central objective of this work is a detailed, richly illustrated description of the osteology of *Satan*. We used High Resolution X-ray Computed Tomography (HRXCT) at the CT Facility at The University of Texas to scan a well-ossified specimen of *Satan* (USNM 195830). Independently, a second specimen of this species (TCWC 8279.01) was scanned at the University of Washington Friday Harbor Laboratories by A. Summers and K. W. Conway who generously made their dataset available to us to confirm and supplement our initial observations.

We also sought to verify known and to discover additional characters of *Satan* for evaluating two published phylogenetic hypotheses on its closest relatives. First, the traditional view, stemming from Hubbs and Bailey's 1947 original description, that *Satan* and *Pylodictis* are, in the parlance of phylogenetics, sister lineages (also, Suttkus, 1961; Taylor, 1969; Lundberg, 1970, 1975, 1982, 1992). Second, the hypothesis that the four ictalurid subterranean catfishes *Satan*, *Trogloglanis*, *Prietella phreatophila* and *P. lundbergi* comprise a monophyletic group informally labelled Troglobites. This latter hypothesis resulted from the cladistic study of ictalurids of Arce-H. et al. (2016, MorphoBank Project P2100) using an expanded taxon sample of 65 extant and fossil ictalurids, seven outgroup taxa, 209 morphological characters, plus existing molecular sequence data.

During this study our comparisons were increasingly challenged by insufficient specimen preparations and incomplete character data for *Trogloglanis* and the two nominal species of *Prietella*. Further, questions arose about the identity of the only specimens attributed to *P. lundbergi* apart from the holotype. To address these issues, new high resolution CT scans were recently made of the holotype and one non-type specimen. The anatomy revealed in these new images suggests that these specimens probably represent a single species, and that *P. lundbergi* is only remotely related to *Prietella phreatophila*. Completing preparation of the new tomographic images and comparative analysis of these are beyond the scope of the present study. If our initial reading is confirmed it will be consistent with molecular based results of Wilcox et al. (2003) that indicate non-monophyly of *Prietella*. Our comparative and phylogenetic treatment herein does not attempt a quantitative phylogenetic analysis of the current data-deficient character matrix. Instead, we focus on describing and discussing newly observed features of *Satan* that are potential autapomorphies within Ictaluridae, and potential synapomorphies shared with other taxa, and we review all the characters from previous studies of *Satan* that have been suggested as informative on its relationships.

MATERIAL AND METHODS

Specimens of Satan.—The 14 specimens of *S. eurystomus* known to us to be in museum collections are listed here with their institutional collection codes following Sabaj (2016) and SL in mm in parentheses: NLU 47110 (60.9), NLU uncataloged (formerly LTU 11342) (74.1), TCWC 8279.01 (108), TCWC 8280.01 (63), TCWC 8281.01 (112), TNHC 18764 (70), TNHC 21702 (96), TNHC 25142 (87.9), TNHC 63279 (69), TU 10809 (77.3), TX State University San Marcos uncataloged teaching collection (102), UMMZ 190922 (68.7), USNM 195830 (88.7), USNM 205383 (73). Ten of these were radiographed to determine the best candidates for CT scanning based on preservation of dense, X-ray-opaque bone tissue and undistorted body form. Eight specimens were judged to be too decalcified to be useful for skeletal study. Six specimens, including the holotype (UMMZ 190922), were sufficiently well preserved to count total vertebrae. We selected USNM 195830, 88.7 mm SL, for our CT scanning at the High-Resolution X-ray CT Facility at The University of Texas, Austin. A second well-calcified specimen, TCWC 8279.01, 108 mm SL, was independently scanned at the Friday Harbor Laboratories, University of Washington by A. Summers and K. W. Conway who made the data available to us. The scan of the second specimen served to clarify the structure of the parasphenoid, basioccipital and anterior vertebrae which are partially distorted in USNM 195830.

Comparative material of Ictaluridae.—The major descriptive and comparative treatments of ictalurid skeletal anatomy are: McMurrich (1884), Kindred (1919), Lundberg (1970, 1975, 1982, 1992), Grande and Lundberg (1988), Egge (2007) and Arce et al. (2016). We compared the skeletal anatomy of *Satan* to representatives of the six living genera of Ictaluridae with a special focus on *Pylodictis olivaris*, *Trogloglanis pattersoni*, *Prietella phreatophila* and *P. lundbergi*. Preparations of these specimens were alcohol preserved (alc), cleared and stained (C&S), dry skeletal (skel), radiographs (X-ray) and tomographic imaging (CT-scan).

Pylodictis olivaris: Alabama: UMMZ 186266, 2, skel; Georgia: ANSP 152189, 1, alc; Kansas: UMMZ 97069, 1, skel; UMMZ 160732, 1, skel; ANSP 89949, 3, alc; ANSP 89970, 1, alc; ANSP 89989, 2, alc; ANSP 90004, 3, alc; ANSP 180246, 3, alc; ANSP 148622, 1, alc; ANSP 147958, 1, alc; ANSP 147970, 2, alc; ANSP 147981, 1, alc; ANSP 148631, 1, alc; Louisiana: USNM 264813, 1, skel; Michigan: UMMZ 186652, 1, skel; Mississippi: UMMZ 173452, 1, skel; Missouri: UMMZ 152549, 1, skel; UMMZ 169029, 3, skel;

Oklahoma: UMMZ 103107, 3, skel; Pennsylvania: ANSP 22084, 1, alc; Tennessee: ANSP 129361, 3, C&S; ANSP 129361, 7 of 102, alc; ANSP 129380, 2, alc; ANSP 129393, 4, alc; ANSP 90288, 1, alc; ANSP 92514, 1, alc; ANSP 99748, 1, alc. Texas: UMMZ 170129, 4, skel; ANSP 135328, 1, C&S; ANSP 150648, 1, C&S; ANSP 135298, 1, alc; ANSP 135328, 2, alc; ANSP 164170, 2, alc; ANSP 18908, 1, alc; ANSP 73929, 1, alc; ANSP 73861, 1; ANSP 135314, 1, alc.

Trogloglanis pattersoni, all from Texas, Bexar County: CAS 58675 (IU 15420), 1, Holotype, alc, X-ray; SIOH-51-350-18A, 1, alc, C&S, X-ray; SIOH-51-379-18A, 2, alc, 1 specimen C&S; UMMZ 190921, 1, alc, X-ray; UMMZ 21190, 1, alc, X-ray; TU 10808, 1, alc, X-ray. TNHC 21701, 1, alc, X-ray, CT-Scan.

Prietella phreatophila, Mexico, Coahuila: USNM 187684, 1, C&S.

Prietella lundbergi, Mexico, Tamaulipas, Cueva del Nacimiento de San Rafael de Los Castros: CNPE-IBUNAM-P7705, 1, Holotype, alc, X-ray (ANSP Ichthyology Image Collection 37086), 2 CT scans.

Prietella cf. *lundbergi*: All from Mexico, Tamaulipas, Cueva del Nacimiento del Rio Frio, Gomez Farias: TNHC 25766, 1, 37 mm SL, alc, X-ray; TNHC 25767, 1, 62 mm SL, alc, X-ray; CT Scan; TNHC 25768, 1, 26 mm SL, alc, X-ray; TNHC 63103 (formerly one of two specimens in TNHC 25767), 33.5 mm SL, C&S.

Specimens examined representing species of *Noturus*, *Ameiurus* and *Ictalurus*, plus †*Astephus* and *Cranoglanis* are previously listed by Lundberg, 1970, 1975, 1982, 1992; Grande and Lundberg, 1988, and Arce-H. et al., 2016.

Methods.—The tomographic images of USNM 205383 were generated by M. Colbert, at the High-Resolution X-ray CT Facility at The University of Texas, Austin. The scanning parameters for the whole specimen scan were: NSI scanner, Feinfocus microfocal X-ray source operating at 130 kV, 0.46 mA, with no X-ray prefiltering. The distance from the X-ray source to the specimen was 47.5 mm and the distance from the X-ray source to the Perkins Elmer detector was 978 mm. The data were collected using a helical continuous CT scan with a vertical extent of 118 mm, pitch of 13.11 mm, 9 revolutions, 9 sets, no frames averaged, 0 skip frames, 18010 total projections, 9 gain calibrations, a 5mm calibration phantom, 0.1 beam hardening correction, a helical sigma of 40 resulting in 3301 transverse slices with a voxel size of 0.0316mm.

The scanning parameters for the scan of the head region were: Zeiss-Xradia micro XCT400 scanner, LFOV objective, X-ray source operating at 70 kV, 10 W, with 0.7 mm SiO2 filte . The data were reconstructed with a center shift of -5.5, 0 beam hardening correction resulting in 1608 transverse slices with a voxel size of 0.02005mm.

The scan was taken along the long axis of the specimen from the snout tip to just posterior to the dorsal-fin spine origin. Visualizations were produced in the commercial software package VG Studio Max. Although the renderings appear similar to photographs, they represent the density differences of the biological tissues as reflected in their X-ray opacit .

The tomographic images of TCWC 8279.01 were generated by Kevin C. Conway and Adam P. Summers, at the Karel F. Liem Biovisualization Center at the University of Washington's Friday Harbor Laboratories. The scanning parameters for the whole specimen scan were: Skyscan 1173 scanner, X-ray source operating at 60 kV, 110 mA with 2K x 2K detector. The data were reconstructed using Bruker NRECON software and resulted in a data set of 3587 transverse slices with a voxel size of 0.027mm.

The HRXCT data were visualized and rendered by KRL at the Academy of Natural Sciences. The illustrations in the following description of the bony skeleton of *Satan* are three dimensional HRXCT reconstructions and two dimensional digital X-rays. Preparation of the figures utilized still frames captured from digital animations of HRXCT and were prepared using Adobe Photoshop CS.

Still images were produced in VGStudioMax 1.2.1 and enhanced using Adobe Photoshop Creative Suite (ver. 6). Animations were produced using VGStudioMax 1.2.1, Adobe Photoshop Creative Suite (ver. 6) and Quicktime Pro. Tomographic image stacks of TCWC 8279.01 are available through the Open Science Framework ScanAllFishes project at https://osf.io/wrcpf/ and on Morphosource.org, along with a selection of animations at http://morphosource.org/Detail/MediaDetail/Show/media_id/16623. Tomographic image stacks and a selection of 3-D animations of USNM 195830 are available on Morphosource.org at http://morphosource.org/Detail/SpecimenDetail/Show/specimen_id/8348 and http://morphosource.org/Detail/MediaDetail/Show/media_id/18048, respecively. Tomographic image stacks and a selection of 3-D animations of both USNM 195830 and TCWC 8279.01 are permanently archived at https://doi.org/10.15781/T27W67N6S in the University of Texas Scholarworks site.

Scale bars were created for each structure or set of structures by viewing the model in dorsal view and inserting a scale on the slice image at the midpoint between the upper and lower margins of the area of interest.

Anatomical terminology.—Anatomical terminology generally follows the Teleost Anatomical Ontology (TAO; Dahdul et al., 2010) an integral part of the Uberon Ontology covering anatomical structures in animals (Mungall et al., 2012; http://uberon.github.io/). Terminology of pectoral- and dorsal-fin spine anatomy follows Vanscoy et al. (2015). Terminology of muscle anatomy follows Winterbottom (1974)

with modification from Datovo & Vari (2014). Abbreviations for anatomical terms used in figures are given in the figur captions and an overall alphabetized list on Page 171-172.

Visualization limitations.—The parameters of the scan data yield high resolution images with sharply delimited bony elements. Paired radio-dense bodies that are in expected positions relative to other structures are first considered to be paired bones, not artifacts. With adjustment of volume opacity using VGStudioMax it is sometimes possible to achieve visualization of cartilage and the edges of cavities as small as laterosensory canals and sensory pores on the skin surface. Most different types of soft tissues are difficul or impossible to distinguish. Radio-transparency in the joint spaces between closely adjacent bones is interpreted as presence of cartilage or ligament in the joint.

DESCRIPTIVE OSTEOLOGY

General.—Figure 1 and Plate I show the external form of *Satan* with its "greatly depressed head, wide transverse mouth, slender body, and a long and flaring adipose fin" (Hubbs and Bailey, 1947, p. 4). Similarly, two-dimensional radiographic images (Figs. 2A, B) of the entire bony skeleton of *Satan* (USNM 195830) in lateral and dorsal views show that the distinctive form of this species extends to the bony head and postcranial skeleton. Our descriptions proceed from general and landmark features of the whole and head skeleton (Figs. 2, 3), to skeletal regions and several individual bony elements (Figs. 3-26).

The complement, arrangement and shapes of bones in the skeleton of *Satan* are similar to other Ictaluridae and most Siluroidei *sensu* Sullivan et al. (2006). The bones of *Satan* are well ossified but many elements have a trabeculated (spongy) texture, apparently containing loose connective and adipose tissue. Most bones are readily delimited by their synchondral or direct bony and fibrous joints. Many joints are deeply and finely interlocking. The dermal skull bones carrying widened cephalic lateralis-sensory canals have correspondingly enlarged tubular passageways and foramina for the main sensory canals and side branches.

The CT-scanned specimen USNM 195830 was found to be damaged by fractures of the left-side dentary, mesethmoid cornua and a possible fracture of the tip of

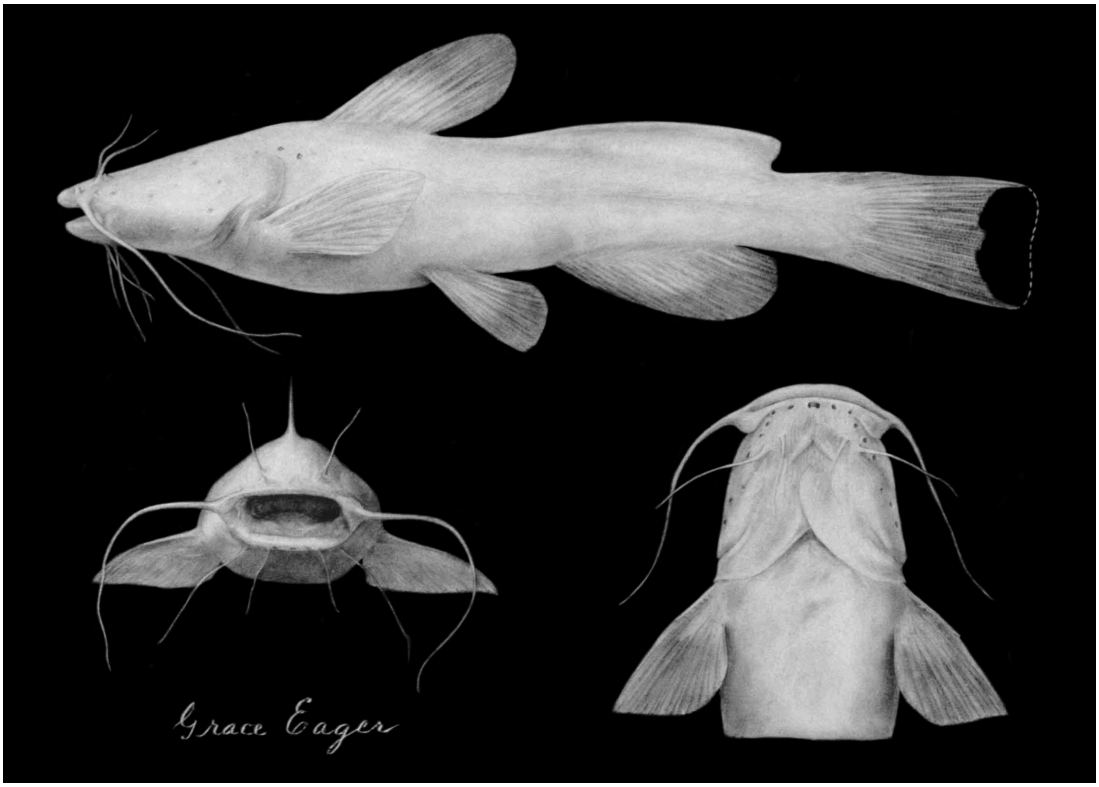

Fig. 1. *Satan eurystomus*, Holotype, UMMZ 190922, 68.7 mm SL. Reprint of Ms. Grace Eager's illustration published in the original description by Carl L. Hubbs and Reeve M. Bailey, 1947. © University of Michigan Museum of Zoology, used with permission.

the right maxilla 3A, C). The contralateral elements show unbroken shapes of these bones. Also, there is a malformation of the left side of the parasphenoid, and left pterosphenoid anterior to the left prootic and trigeminofacial foramen (Fig. 4B). The corresponding right-side elements closely resemble the normal bilaterally symmetrical shapes seen in other ictalurid catfishes. USNM 195830 is further distorted by fusions between the basioccipital and first centrum, and between the fifth centrum and Weberian compound centrum (Figs. 3C, D, 20). Unfused vertebral elements are observed in the CT-scanned specimen TCWC 8279.01 (Fig. 21) and radiographs of other specimens. Accordingly, in the following descriptions we emphasize the unbroken elements and unfused/undistorted bone shapes.

The articulated head skeleton is roughly quadrangular in dorsoventral views (Fig. 3A, C), its sides scarcely taper before the opercles to the broad, bluntly-rounded snout. The mouth is subterminal below the anteriorly projecting premaxillae (Fig. 3B, D). The head skeleton is narrow and moderately depressed; its length from the anterior limit of the premaxillary symphysis to the posterodorsal corner of the opercle is about 1.5 times longer than its greatest width across the opercles. The greatest depth of the head skeleton is at the occiput and contained about 2.1 times in its length. Cross-sectional profiles of the head skeleton are flattened anteriorly and become scarcely arched across the dorsal midline along the otic and occipital regions; ventral cross-sectional profiles are gently convex

Landmark features of the articulated head skeleton, anterior vertebrae, dorsal-fin and pectoral-fin skeletons are noted below and identified in Figs. 3A-D. The dorsal view (Fig. 3A) shows the mesethmoid bone with its tapering lateral cornua that articulate ventrally with the toothed premaxillary bones. The olfactory organ fossa is bounded medially by the mesethmoid and nasal bones, laterally by the first infraorbital, autopalatine and maxilla, anteriorly by the premaxilla and posteriorly by the thick bony antorbital process of the lateral ethmoid. Along the dorsal midline of the skull roof are the open anterior cranial fontanel, epiphyseal bar bridging the contralateral frontals and the posterior cranial fontanel that is subdivided by additional symphyses of the frontals and supraoccipital. The five tubular infraorbital bones and the lateral margin of the frontal frame the eye-less orbit. At the frontal-sphenotic joint on the skull roof margin, the junction of infraorbital, supraorbital and otic cephalic sensory canals has a large common foramen. A deep, circular temporal fossa dominates the skull roof in the otic and occipital region. The temporal fossa is bounded and floored by the supraoccipital, sphenotic, pterotic and epioccipital bones and their cartilaginous joints. The supraoccipital posterior process is short and thinly compressed. Sharply raised parasagittal and occipital crests on the supraoccipital and epioccipital are well developed as attachment sites of jaw adductor and epaxial musculature. The posttemporo-supracleithrum links the pectoral girdle to the skull at the epioccipital and supraoccipital, and carries the lateral line sensory canal to the cephalic lateralis sensory canals in the extrascapular, pterotic, sphenotic, frontal, nasal and infraorbitals. Also, seen in dorsal view are parts of the Weberian apparatus including the enlarged transverse processes of the fourth vertebra and the neural arches and spines of the third and fourth vertebrae. The dorsal-fin, its locking fin-spines and pterygiophores articulate internally with the neural spines of the Weberian apparatus and a few following precaudal vertebrae.

The lateral view (Fig. 3B) illustrates the bones of the maxillary-autopalatine joint (the large autopalatine cartilage is not visible in CT image) that is seated on and just posterior to the adjacent premaxilla. The lower jaw, including the well-toothed dentary and compound angular-articular-retroarticular, contains the mandibular section of the preoperculo-mandibular sensory canal and enlarged foramina for passage of side branches to sensory pores. The main sensory canal passes posteriorly into the preopercle where it ascends to join the postotic canal in the pterotic. The thick coronoid process of the mandible rises from the dentary and articular-angular-retroarticular as the main insertion site for jaw adductor muscles. The mandibular jaw joint between the articular and quadrate is large and transversely broad. The hyomandibula is the keystone skeletal element for support and movement of the lower jaw, operculum and hyobranchial skeleton. The hyomandibular joints with the quadrate and metapterygoid are long and firmly interlocking. The hyomandibula-cranial hinge joint is prominent along the sphenotic and pterotic margins. Off the anterior end of the hyomandibula its sharp anterodorsal process projects to the pterosphenoid. The hyomandibula-opercle articulation is a prominent synchondral ball and socket joint. The opercle, preopercle and interopercle form a triangular frame around a membranous opercular panel in the gill cover. The pectoral-fi with its strong, locking fin-spine, soft rays and radials, articulate internally with the pectoral girdle's cleithrum and scapulocoracoid. The pectoral girdle is firmly braced by joints with the fourth transverse processes, the temporal and basicranial parts of the skull, and its own midline cleithral and scapulocoracoid symphyses.

The ventral view (Fig. 3C) recaps the premaxillae, maxillary-autopalatine joint, preopercle and interopercle, and adds the hyoid arch skeleton. The hyoid skeleton includes the median urohyal and posteriorly diverging hyoid bars from the ventral and dorsal hypohyals, to the anterior and posterior ceratohyals and the branchiostegal

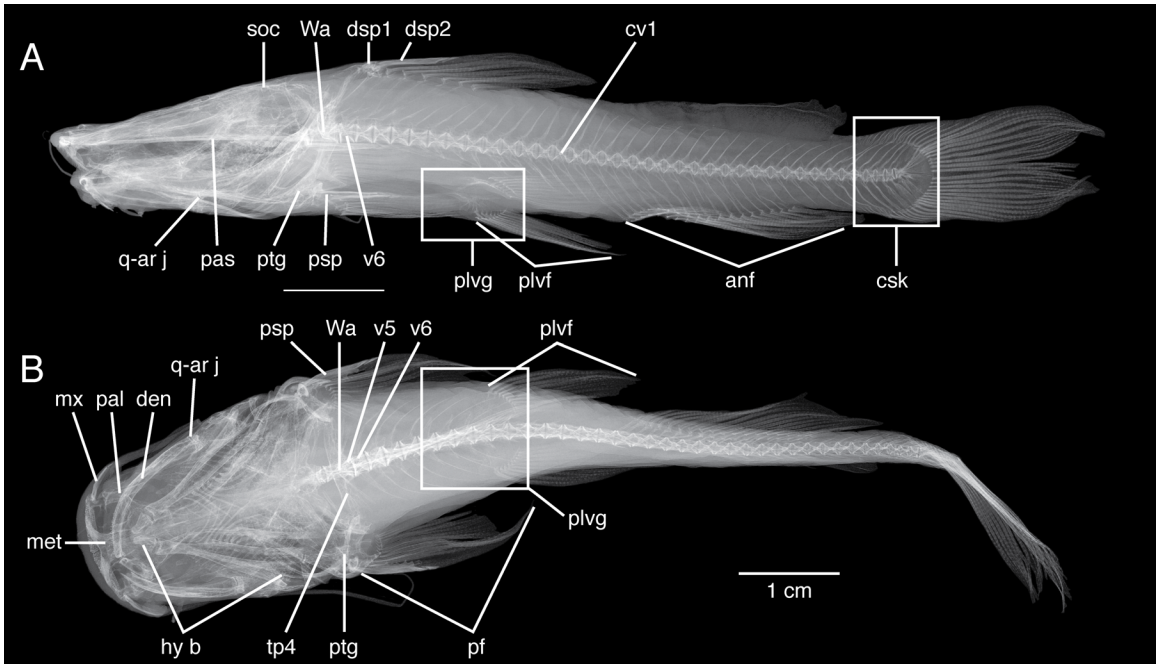

Fig. 2. *Satan eurystomus*, USNM 195930, 88.7 mm SL. Radiographs of whole specimen in A. lateral view, B. dorsoventral view. Abbreviations: anf, anal fin; csk, caudal skeleton; cv1, first caudal vertebra; den, dentary; dsp 1, dorsal-fin spine 1; dsp 2, dorsal-fin spine 2; hy b, hyoid bar; met, mesethmoid; mx, maxilla; pal, autopalatine; pas, parasphenoid; pf, pectoral fin; plvf, pelvic fin; plvg, pelvic girdle (basipterygium); psp, pectoral-fin spine; ptg, pectoral girdle; q-ar j, quadrate-articular jaw joint; soc, supraoccipital; v5, vertebra 5; v6, vertebra 6; tp4, Weberian apparatus transverse processes; Wa, Weberian apparatus.

Fig. 3. (Pages 124-125) *Satan eurystomus*, USNM 195930, 88.7 mm SL. 3-D HRXCT model of head skeleton, anterior vertebrae and pectoral girdle and pectoral fins. A. Dorsal, with dotted line indicating outline of temporal fossa, B. Right lateral, C. Ventral, D. Left medial from near sagittal plane. Abbreviations: aan, angulo-articular-retroarticular; acf, anterior cranial fontanel; boc/c1, basioccipital and fused first centrum; br, branchiostegal rays; cha, anterior ceratohyal; chp, posterior ceratohyal; cl, cleithrum; cor, scapulocoracoid; cor s, scapulocoracoid symphysis; den, dentary; df s, dorsal-fin skeleton; dfp1, dorsal-fin pterygiophore 1; dfp2, dorsal-fin pterygiophore 2; eb, epiphyseal bar; ext, extrascapula; f pop s, preopercular-mandibular sensory canal foramina; fm 7, fm 8, mandibular sensory canal foramina; fr, frontal; hhd, dorsal hypohyal; hhv, ventral hypohyal; hy b, hyoid bar; hyo, hyomandibula; hyo ap, hyomandibular anterodorsal process; hyo oc, hyomandibular-opercular condyle; hyo-sk, hyomandibula-cranial joint; io1, infraorbital 1; io5, infraorbital 5; iop, interopercle; ios f, foramen at union of infraorbital, supraorbital, otic canals; la o, lagenar (asteriscus) otolith; let, lateral ethmoid; let ap, antorbital process; mco p, coronoid process of mandible; met, mesethmoid; met cl, mesethmoid cleft; met co, mesethmoid cornu; mpt, metapterygoid; mn s, mandibular (dentary) symphysis; mx, maxilla; mx-pal j, maxillary-autopalatine joint; na, nasal; ns4, neural spine 4; olf, olfactory organ fossa; op, opercle; op f, optic nerve foramen; op p, opercular panel; ors w, orbitosphenoid wall; otl, ossified transcapular ligament; pal, autopalatine; pal-let j, autopalatine-lateral ethmoid joint; pcf a, posterior cranial fontanel, anterior subdivision; pcf p, posterior cranial fontanel, posterior subdivision; pf, pectoral-fin; pfr, pectoral-fin radials; pmx, premaxilla; pmx s, premaxillary symphysis; po f, post-otic sensory canal foramina; pop, preopercle; pro, prootic; ps cr, parasagittal crest; psp, pectoral-fin spine; psp lj, pectoral-fin spine locking joint; pto, pterotic; pto w, pterotic wing; ptt, posttemporo-supracleithrum; ptt dp, posttemporo-supracleithrum dorsal (pterotic) limb; q, quadrate; q-ar j, quadrate-articular jaw joint; sa o, saccular otolith; sc, scaphium ossicle; sn4, supraneural 4; so f, supraorbital sensory canal foramina; soc, supraoccipital; soc pp, supraoccipital posterior process; spo, sphenotic; spo p, sphenotic process; tf f, trigeminofacial foramen; tm f, temporal fossa; uh, urohyal; ut o, utricular otolith; v5, vertebra 5; v6, vertebra 6; Wa cc, Weberian compound centrum.

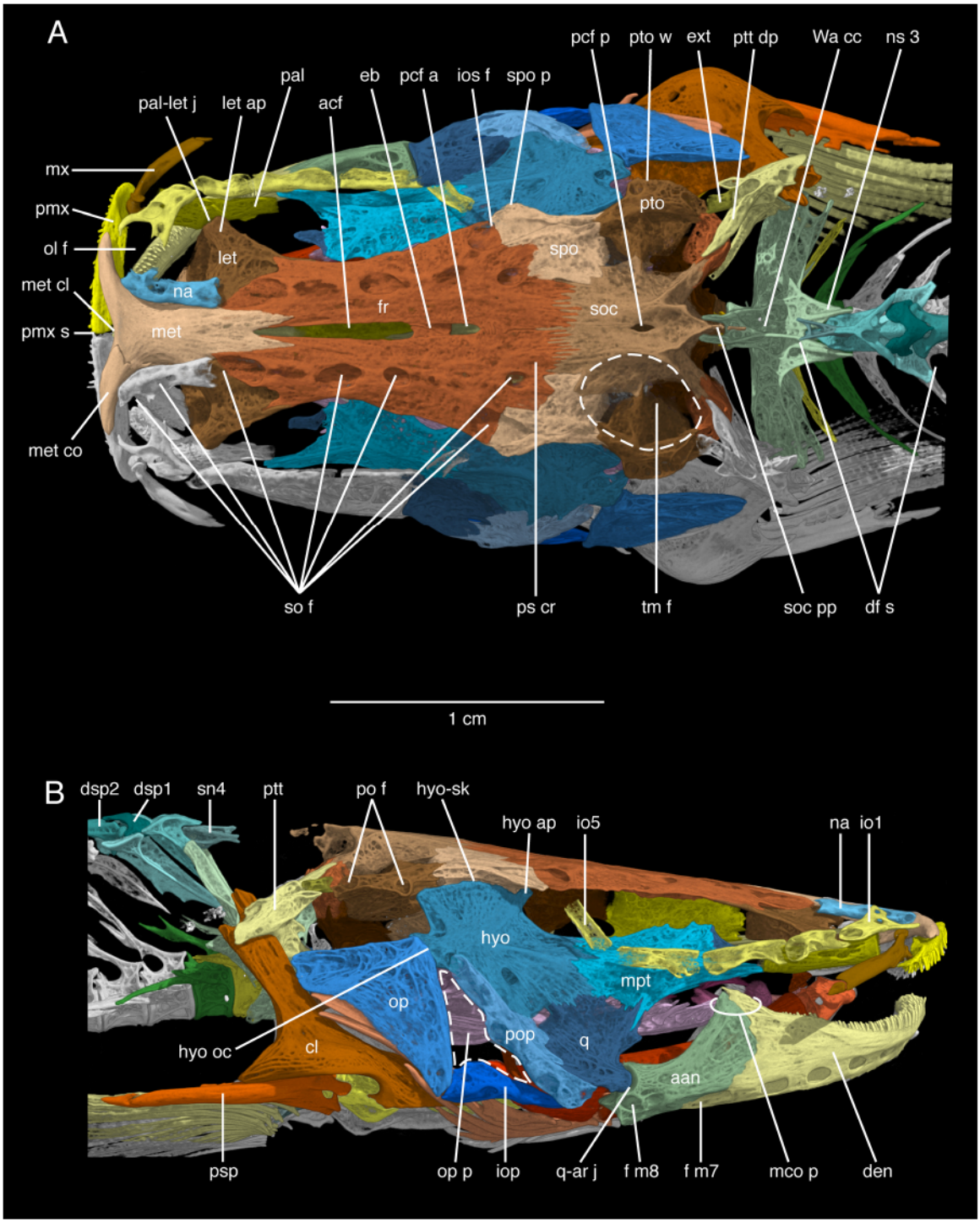
A
pcf p
pto w
ext
ptt dp
Wa cc
ns 3
pal
eb
pcf a
ios f
spo p
pal-let j
let ap
acf
mx
pmx
ol f
met cl
pmx s
met co
let
na
met
fr
spo
pto
soc
so f
ps cr
tm f
soc pp
df s
1 cm
B
dsp2
dsp1
sn4
ptt
po f
hyo-sk
hyo ap
io5
na
io1
hyo
mpt
op
pop
q
hyo oc
cl
aan
psp
op p
iop
q-ar j
f m8
f m7
mco p
den

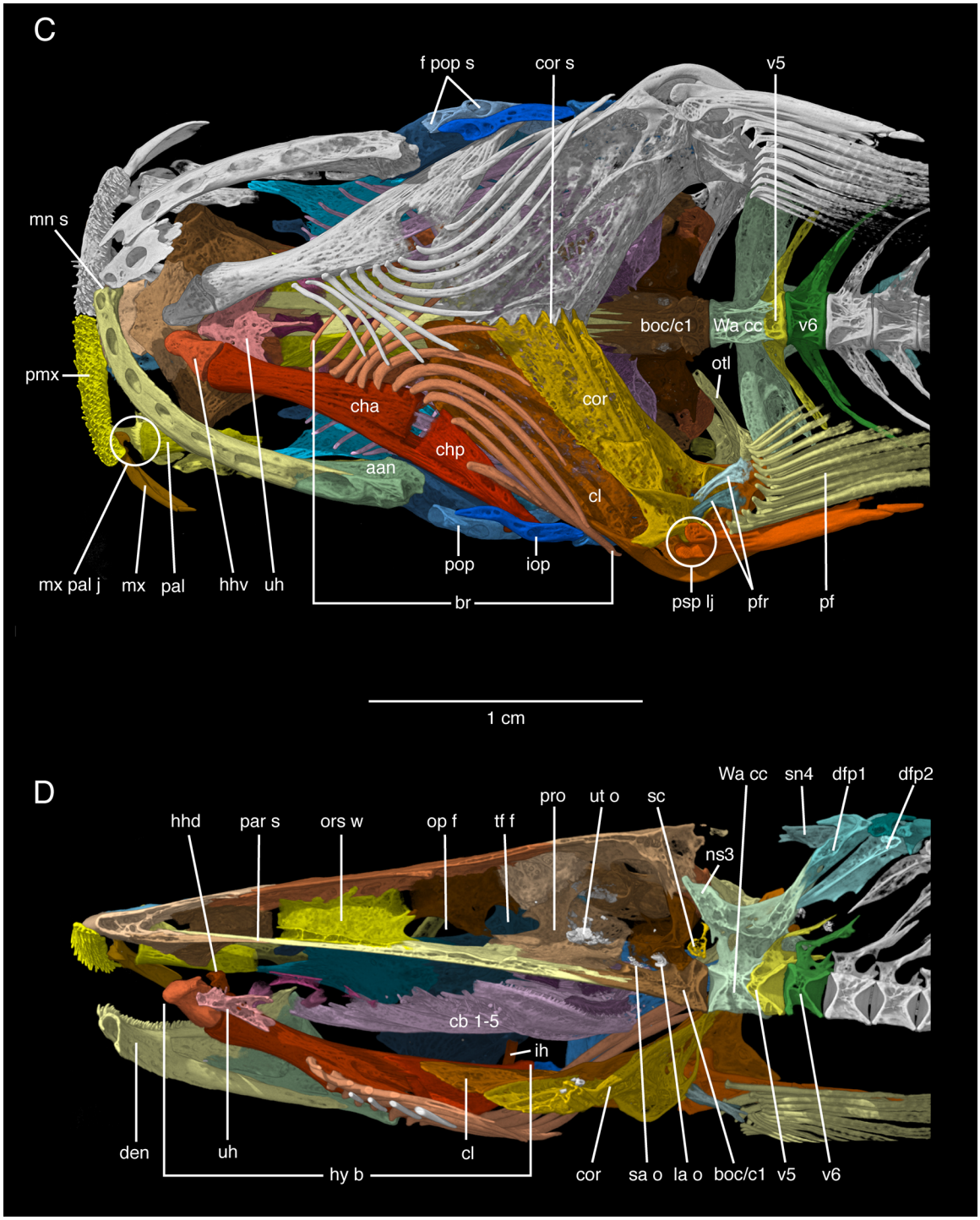
C
f pop s
cor s
v5
mn s
boc/c1
Wa cc
v6
otl
pmx
cha
cor
chp
aan
cl
mx pal j
mx
pal
hhv
uh
pop
iop
br
psp lj
pfr
pf
1 cm
D
Wa cc
sn4
dfp1
dfp2
pro
ut o
sc
hhd
par s
ors w
op f
tf f
ns3
cb 1-5
ih
den
uh
cl
hy b
cor
sa o
la o
boc/c1
v5
v6

rays supporting the opercular membrane. Posterior to the hyoid bars and branchiostegals are the symphyses of the cleithra and scapulocoracoids and, at the sides, the expansive pectoral fins and the pectoral spine locking joint with the cleithrum. Posteriormost, in this view are the basioccipital (with fused first centrum), ossified transcapular ligament of the posttemporo-supracleithrum, the Weberian apparatus and precaudal vertebrae.

The sagittal section view (Fig. 3D) recaps the ethmoid region, jaws and skull roof, lower hyoid skeleton, pectoral girdle and fin, Weberian apparatus, precaudal vertebrae and dorsal-fin skeleton. This view adds the branchial arch skeleton in the pharynx below the braincase, the medial face of the right wall of the braincase and the parasphenoid stem in section from the ethmovomerine region to the basioccipital. Also, added are the orbitosphenoid wall, optic and trigeminofacial foramina, otic capsule inner wall with three otoliths and their chambers, and the occiput from supraoccipital to basioccipital (with fused first centrum)

Neurocranium.—Figure 4 illustrates the neurocranium and right-side premaxilla, maxilla, autopalatine, nasal, infra-orbitals and posttemporo-supracleithrum. Figures 5-14 illustrate details of individual and groups of neurocranial elements.

In dorsal view, the median, smooth-surfaced and broadly T-shaped mesethmoid (Figs. 2-6, 13, 14) is a little wider anteriorly across its cornua than the bone is long. The relatively thick mesethmoid cornua extend laterally over the toothed premaxillae; these bones are closely joined dorsoventrally. Across the midline the mesethmoid cleft is wide and shallow exposing the premaxillary symphysis (Fig. 3A). The anterior margins of the cornua lack mesially-directed processes projecting back into the cleft and instead the cornua are smoothly curved and tapering above the medial approximately two-thirds of each premaxilla. In dorsal view and posterior to the cornua, the lateral margins of the mesethmoid are nearly straight-sided and constricted to form the relatively wide mesethmoid neck. The least width of the mesethmoid neck, between the flanking nasals, is about 30% of the width across the cornua tips and 32% of the mesethmoid midline length. Posteriorly, the mesethmoid has an overlapping joint with the frontals and is broadly divided on the midline forming the anterior margin of the open anterior cranial fontanel.

The vertical sides of the mesethmoid are the shallowly concave medial walls of the olfactory organ fossa. Each side of the mesethmoid has a short posterodorsal bony joint with the adjacent lateral ethmoid and, more ventrally, the mesethmoid-lateral ethmoid joints are synchondral. In ventral view (Fig. 5B, C, 13, 14) the mesethmoid is a flattened plate with biconcave margins anterior and dorsal to the vomer and posterior to its cornua and the premaxillae. The mesethmoid is ventrally shortened; its ventral midline length from the cleft margin to the vomer is less than one-third its dorsal midline length. Its ventral surface is incised with a recess that receives the bilobed anterior end of the vomer.

The nasal bone (Figs. 3, 4) lies dorsomedial to the olfactory organ fossa adjacent to, but free from, the mesethmoid neck. The nasal is a simple, tubular, sensory canal bone with three foramina. The bone is straight posteriorly and its anterior third curves laterally along the posterior margin of the mesethmoid cornu. The nasal is relatively wide (its outside width is about 25% of its length) and lacks marginal laminar bone extensions. The supraorbital sensory canal passes from the frontal through the nasal's posterior and then anterior foramina to terminate on the snout at the first supraorbital sensory pore. The lateral foramen in the nasal bone provides passage for a side branch of the supraorbital sensory canal that fuses with the anterior end of the infraorbital sensory canal such that they have a common sensory pore (Taylor, 1969).

The lateral ethmoid (Figs. 4, 6, also 3, 5, 13, 14) projects horizontally off the mesethmoid, frontal and orbitosphenoid as a thickly ossified antorbital process between the olfactory organ fossa and eyeless orbit. In dorsoventral views the lateral ethmoid is subtriangular, tapering distally to its autopalatine condyle. This bony condyle is truncated and capped with cartilage. In the skull roof, the dorsal surface of the lateral ethmoid is irregularly trabeculated and without a thin projecting wing or superficial ornamentation of dense bone. The lateral

Fig. 4. (Page 127) *Satan eurystomus*, USNM 195930, 88.7 mm SL. 3-D HRXCT model of articulated neurocranium plus right side premaxilla, maxilla, autopalatine, nasal, infraorbital, and posttemporo-supracleithrum. A. Dorsal, B. Ventral, C. Right lateral, D. Detail of left-side optic and trigemino-facial foramina with surrounding bones. Abbreviations: acf, anterior cranial fontanel; boc/c1, basioccipital and fused first centrum; eb, epiphyseal bar; eoc, exoccipital; epo, epioccipital; ext, extrascapula; fb j, frontal abutting joint; fr, frontal; fs j, frontal sutural joint; io1-5, infrorbitals 1-5; ios f, foramen at union of infraorbital, supraorbital, otic canals; let, lateral ethmoid; lop f, left optic nerve foramen; ltf t, left trigemino-facial nerve foramen; met, mesethmoid; met cl, mesethmoid cleft; met co, mesethmoid cornu; mx, maxilla; na, nasal; ors, orbitosphenoid; otl, ossified transcapular ligament; pal, autopalatine; pas, parasphenoid; pcf a, posterior cranial fontanel, anterior subdivision; pcf p, posterior cranial fontanel, posterior subdivision; pmx, premaxilla; po f, post-otic sensory canal foramina; pro, prootic; pto, pterotic; pts, pterosphenoid; ptt, posttemporo-supracleithrum; rop f, right optic nerve foramen; rtf f, right trigemino-facial nerve foramen; sb j, supraoccipital abutting joint; so f, supraorbital sensory canal foramina; soc, supraoccipital; spo, sphenotic; vo, vomer.

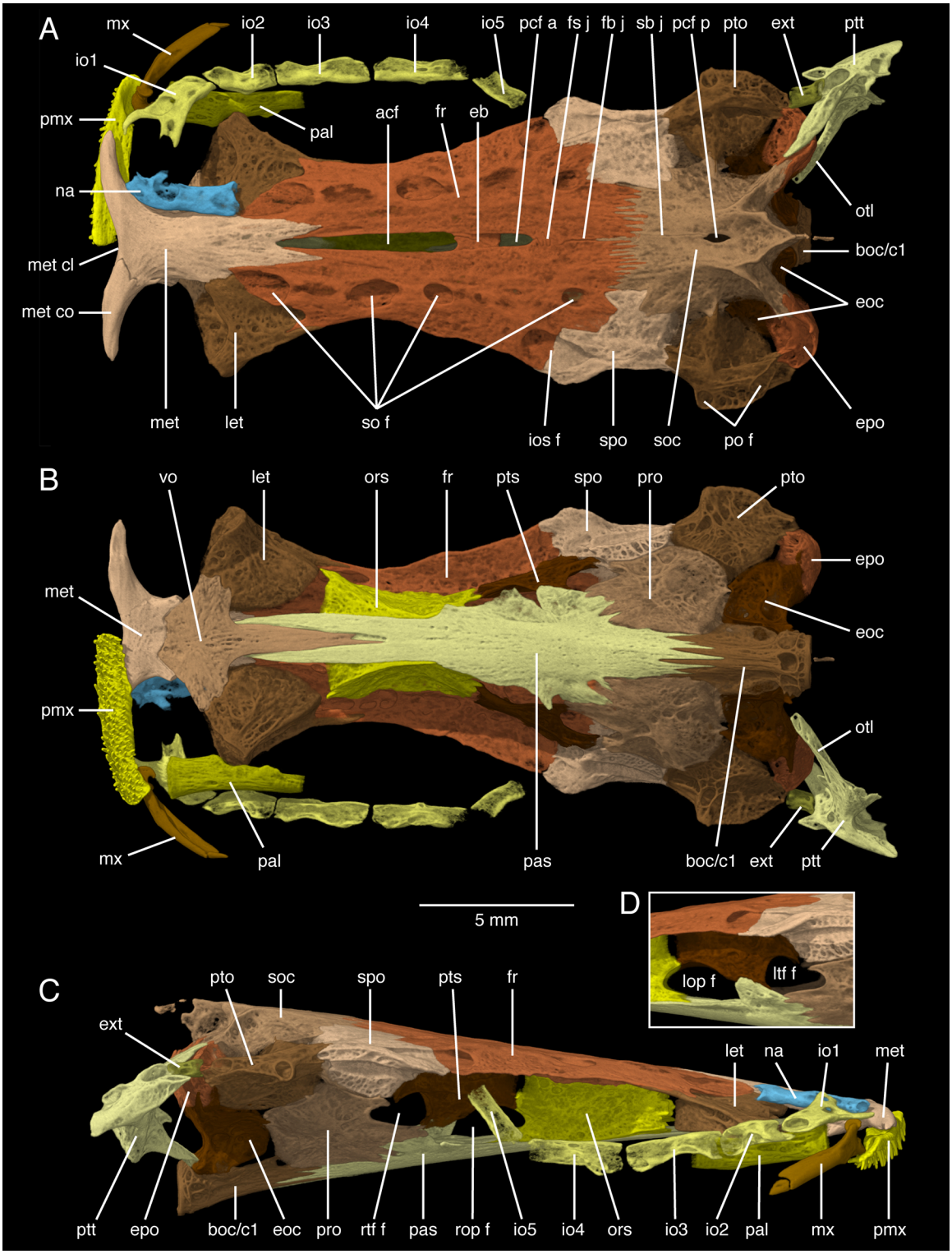
A
mx
io2
io3
io4
io5
pcf a
fs j
fb j
sb j
pcf p
pto
ext
ptt
io1
pmx
pal
acf
fr
eb
na
otl
met cl
boc/c1
met co
eoc
met
let
so f
ios f
spo
soc
po f
epo
B
vo
let
ors
fr
pts
spo
pro
pto
epo
met
eoc
pmx
otl
mx
pal
pas
boc/c1
ext
ptt
5 mm
D
lop f
ltf f
C
pto
soc
spo
pts
fr
ext
let
na
io1
met
ptt
epo
boc/c1
eoc
pro
rtf f
pas
rop f
io5
io4
ors
io3
io2
pal
mx
pmx

ethmoid has a narrow posterior process extending along the edge and below the frontal bone margin (Fig. 6A-C, 13). Medially the supraorbital sensory canal passes over the lateral ethmoid in the gap between the frontal and nasal. Posteriorly, the wide superficial ophthalmic nerve foramen passes obliquely through the otherwise non-interdigitating overlapping frontal-lateral ethmoid joint.

In the olfactory organ fossa (Figs. 3, 4, 6) the anterior wall of the lateral ethmoid contains the large foramen of the olfactory nerve. The lateral side of the anterior wall of the lateral ethmoid has an irregular spongy texture that obscures the exact position of the orbital nerve foramen. More deeply in the orbit and ethmoid region, the lateral ethmoid broadly articulates with the orbitosphenoid and mesethmoid via wide synchondral joints and a few small points of direct bony contact. Ventrally, on the palate, the vomer superficially overlaps the deeper anteromedial corner of the lateral ethmoid.

The frontal bone (Figs. 3-7) is roughly trapezoidal in outline and elongate, its length along the dorsal midline between the joints with the mesethmoid and supraoccipital comprises about half of the dorsal midline length of the skull roof. The narrowest width of the frontal is before the level of the epiphyseal bar across the eyeless orbits, and is about 40% of its own length. At the epiphyseal bar the width of the skull across the frontals is about 28% of the dorsomedial skull length from the tip of the mesethmoid to the end of the supraoccipital bone excluding the posterior process. Anteriorly, the frontal articulates with the mesethmoid and lateral ethmoid, its margin is notched above the lateral ethmoid at the wide superficial ophthalmic nerve foramen, and is underlain by the thin posterior process of the lateral ethmoid (Fig. 6). The free lateral margin of the frontal bordering the orbit has a shallowly concave profil that posteriorly gently slopes outward toward its joint with the sphenotic. The bony frontal-sphenotic joint is thin and scarcely interlocking; at the skull roof margin the frontal and sphenotic share a large foramen above the junction of the supraorbital, postotic and infraorbital sensory canals. The supraorbital sensory canal passes lengthwise through the middle of the frontal. The frontal has five sensory canal foramina: the anteriormost faces the matching posterior foramen in the nasal bone; two dorsal foramina lie in series over the orbit; the posteromedial parietal branch of the supraorbital canal leads to its foramen near the border with the sphenotic and supraoccipital; the posteriormost foramen is posterolateral between the frontal and sphenotic as noted above.

Medially and anterior to the epiphyseal bar (Fig. 4) the frontals flank the narrowly ovate anterior cranial fontanel. There is no contact between the frontals anterior to the epiphyseal bar. The anterior edge of the fontanel falls posterior to the lateral ethmoid wing. The stout epiphyseal bar is a little behind the frontal midlength and set below the general surface of skull roof. Posterior to the epiphyseal bar is a short, open anterior subdivision of the posterior cranial fontanel. Posterior to this fontanel remnant, the frontals meet again on the midline to close the posterior cranial fontanel in front of the supraoccipital, first in a short and coarsely interlocking frontal symphysis and then in a straight-sided butt joint. Posteriorly, across dorsal midline, each frontal articulates with the supraoccipital in a deeply and finely interlocking joint.

Jaw adductor muscle crests are scarcely developed on the frontal. The low, but sharp-edged parasagittal crests on the supraoccipital continue anteriorly onto the frontals medial to the foramina of the parietal branch sensory canals (Figs. 4, 7). Each parasagittal crest fades out anterior to the parietal branch foramen and lateral to the short, coarsely interlocking frontal symphysis. No muscle crests are

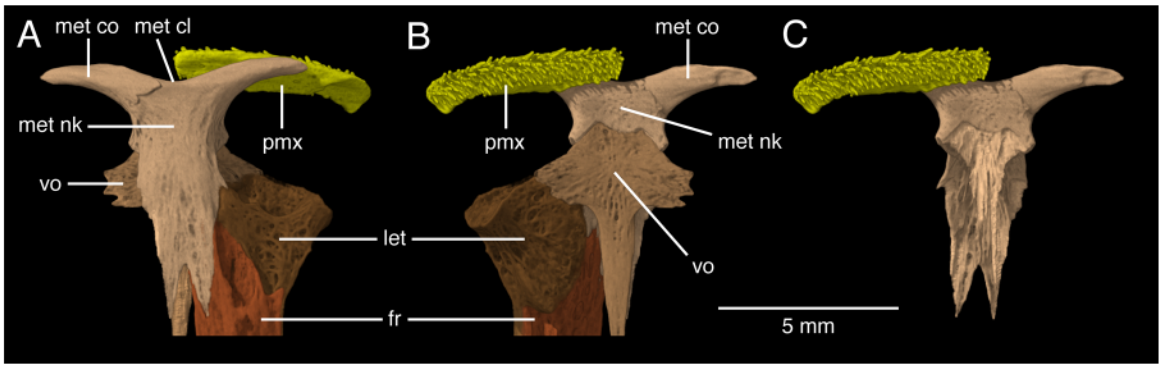

Fig. 5. *Satan eurystomus*, USNM 195930, 88.7 mm SL. 3-D HRXCT model of ethmoid region with right premaxilla. A. Dorsal, B. Ventral, C. Mesethmoid and right premaxilla, ventral view. Abbreviations: fr, frontal; let, lateral ethmoid; met cl, mesethmoid cleft; met co, mesethmoid cornu; met nk, mesethmoid neck; pmx, premaxilla; vo, vomer.

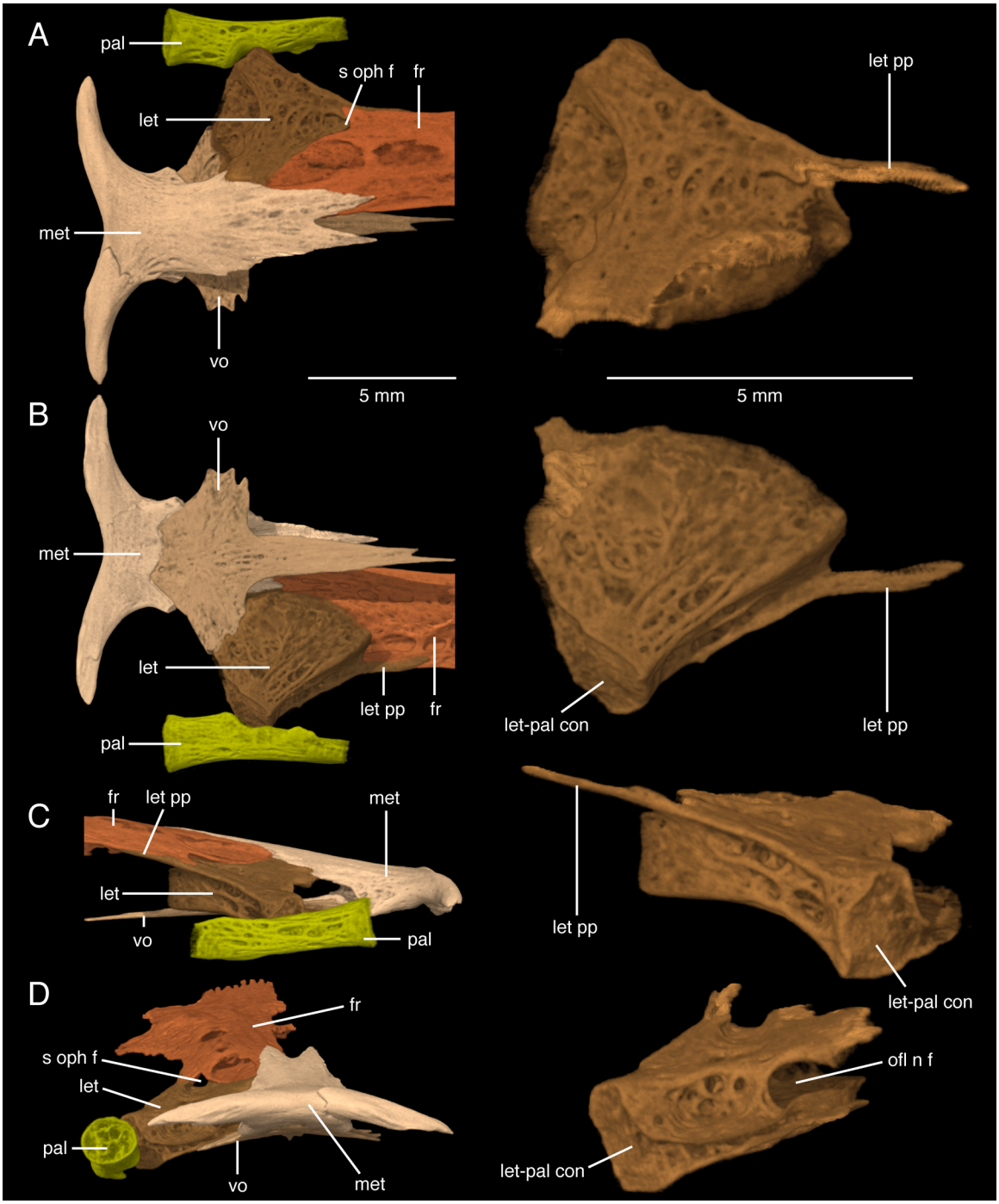

Fig. 6. *Satan eurystomus*, USNM 195930, 88.7 mm SL. 3-D HRXCT model of ethmoid and autopalatine region bones and isolated right-side lateral ethmoid bone. A. Dorsal, B. Ventral, C. Lateral right-side, D. Anterior. Abbreviations: fr, frontal; let-pal con, lateral ethmoid palatine condyle; let pp, lateral ethmoid posterior process; met, mesethmoid; pal, autopalatine; olf n f, olfactory nerve foramen; s oph f, superficial ophthalmic nerve foramen; vo, vome .

developed more anteriorly on the frontal. Ventrally (Figs. 3, 4, 7) the frontals have shallow vertical walls projecting to and along the articulations with the dorsal margins of the orbitosphenoid and pterosphenoid.

There are five wide, tubular infraorbital bones (Figs. 3, 4). Infraorbital 1 (= lachrymal) is anteromedially-oriented and anteriorly bears a slender and medially hooked process that passes over the maxillary-autopalatine joint to terminate in the skin at the anterior end of the olfactory organ and above the premaxilla and distal tip of the mesethmoid cornu. Infraorbital 1 has anteromedial and anterior foramina for passage of its terminally bifurcated sensory canal. The infraorbital sensory canal branch emanating from the anteromedial foramen of infraorbital 1 joins the supraorbital sensory canal coming from the second foramen in the nasal bone and these terminate in a common pore (Taylor, 1969). The second sensory canal branch of infraorbital 1 exits the anterior foramen and ends in the separate second infraorbital sensory pore. The posterior foramen of infraorbital 1 is aligned with the anterior foramen of infraorbital 2, and the foramina of the following infraorbital ossicles are similarly aligned with their serial neighbors. At each gap between the infraorbital bones a sensory canal side branch leads to a surface pore (infraorbital sensory canal pores 3-7). Infraorbital 2 is lateral to the lateral ethmoid antorbital process and does not overlap ossicle IO1; ossicles IO3 and IO4 ventrally frame the eyeless orbit; ossicle IO5 is oriented posterodorsally behind the orbit toward the frontal-sphenotic joint and large common foramen at the junction of the infraorbital, supraorbital and otic sensory canals.

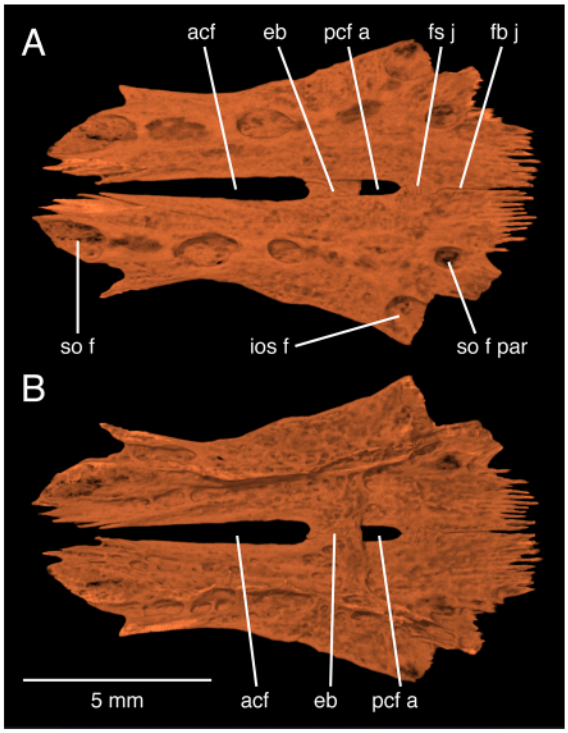

Fig. 7. *Satan eurystomus*, USNM 195930, 88.7 mm SL. 3-D HRXCT model of the frontal bones in dorsal view showing detail of supraorbital canal foramina, frontal midline joints and cranial fontanels. A. Dorsal, B. Ventral. Abbreviations: acf, anterior cranial fontanel; eb, epiphyseal bar; fb j, frontal abutting joint; fs j, frontal sutural joint; ios f, foramen at union of infraorbital, supraorbital, otic canals; pcf a, posterior cranial fontanel, anterior subdivision; so f, supraorbital sensory canal foramen; so f par, parietal branch of supraorbital sensory canal.

The supraoccipital (Figs. 2-4, 8-11) articulates with the frontals, sphenotics, pterotics, epioccipitals, exoccipitals, posttemporo-supracleithra, third supraneural and distally-bifid third neural spine of the Weberian apparatus. The joints of the supraoccipital with the sphenotics, pterotics, epioccipitals and exoccipitals are mixed synchondral (the cartilage contributed by the endochondral elements) and directly abutting, or coarsely interdigitating with the exoccipital. The dermal bone articulation between the supraoccipital and frontal is strongly interdigitating, and the supraoccipital articulations with posttemporo-supracleithra, third supraneural and anterior neural arch and spine are loose and presumably ligamentous.

In dorsal view (Figs. 3A, 4A, 8-11), the supraoccipital is large and roughly quadrangular except for the short posterior process off the occipital midline and its projecting posterolateral corners. The sharply raised margins of the base of the supraoccipital posterior process define the posterior end of a dorsomedian sulcus. The posterior process tapers abruptly behind the occiput to a narrowly pointed tip remote from the dorsal-fin origin. The posterior process is not horizontally expanded in the integument of the nape. Instead, a thin blade-like vertical ventromedial keel continues the posterior process ventrally to the posterior face of the supraoccipital above the foramen magnum. A small terminal piece of the keel is broken and floating in USNM 195830, Fig. 3A, B, 19D.

Proximally on the supraoccipital roof, the raised margins of the posterior process are continuous with the pair of longitudinally oriented parasagittal crests that also have sharply defined, angular margins. The parasagittal crests, in addition to delimiting the shallow dorsomedian sulcus, are the medial limit of origin of the main jaw adductor muscles on the skull roof. More anteriorly on the frontals the parasagittal crests are low and rounded, and they terminate behind the level of the epiphyseal bar. The small, dorsomedian and lozenge-shaped posterior subdivision of the posterior cranial fontanel persists within the sulcus of the supraoccipital. Anterior to the fontanel

and forward to the frontal-supraoccipital joint, the left and right sides of the supraoccipital abut in a dorsomedial joint. Thus, closure of a middle span of the posterior cranial fontanel results from the formation of three dorsal midline joints, one within the supraoccipital and two between the frontals posterior to the anterior remnant of the posterior cranial fontanelle. Lateral to each parasagittal crest is a wide and deep, subcircular temporal fossa (Fig. 3A, 4) floored and bounded by the supraoccipital, epioccipital, pterotic and sphenotic.

The transverse occipital crests are well developed along the occipital margin of the skull roof. These crests arise on the base of the supraoccipital posterior process adjacent parasagittal crests and run posterolaterally to join the similarly raised posterodorsal margins of the epioccipitals and dorsal (pterotic) limbs of the posttemporo-supracleithra. The transverse crests make an acute angle with the posterior process of the supraoccipital and they are tilted anteriad. The anterior faces of the transverse occipital crests mark the posterior limit of jaw adductor musculature on the skull roof, and their posterior faces mark the anterior extent of epaxial musculature onto the skull roof.

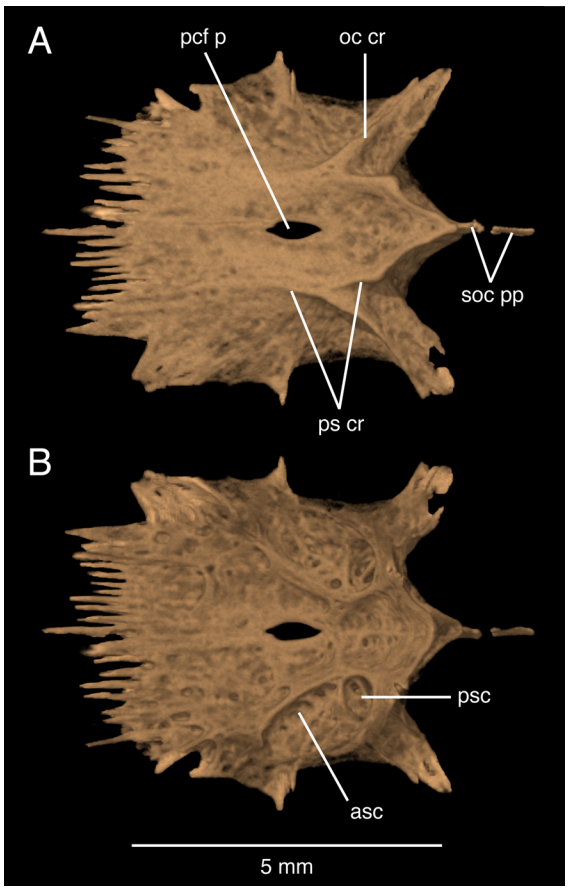

Fig. 8. *Satan eurystomus*, USNM 195930, 88.7 mm SL. 3-D HRXCT model of supraoccipital bone in A. Dorsal, B. Ventral. Abbreviations: asc, anterior semicircular canal; oc cr, occipital crest; pcf p, posterior cranial fontanel, posterior subdivision; psc, posterior semicircular canal; ps cr, parasagittal crest; soc pp, supraoccipital posterior process.

The occipital wall of the supraoccipital (Fig. 11) borders the foramen magnum and carries the pair of foramina for the recurrent (lateral accessory) branches of the facial nerve. Internally, the supraoccipital surrounds dorsomedial portions of anterior and posterior vertical bony semicircular canals.

The sphenotic bone (Figs. 3, 4, 9) is wedged between frontal, supraoccipital and pterotic in skull roof, and between pterosphenoid, pterotic and prootic in braincase sidewall. The anterior end of the sphenotic lies well posterior to the level of the epiphyseal bar. The otic sensory canal courses through the dorsolateral margin of the sphenotic. This bone provides the anterior and anteroventral wall of the deeply concave temporal fossa.

The dorsolateral margins of the sphenotic and pterotic form a long, narrow cranial facet of the hyomandibular hinge joint (Figs. 4, 9, 10). The sphenotic accounts for about two-thirds of the length of this joint, and the pterotic about one-third. Anterior to the hyomandibular hinge joint, the sphenotic and pterosphenoid together form a separate coarsely textured and slightly concave articulation point for the narrow anterodorsal process of the hyomandibula. The sphenotic margin posterior to its joint with the frontal and above the anterior end of anterodorsal process of the hyomandibula, protrudes as a laterally-rounded and horizontal sphenotic process.

Ventrally (Fig. 9 B-D), below the hyomandibular articulation, the lateral face of the sphenotic is slightly concave. Its ventral and posterior margins are curved convexly at their synchondral joints with the pterosphenoid, prootic and pterotic. Internally the sphenotic contains the lateral portion of the bony anterior vertical semicircular canal, the anterior end of the bony horizontal semicircular canal, and the bony ampulla chamber at the junction of these semicircular canals.

The pterotic bone (Figs. 3, 4, 10, 11) on the skull roof lies between the sphenotic, supraoccipital, epioccipital and extrascapula, and anterior to the posttemporo-supracleithrum. The pterotic provides the lateral and lateroventral wall of the temporal fossa. The pterotic wing is scarcely developed at the bluntly rounded posterolateral corner of the skull roof. The dorsal margin of the pterotic wing is shallowly pitted. This bone barely extends beneath the superficial and tubular extrascapula and does not directly contact the posttemporo-supracleithrum.

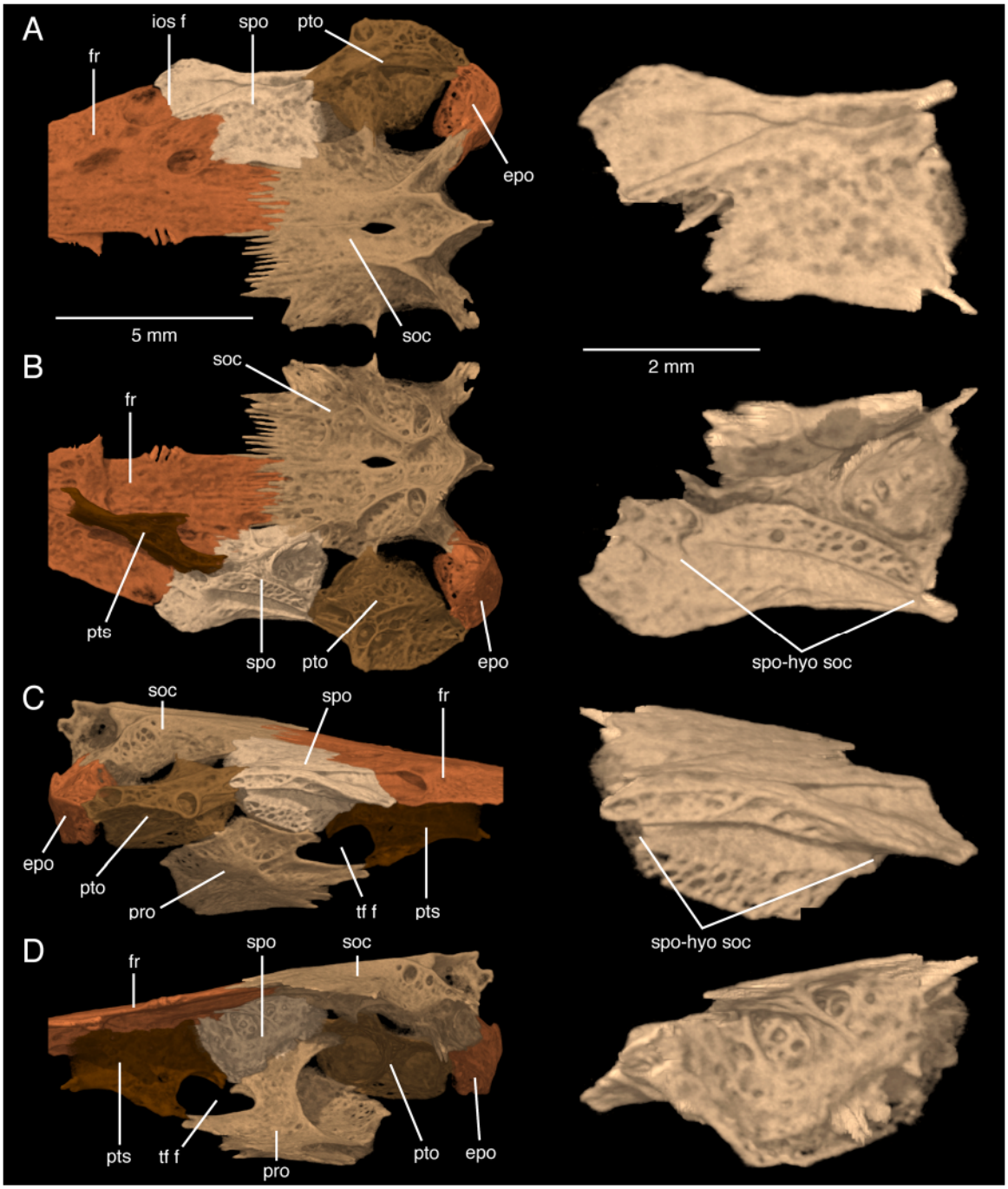

Fig. 9. *Satan eurystomus*, USNM 195930, 88.7 mm SL. 3-D HRXCT model of right-side sphenotic bone detail with adjacent supraoccipital, frontal, pterotic, epioccipital, prootic and pterosphenoid, and isolated right-side sphenotic bone. A. Dorsal, B. Ventral, C. Lateral, anterior to right, D. Medial of right-side, anterior to left from near sagittal plane. Abbreviations: epo, epioccipital; ios f, foramen at union of infraorbital, supraorbital, otic canals; fr, frontal; pro, prootic; pto, pterotic; pts, pterosphenoid; soc, supraoccipital; spo, sphenotic; spo-hyo soc, sphenotic sulcus at hyomandibula joint; tf f, trigeminofacial foramen.

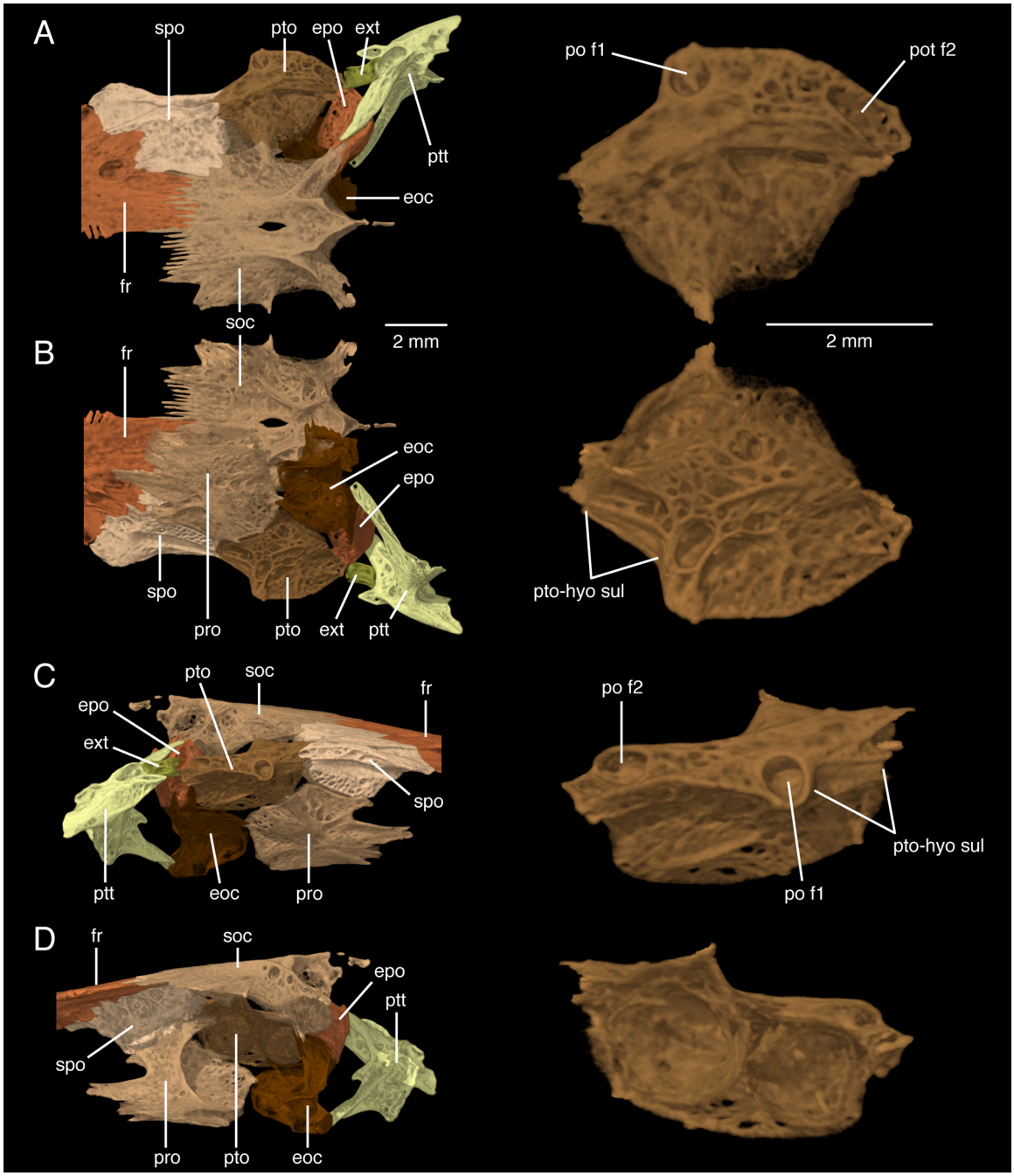

Fig. 10. *Satan eurystomus*, USNM 195930, 88.7 mm SL. 3-D HRXCT model of right-side pterotic bone detail with adjacent supraoccipital, frontal, sphenotic, epioccipital, posttemporo-supracleithrum, exoccipital and prootic, and isolated right-side pterotic bone. A. Dorsal, B. Ventral, C. Lateral, anterior to right, D. Medial of right-side, anterior to left from near sagittal plane. Abbreviations: eoc, exoccipital; epo, epioccipital; ext, extrascapula; fr, frontal; po f1, pterotic foramen for passage of preopercular-mandibular sensory canal; po f2, posterior foramen in pterotic for postotic canal; pro, prootic; pto, pterotic; pto-hyo sul, pterotic sulcus at hyomandibular joint; ptt, posttemporo-supracleithrum; soc, supraoccipital; spo, sphenotic.

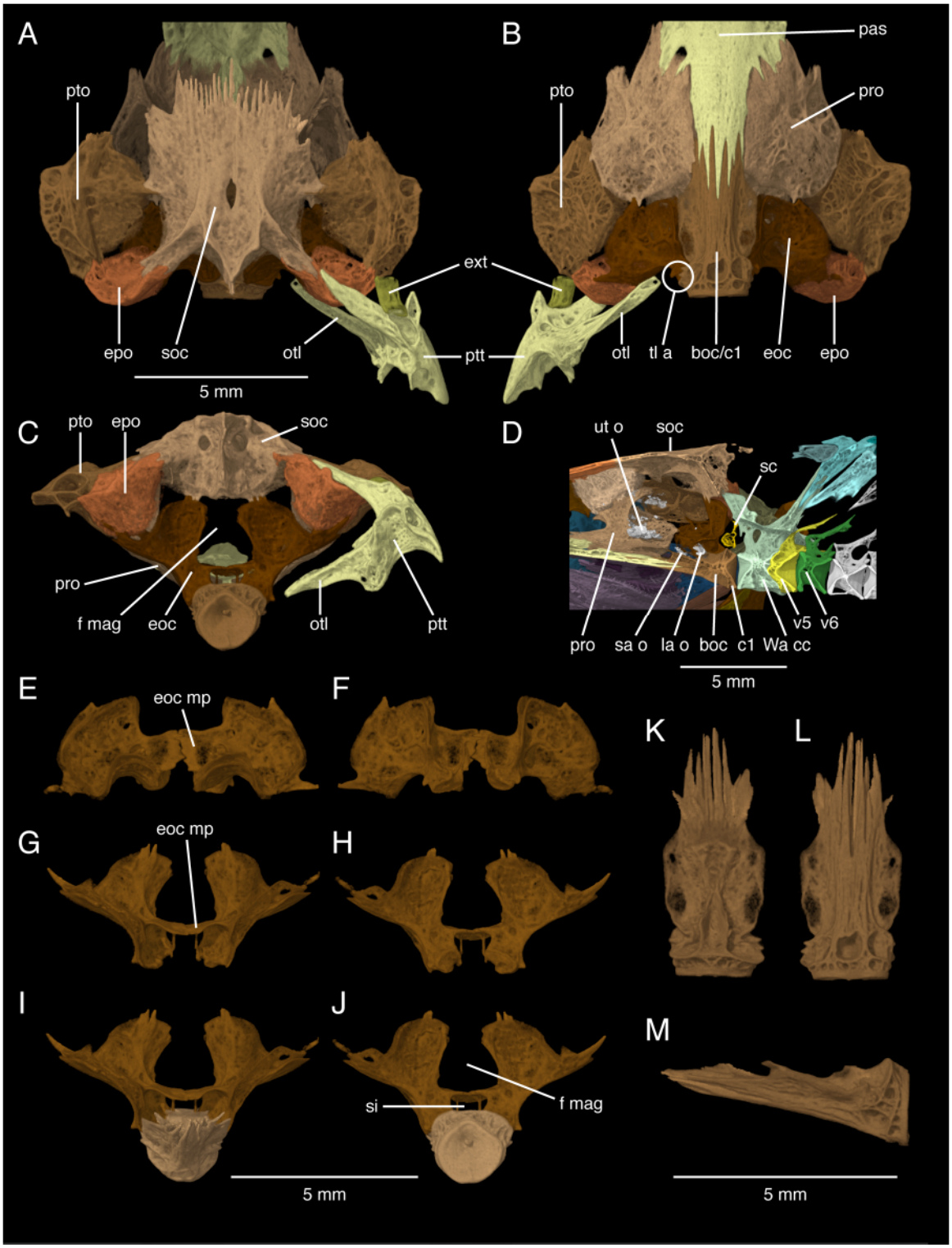
A
pto
epo
soc
otl
ext
ptt
5 mm
B
pto
pas
pro
otl
tl a
boc/c1
eoc
epo
C
pto
epo
soc
pro
f mag
eoc
otl
ptt
D
ut o
soc
sc
pro
sa o
la o
boc
c1
Wa
cc
v5
v6
5 mm
E
eoc mp
F
G
eoc mp
H
I
J
si
f mag
5 mm
K
L
M
5 mm

The postotic sensory canal (Fig. 10) runs through the elevated dorsolateral margin of the pterotic from the otic canal in the sphenotic to the posterior passage of the postotic canal to the extrascapula; the foramen for passage of the preoperculo-mandibular sensory canal opens from the pterotic above the posterior end of the pterotic-hyomandibular joint. There are no sensory canal side branches from the postotic canal to sensory pores. In the lateral walls of the braincase and otic capsule (Figs. 10, 11), the pterotic is synchondrally joined to the sphenotic, prootic, epioccipital and exoccipital. Internally, the pterotic contains the lateral portion of the bony horizontal semicircular canal.

The extrascapula (Figs. 3, 4, 11) is a short, tubular canal bone that is aligned with, but separate from, the postotic sensory-canal ossifications in the posttemporo-supracleithrum and pterotic. The thin walls of the extrascapula are perforated by a few small, irregularly shaped holes that are not foramina of passage for sensory-canal side branches. There is no lamellar-bone associated with the tubular extrascapula.

The epioccipital (Figs. 3, 4, 9-11) lies between the pterotic, supraoccipital, exoccipital and posttemporo-supracleithrum in the skull roof and occipital wall. The epioccipital forms the posterior and posteroventral wall of the temporal fossa. The joints between the epioccipital and neighboring bones are synchondral and membranous, but ligamentous with the posttemporo-supracleithrum. Along the occipital margin of the skull and otic capsule the epioccipital has a trenchantly elevated ridge continuing the transverse occipital crest of the supraoccipital and the overlying upper limb of the posttemporo-supracleithrum. Internally the epioccipital forms the posterior span of its posterior vertical semicircular canal.

The exoccipital (Figs. 4, 11, 12) in the posterolateral corner of the neurocranium forms much of the occipital and posterior wall of the otic capsule. The exoccipitals lie ventral to the supraoccipital, ventromedial to the epioccipitals, dorsal to the basioccipital, and the contralateral exoccipitals meet on the midline to frame the foramen magnum with

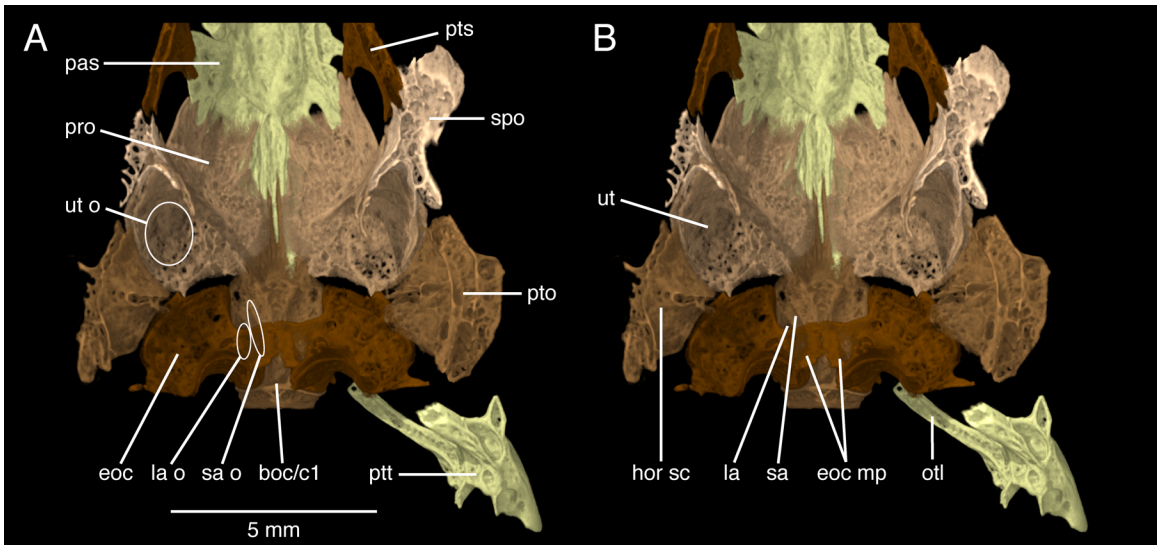

Fig. 12. *Satan eurystomus*, USNM 195930, 88.7 mm SL. 3-D HRXCT model of otic-occipital region in dorsal (interior) view A. Otolith positions shown by ovals, B. Without otolith positions. Abbreviations: boc/c1, basioccipital and fused first centrum; eoc, exoccipital; eoc mp, exoccipital medial processes; hor sc, horizontal semicircular canal; la, lagenar chamber; la o, lagenar (asteriscus) otolith; otl, ossified transcapular ligament; pas, parasphenoid; pro, prootic; pto, pterotic; pts, pterosphenoid; ptt, posttemporo-supracleithrum; sa, saccular chamber; sa o, saccular otolith; spo, sphenotic; ut, utricular chamber; ut o, utricular otolith.

Fig. 11. (Page 134) *Satan eurystomus*, USNM 195930, 88.7 mm SL. 3-D HRXCT models of otic-occipital region skeleton. (A-D) and isolated occipital bones (E-M). A. Dorsal, B. Ventral, C. Posterior, D. Medial of right-side, anterior to left from near sagittal plane. E-H. Isolated exoccipital bones, E. Dorsal, F. Ventral, G. Anterior, H. Posterior. I, J. Articulated exoccipital and basioccipital bones, I. Anterior, J. Posterior. K-M. Isolated basioccipital bone, K. Dorsal, L. Ventral, M. Left lateral. Abbreviations: boc, basioccipital; boc/c1, basioccipital and fused first centrum; c1, first centrum; eoc, exoccipital; eoc mp, exoccipital medial processes; epo, epioccipital; ext, extrascapula; f mag, foramen magnum; la o, lagenar (asteriscus) otolith; otl, ossified transcapular ligament; pas, parasphenoid; pro, prootic; pto, pterotic; ptt, posttemporo-supracleithrum; sa o, saccular otolith; sc, scaphium ossicle; si, sinus impar; soc, supraoccipital; tl a, transcapular ligament attachment site; ut o, utricular otolith; v5, vertebra 5; v6, vertebra 6; Wa cc, Weberian compound centrum.

bone laterally and ventrally, and with cartilage dorsally. The vertical exoccipital-supraoccipital joint is cartilaginous medially and laterally, but bony and coarsely interdigitating at midlength. The joints between the exoccipital, epioccipital, pterotic and prootic are synchondral. Low on the braincase and otic walls, the exoccipital contacts the basioccipital and prootic. The posterior half of the exoccipital-basioccipital joint in the ventrolateral wall and floor of the otic capsule is bony and weakly sutural but the anterior half of this contact is synchondral. Dorsal to the basioccipital, the exoccipital rises vertically as a steep, outwardly concave and mostly smooth-faced wall of the otic capsule and then slopes laterally toward its joint with the pterotic. Ventral to the exoccipital-epioccipital joint, the exoccipital projects posterolaterally expressing the posterior vertical semicircular canal. The large vagal nerve foramen pierces the exoccipital ventrally, just anterior to the posterolateral corner of the neurocranium and between the posterior vertical semicircular duct and the lagenar and saccular chambers.

Internally (Fig. 12), the exoccipital surrounds the ventrolateral portion of the bony posterior vertical semicircular canal, the posterior part of the bony horizontal

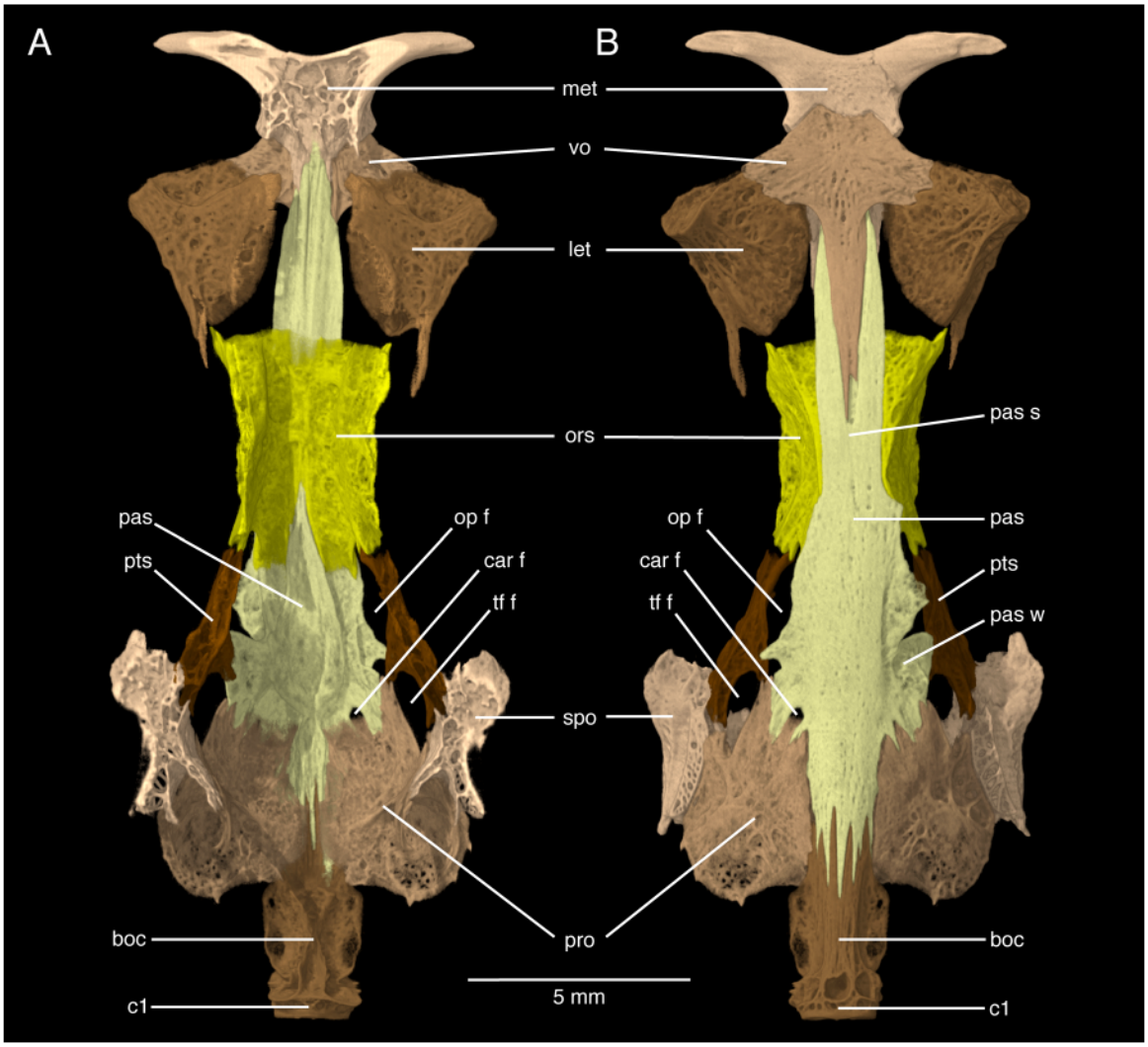

Fig. 13. *Satan eurystomus*, USNM 195930, 88.7 mm SL. 3-D HRXCT model of basicranium. A. Dorsal (interior). B. Ventral. Abbreviations: boc, basioccipital; c1, first centrum; car f, carotid foramen; let, lateral ethmoid; met, mesethmoid; op f, optic nerve foramen; ors, orbitosphenoid; pas, parasphenoid; pas s, parasphenoid stem; pas w, parasphenoid wing; pro, prootic; pts, pterosphenoid; spo, sphenotic; tf f, trigeminofacial foramen; vo, vomer.

semicircular canal, and the bony ampullae chamber at the junction of those canals. The exoccipital also forms the lateral and posterior walls of the lagenar chamber containing the asteriscus otolith. Between the lagenar chambers, the prominent medial processes of the contralateral exoccipitals meet on the midline to form a symphyseal wall separating the ventrally placed sinus impar from the dorsally placed foramen magnum and neural canal. The exoccipital medial processes are horizontal, in the same plane as the sinus impar and horizontal axis of the neural canal.

The basioccipital and exoccipital together form a coarse-textured, bony attachment site for the medial ligamentous end of the otherwise ossified transcapular ligament of posttemporo-supracleithrum (Figs. 4, 11, 12). This attachment site is dorsolaterally adjacent to the occipital condyle at the tight articulation of these occipital bones.

The median basioccipital (Figs. 3, 4, 11-13, 19, 20) is the posteriormost element of the neurocranial floo . The basioccipital is part of the occipital wall and otic capsule between the exoccipital, prootic and parasphenoid. Posteriorly, the basioccipital is normally jointed with a separate firs vertebral centrum as in TCWC 8279.01 (Fig. 20). As noted however, the basioccipital and first centrum are fused in USNM 195830 (Figs. 3, 11, 12, 19). In both conditions the basioccipital and first centrum are closely associated with the scaphia, the second pair of Weberian ossicles.

The ventral side of the basioccipital is transversely rounded and cylindrically shaped at and anterior to the occipito-vertebral condyle except for a single median pit (Fig. 20). There is no midventral aortic groove on the basioccipital or first centrum. Anteriorly, the basioccipital-parasphenoid joint is deeply interlocking. Anterolaterally and across the ventral midline the basioccipital articulates with the prootics via narrow synchondral joints.

The basioccipital-exoccipital joint is narrowly synchondral along the ventrolateral sidewall of the otic capsule and ventrally along the base of the occipital wall. The ventral profile across the occipito-vertebral joint and below the Weberian apparatus is horizontal and straight in both TCWC 8279.01 and USNM 195830. The sinus impar, floored by the basioccipital and enclosed above by the exoccipital medial processes, is similarly horizontally straight. On the floo of the otic capsule (Fig. 12), the basioccipital provides the floors of the paired saccular and lagena chambers housing, respectively, the sagitta and astericus otoliths.

The flattened prootic (Figs. 3, 4, 11-13) is roughly pentagonal in outline in the otic capsule wall and braincase between the parasphenoid, contralateral prootic, basioccipital, exoccipital, pterotic, sphenotic and pterosphenoid. The prootic forms the posterodorsal border of the trigeminofacial nerve foramen. The lateral surface of the prootic is weakly bulging lateral to its otolith chambers.

The elongate parasphenoid (Figs. 3, 4, 11-13) is the floor of the braincase from the mesethmoid and vomer to the basioccipital. The anterior stem of the parasphenoid lies ventral to the mesethmoid and orbitosphenoid and dorsal to the vomer; anteriorly the parasphenoid stem is a little narrower than the overlying orbitosphenoid walls. The parasphenoid has wing-like expansions adjacent to the orbitosphenoid, pterosphenoids and prootics. The right and left parasphenoid wings form the ventral margins of the optic foramina. The left parasphenoid wing has the normal relationships with the left margin of the trigeminofacial foramen, the prootic and pterosphenoid, whereas the right parasphenoid does not enter the margin of the right due to an atypical contact in USNM 195830 between the right prootic and pterosphenoid.

The pterosphenoid (Figs. 3, 4, 9, 13) is a vertical, longitudinally oriented plate of bone in the braincase and orbital wall where it forms the anterior and dorsal margins of the large trigeminofacial nerve foramen and the dorsal margin of the optic nerve foramen. The pterosphenoid articulates with the frontal dorsally, orbitosphenoid anteriorly, sphenotic posteriorly, and the prootic above and below the trigeminofacial foramen. The joints of the pterosphenoid are narrowly synchondral and membranous.

The median orbitosphenoid (Figs. 3, 4, 13), situated between the lateral ethmoids, vomer, parasphenoid, pterosphenoids and frontals, has a broad horizontal floor and tall vertical sidewalls. There are no bony horizontal shelves developed on the lateral faces of the orbitosphenoid sidewalls. The surface and internal textures of the orbitosphenoid are mostly coarse and spongy. There are no evident foramina except that the orbitosphenoid forms the anterior margin of the large optic foramen. The orbitosphenoid is completely subtended by the anterior stem of the parasphenoid and vomer and is scarcely exposed on the palatal surface along the sides of the parasphenoid stem. The dorsal margins of the orbitosphenoid sidewalls articulate with matching but shallow ventral ridges of the frontals. Anteriorly the orbitosphenoid has mixed synchondral and bony joints with the paired lateral ethmoids. Posteriorly, above the optic foramen the orbitosphenoid articulates via a narrow synchondral joint with the anterior vertical edge of the pterosphenoid.

The median, T-shaped vomer (Figs. 3-5, 13) is a large, well-ossified and edentulous plate directly jointed with the overlying mesethmoid, lateral ethmoids and parasphenoid. The anterior margin of the vomer is shallowly concave between a pair of low projections, its lateral wings are broad and blunt-tipped, and its narrowly pointed posterior end flanked by the parasphenoid reaches to below the middle of the orbitosphenoid.

Splanchnocranium.—Figures 3-5 and 14 illustrate the arrangement and shapes of the bones of the right upper jaw and maxillary barbel: premaxilla, maxilla, autopalatine. In dorsoventral view the premaxilla is narrowly subrectangular, transversely broad and nearly straight but laterally a little curved posteriorly beyond the mesethmoid cornu and below the maxillary head. Its posterolateral corner is bluntly rounded and without a posterior projection. On the lateral quarter of its dorsal surface, the premaxilla has a shallow fossa wherein sits the head of the maxilla. A shallow trench obliquely crosses the medial two-thirds of the premaxillary dorsal surface. This groove receives the matching long, narrow mesethmoid cornu in a direct, likely-firm premaxillary-mesethmoid joint

The ventral surface of the premaxilla is covered with narrowly conical, slightly recurved and acutely tipped teeth; those of the outer row are about three times taller than the inner-row teeth. The premaxillary teeth are close-set and arranged in approximately four to fiv irregular rows with about 30 teeth in the outer row and 28 in the inner row. The bands of premaxillary teeth mostly overbite the occluding dentary teeth. There is no direct bony contact of the contralateral premaxillaries at their ligamentous symphysis.

The edentulous maxilla is excluded from the gape and, with the autopalatine, supports and controls movements of the maxillary barbel. The maxilla is crescentic in form and relatively long, its length is about two-thirds of the premaxillary width; its tip has a fracture in USNM 195830. The maxillary shaft is robust, deeply grooved post-axially wherein lies the elastocartilage core of the maxillary barbel, and the shaft narrows distally in the base of the maxillary barbel. The maxillary head is bifid with a dorsoventral pair of rounded maxillary condyles that moveably articulate with the anterior cartilage of the autopalatine. The autopalatine and maxilla are lateral to the olfactory organ fossa.

The autopalatine is longitudinally oriented lateral to the lateral ethmoid, posterior to the maxilla and moveably articulated with both. The bone is stout and rod-like with both ends sharply truncated and cartilage-capped. Its bony anterior end is circular in end view with its diameter contained about three times in the autopalatine length; its posterior end is laterally compressed. The anterior cartilage of the autopalatine is relatively large as estimated by the size of the radiotransparent space between the bony maxilla and autopalatine, and is contained about nine times in the length of the autopalatine. The synchondral lateral ethmoid-

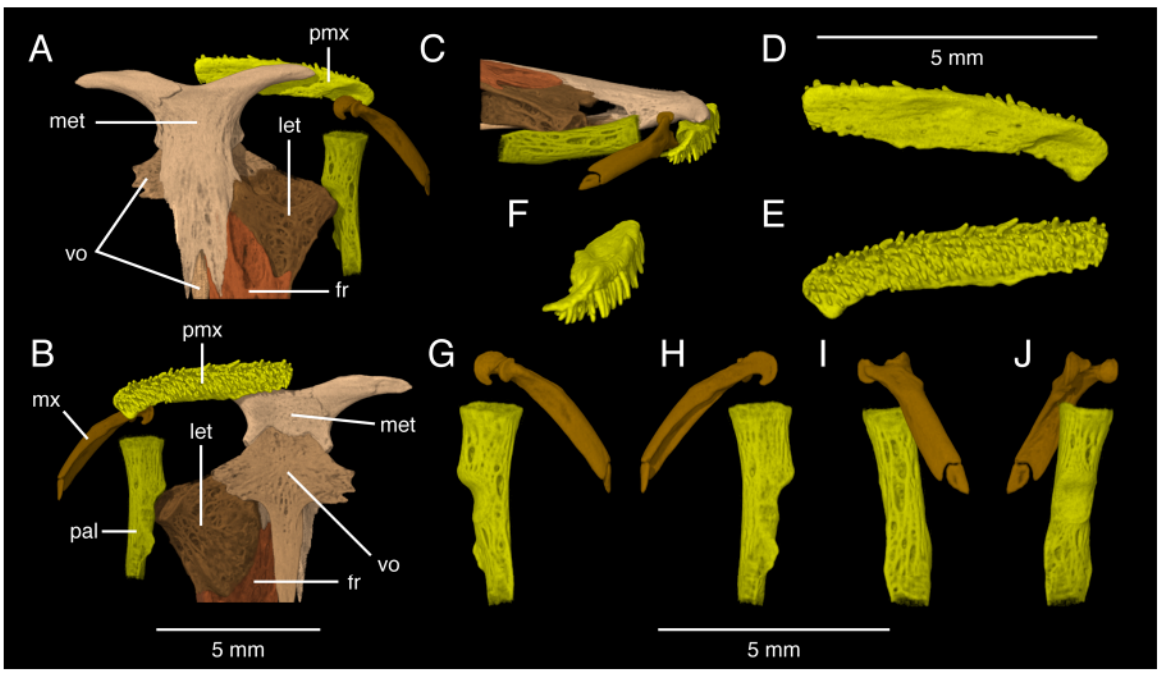

Fig. 14. *Satan eurystomus*, USNM 195930, 88.7 mm SL. 3-D HRXCT model of ethmoid region with right-side premaxilla, maxilla and autopalatine bones. A. Dorsal, B. Ventral, C. Right lateral. Premaxilla. D. Dorsal, E. Ventral, F. Lateral. Maxilla and autopalatine. G. Dorsal, H. Ventral, I. Lateral, J. Medial view. Abbreviations: fr, frontal; let, lateral ethmoid; met, mesethmoid; mx, maxilla; pal, autopalatine; pmx, premaxilla; vo, vomer.

autopalatine joint is at the distal end of the antorbital process between its anteroventral, gently convex condyle and the shallowly concave medial articular face of the autopalatine.

Figures 3 and 15 illustrate the arrangement and shapes of the bones of the large mandible including the well-toothed dentary, fused angulo-articular-retroarticular (Arratia, 2003) and separate coronomeckelian. Together the lower jaws are wide across their posterior ends at the quadrate-articular joint (about 55% of HL and long (about 60% of HL). The coronoid process is moderately deep (about 30% of the straight line distance from the anterior end of its symphysis to the end of the articular condyle) and steep-sided with the dorsal margins of the dentary and angular meeting apically in an angle of nearly 90°. The medial wall of the mandible between the dentary and angulo-articular-retroarticular is a wide trench occupied by the mandibular (Meckel's) cartilage and the small coronomeckelian bone.

In siluriforms the angular, articular and retroarticular bones are fused. The articular facet of the jaw joint is transversely wide and moderately concave centrally. A short, blunt retroarticular process projects posteriorly off the bone just below the articular facet. The posterior foramen for passage of the mandibular sensory canal is visible laterally on the outer face the angulo-articular-retroarticular ventrally adjacent to the articular facet.

The dentary is narrow and shallow at the symphysis and has a sharp, low ventral keel below the first to fifth sensory-canal foramina. The symphysis is loosely constructed and the paired postsymphyseal process is weakly developed. The broad band of dentary teeth extends posteriorly onto the base of the coronoid process. The dentary teeth are like the premaxillary teeth in size and shape, close-set and arranged in approximately four to five irregular rows near the symphysis, diminishing to a single row lateroposteriorly; there are at least 45 teeth in the outer row and about 40 teeth in the inner row. There are seven enlarged sensory pore foramina along the mandibular canal; the first or symphyseal foramen is adjacent to the symphysis and directed anteroventrally reflecting the union of the contralateral first sensory canals and their common sensory pore on the midline of the chin. The seventh mandibular-canal foramen spans the dentary-angulo-articular-retroarticular joint, and the eighth foramen is just below and lateral to the jaw joint. Here the main canal passes between the mandible and preopercle.

Figures 2, 3, 16 illustrate the arrangement and shapes of the bones of the suspensorium and opercle including the entopterygoid, metapterygoid, quadrate, hyomandibula, preopercle, interopercle and opercle. The ectopterygoid, supra- and sub-preopercular ossicles are absent.

The entopterygoid is a small, edentulous and comma-shaped plate that loosely abuts the anteromedial corner of the metapterygoid. The entopterygoid has no other bony contacts with neighboring bones.

The metapterygoid is a large, edentulous and roughly rhomboidal plate lying obliquely (about 45°) above the horizontal plane in the orobranchial wall. The metapterygoid articulates with the entopterygoid, quadrate and hyomandibula. The anteromedial corner of the meta-

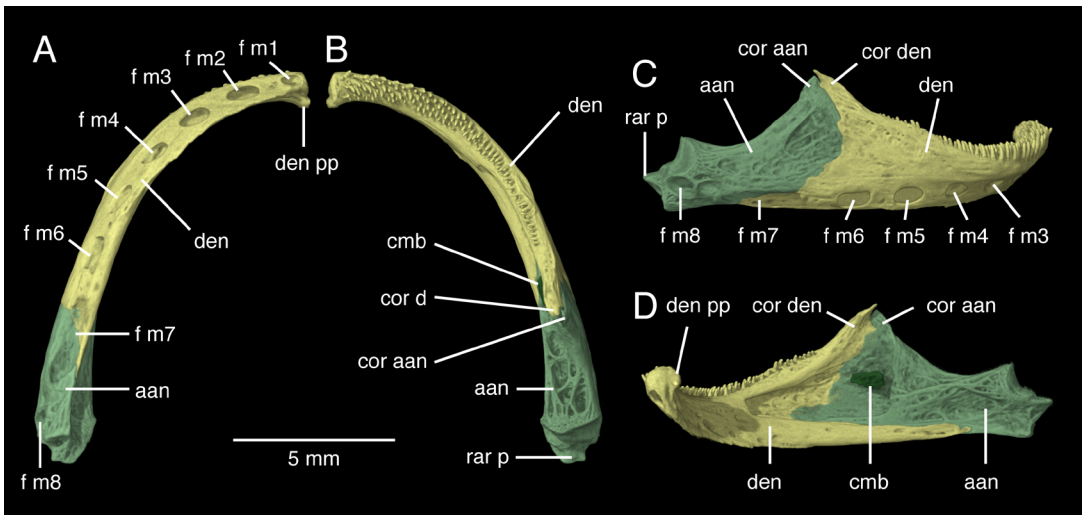

Fig. 15. *Satan eurystomus*, USNM 195930, 88.7 mm SL. 3-D HRXCT model of right-side lower jaw. A. Ventral, B. Dorsal, C. Lateral, D. Medial. Abbreviations: aan, angulo-articular-retroarticular; cmb, coronomeckelian; cor aan, coronoid process of anguloarticular; cor den, coronoid process of dentary; den, dentary; den pp, dentary postsymphyseal processes; f m1-8, foramina for mandibular sensory canal and its side branches; rar p, retroarticular posterior process.

pterygoid is truncated at its joint with the entopterygoid. Its anterolateral corner is narrowly elongated and terminates posterolateral to the autopalatine. Its medial margin has four low cusps before a weakly concave span to its joint with the hyomandibula. The lateral margin of the metapterygoid is shallowly and smoothly concave; its posterolateral corner and about one-third of its posterior margin articulate with the quadrate via a deeply interdigiting bony plus a short synchondral joint of the pterygoquadrate cartilage. The remaining posterior margin of the metapterygoid is a long, shallowly interdigitating joint with the hyomandibula.

The quadrate is expanded and fan-like dorsal to its robust, wide and gently convex condyle at the quadrate-articular (jaw) hinge joint. The quadrate also articulates with the metapterygoid, hyomandibula and preopercle. The quadrate-hyomandibular joint is bony and firmly interdigitating posterior to the metapterygoid, then, more posteriorly and medial to the preopercle, the quadrate-hyomandibular joint is fully synchondral via the hyosymplectic cartilage. The dorsal end of the quadrate-preopercle joint has a thin sheet of the preopercle laterally overlapping the quadrate. The ventrolateral margins of the quadrate and preopercle are shallowly sutured whereas those elements are more broadly articulated internally just below the hyosymplectic cartilage. The quadrate has a broad, shallow trench above the ventralmost end of the preopercle and posterior to its articular condyle. The symplectic canal, the passageway of the external mandibular branch of the facial cranial nerve, pierces the quadrate immediately adjacent to the lower limb of the preopercle.

The hyomandibula is broad and squarish but with a wide anterior sheet extending anteroventrally to its joints with the metapterygoid and quadrate. The hyomandibula also has a robust opercular condyle off its posterior margin and a sharply prominent anterodorsal process that tilts medially to contact the pterosphenoid. The long, narrow and dorsally convex articular head of the hyomandibula makes a synchondral hinge joint with the matching sulcus along the margins of the sphenotic and pterotic.

With few exceptions sites of muscle attachment are not strongly developed on the hyomandibula. On its lateral face the centrally placed and horizontal *levator arcus palatini* crest is a low rounded ridge from the hyomandibula-metpterygoid joint to its termination at the vertical crest of attachment of the A3 (*pars stegalis*) deep layer of the *adductor mandibulae*. The A3 crest continues ventrally to the lower foramen of the facial nerve canal. The A3 crest also marks the anterior limit of the flat to scarcely concave surface of the *adductor mandibulae* crest. The adductor crest is the surface of origin of the superficial main *adductor mandibulae* muscle and it broadly extends posteriorly to the hyomandibula-preopercle joint. Dorsally, at the level of the opercular condyle, the adductor crest is diminished and there is no bony indication of the separation between the *dilitator operculi* muscle and *adductor mandibulae* muscle. At the posterodorsal corner of the hyomandibula there is no development of a vertical levator operculi crest, but the large *adductor hyomandibularis* process prominently projects off the dorsal margin of the opercular condyle. On the medial face of the hyomandibula a typical C-shaped *adductor arcus palatini* crest is present.

The upper foramen of the facial canal, for passage of the hyomandibular trunk of the facial nerve, opens on the medial face of the hyomandibula posteroventral to its anterodorsal process. The facial canal has two large lower foramina. Of these, one opens posteromedially immediately below the opercular condyle, at a gap between the hyomandibula and preopercle. We interpret this as the foramen of exit of the hyoidean branch of the hyomandibular trunk innervating the lower hyoid arch. The second lower foramen of the facial canal is on the lateral face of the hyomandibula dorsal to the hyosymplectic cartilage and near the preopercle. This foramen carries the mandibular branch of the facial nerve to the lateral side of the suspensorium. The main trunk of the mandibular branch courses ventrally to pass through the symplectic canal back to the medial side of the quadrate and then on to the mandibular region.

The preopercle is closely applied to the posterolateral margin of the hyomandibula and posteroventral edge of the quadrate. It is an outwardly swollen, sensory-canal bone with a flat anterior expansion that laterally covers and unites with the hyomandibula, hyosymplectic cartilage and quadrate. The preopercle lacks flat or concave bony extensions from its posterior margin. Its preopercular dorsal limb, above the hyosymplectic cartilage, terminates bluntly lateral to the opercular condyle of the hyomandibula. The preopercular ventral limb articulates with the quadrate as described above. The preopercular sensory-canal has four foramina: dorsal and ventral foramina of passage for the main preoperculo-mandibular sensory canal, and two large foramina of exit for side branches of the preopercular sensory canal, the upper of these foramina is anterodorsal of the opercle-interopercle joint, and the lower foramen is laterally adjacent to the anterior end of the interopercle.

The opercle, as in most catfishes, is nearly right-triangular with the dorsal and anterior margins intersecting at about 90°, and moderately broad (its width along the dorsal margin contained about 1.2 times in depth along anterior margin). The dorsal margin is slightly concave and flatt ned without a dorsal crest along the insertion of the *levator operculi* muscle. The opercle, interopercle and preopercle do not meet and instead form a triangular frame around an apparent gap in the operculum that is covered by a panel of integument.

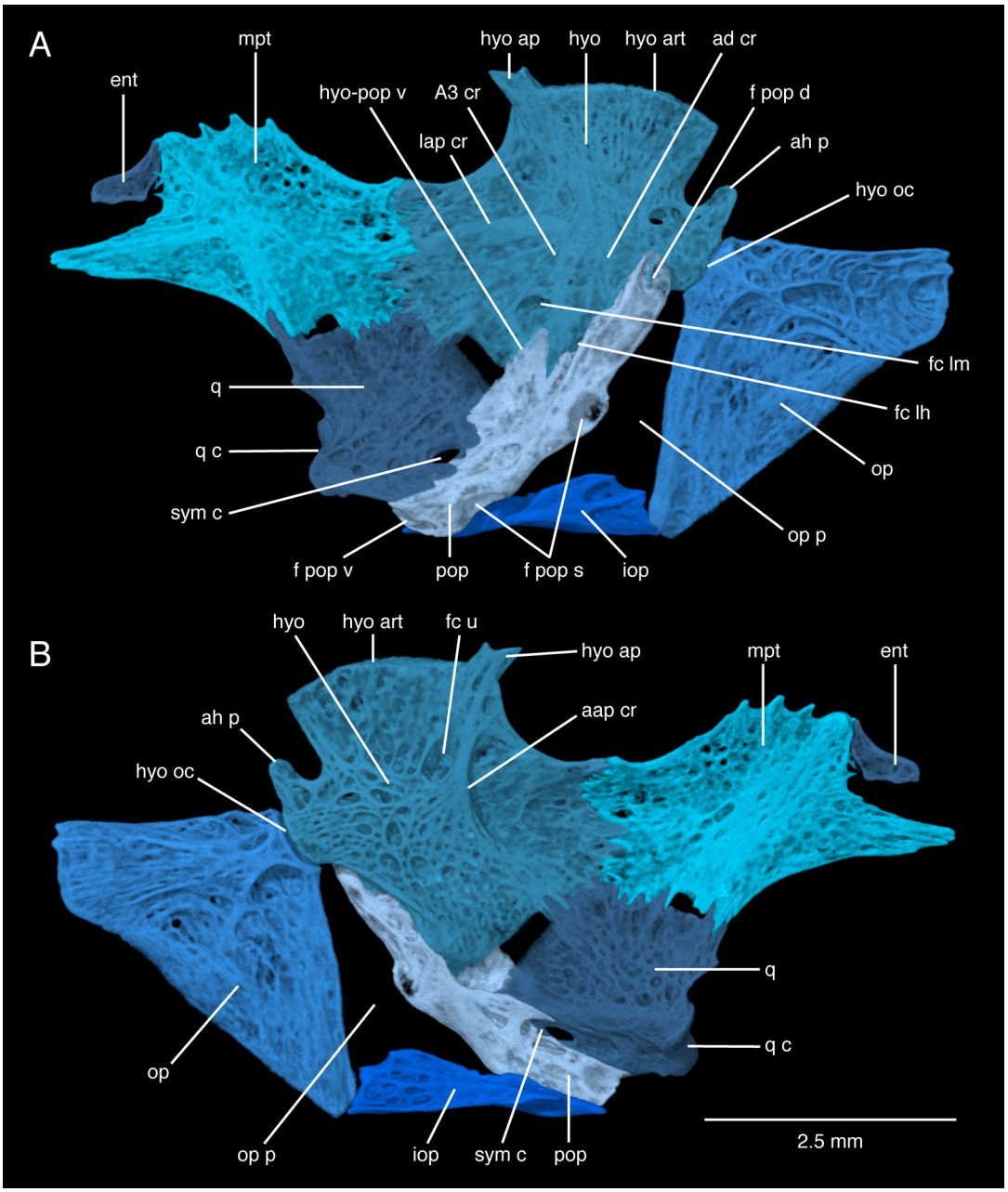

Fig. 16. *Satan eurystomus*, USNM 195930, 88.7 mm SL. 3-D HRXCT model of left-side suspensorium and opercular bones. A. Lateral, B. Medial. Abbreviations: A3 cr, deep *adductor mandibulae* (A3) crest; aap cr, *adductor arcus palatini* crest; ad cr, main adductor mandibulae crest; ah p, *adductor hyomandibularis* process; ent, endopterygoid; fc u, facial canal upper foramen; fc lh, facial canal lower foramen for hyoidean branch; fc lm, facial canal lower foramen for mandibular branch; f pop d, preopercle main sensory canal dorsal foramen; f pop s, preopercle sensory canal side-branch foramen; f pop v, preopercle main sensory canal ventral foramen; hyo ap, hyomandibular anterodorsal process; hyo art, hyomandibular articular head; hyo oc, hyomandibular-opercular condyle; hyo, hyomandibula; hyo-pop v, hyomandibula-preopercle ventral articulation; iop, interopercle; lap cr, *levator arcus palatini* crest; mpt, metapterygoid; op, opercle; op p, opercular panel; pop, preopercle; q, quadrate; q c, quadrate articular condyle; sym c, preopercle symplectic canal.

The interopercle is narrowly triangular and tapering anteriorly below the preopercle from its posterior margin that articulates loosely with the anteroventral corner of the opercle. It is shallowly elongate with its greatest depth contained about four times in its length along the straight ventral margin. The medial face of the interopercle is shallowly concave and lacks a raised crest at its moveable articulations with the head of the posterior ceratohyal and interhyal.

Figures 3 and 17 illustrate the arrangement and shapes of the bones of the long, slender hyoid bar including the interhyal, ceratohyals, hypohyals, branchiostegal rays and urohyal. The interhyal is a long, bony cylinder presumably surrounding the persistent interhyal cartilage; it is oriented vertically in USNM 195830 with its hyoid bar elevated and mouth closed. The ventral end of the interhyal is loosely and presumably attached by ligaments to the subterminal, posterolateral face of the posterior ceratohyal and adjacent dorsomedial face of the interopercle. The dorsal end of the interhyal is presumably tied by ligaments to the medial face of the preopercle and adjacent hyomandibula.

The hyoid bar is elongate, its length measured from the anterior tip of the ventral hypohyal to the posterior tip of posterior ceratohyal is about 65% of the basicranial midline length. The anterior and posterior ceratohyals are shallow and compressed with rounded and unkeeled dorsal edges and gently concave medial faces near their joint. The anterior ceratohyal-posterior ceratohyal joint is dorsally bony and deeply interdigitating, whereas ventrally the joint is widely synchondral but lacking cartilaginous extension along their adjacent ventral margins.

The dorsal hypohyal is a small, three-cornered, cap-shaped bone synchondrally joined to the much larger ventral hypohyal and anterior ceratohyal. The ventral hypohyal is roughly five times the size of the dorsal hypohyal and has synchondral joints with the dorsal hypohyal and anterior ceratohyal, and ligamentous articulations with the urohyal and contralateral ventral hypohyal.

The horizontal lamina of the urohyal is broadly trapezoidal in form; its prominent posterolateral wings are swept-back and pointed. Anteriorly the urohyal terminates bluntly and without paired ventral facets behind the rounded tips of the ventral hypohyals. Anterodorsally, between the hypohyals, the vertical lamina of the urohyal has a median cup-shaped facet that is posteriorly continuous with its narrow, flat-topped crest. Posteriorly the vertical lamina extends as a thin plate beyond the horizontal lamina to reach the level of the posterior end of the overlying second basibranchial bone.

The branchiostegal rays number 11 on each side, the anteriormost pair are floating in soft tissue medial to the anterior ceratohyal, eight articulate with the anterior ceratohyal, and two with the posterior ceratohyal and none entirely on the cartilage between these bones. All the articulations are loose and moveable. The medial-most two branchiostegal rays are the smallest and curve slightly medially, the third rays are nearly straight, and the remaining rays are increasingly curved posteriorly. Figure 3C shows that the paired anteriormost five six rays broadly overlap on the ventral midline in this specimen with its mouth closed and orobranchial cavity unexpanded. Branchiostegal rays 8-11 are the longest and most robust; the last two rays lie medially under the interopercle and ventral end of the opercle and they reach the vertical limb of the cleithrum.

Figure 18 illustrates the arrangement and shapes of the bones comprising the branchial arches including the basi-, hypo-, cerato-, epi-, and pharyngo-branchials, gill rakers and pharyngeal tooth plates. Branchial cartilages are not visible but their extent between adjacent bones can be estimated by radiotransparent space.

Two simple rod-shaped basibranchial bones are present, identified here as the second and third basibranchials, neither of which has direct bony contact with other elements; their joints with the cartilaginous branchial elements are presumed synchondral as in other ictalurids and most catfishes. The second basibranchial lies dorsal to the vertical lamina of the urohyal and medial to first and second hypohyals; it is twice or more the volume of the third basibranchial. The third basibranchial lies medial to anterior end of the second ceratobranchial and anterior to the third ceratobranchial.

The first two pairs of hypobranchials are ossified. These vary from quadrangular to roughly triangular. The first hypobranchial is situated dorsal to the posterior wings of the urohyal and directly posterior to the hypohyals. The second hypobranchial lies above the anterior end of the second ceratobranchial and in line with first hypobranchial and ceratobranchial.

The five, paired ceratobranchials are well ossified. The anterior four ceratobranchials have a slender, elongated and ventrally concave form typical of most catfishes; the last or fifth ceratobranchials, carrying the ventral pharyngeal tooth patches, are paddle shaped, slightly concave dorsally and broadest at mid-length. The first ceratobranchial is the longest, about half the length of the ventral basicranial length and the following ceratobranchials are shorter, the fourth ceratobranchial is about one third of the ventral basicranial length. Long, well-ossified gill rakers are present on all ceratobranchials with the first, second, and fifth having rakers developed on their anterior margins only, whereas the third and fourth have gill rakers on both anterior and posterior margins. The left and right side counts of ceratobranchial gill rakers are:

First ceratobranchial: 12-13 anterior rakers;
Second ceratobranchial: 12-14 anterior rakers;
Third ceratobranchial: 15-15 anterior, 14-16 posterior rakers;
Fourth ceratobranchial: 15-16 anterior, 15-15 posterior rakers;
Fifth ceratobranchial: 13-13 anterior rakers.

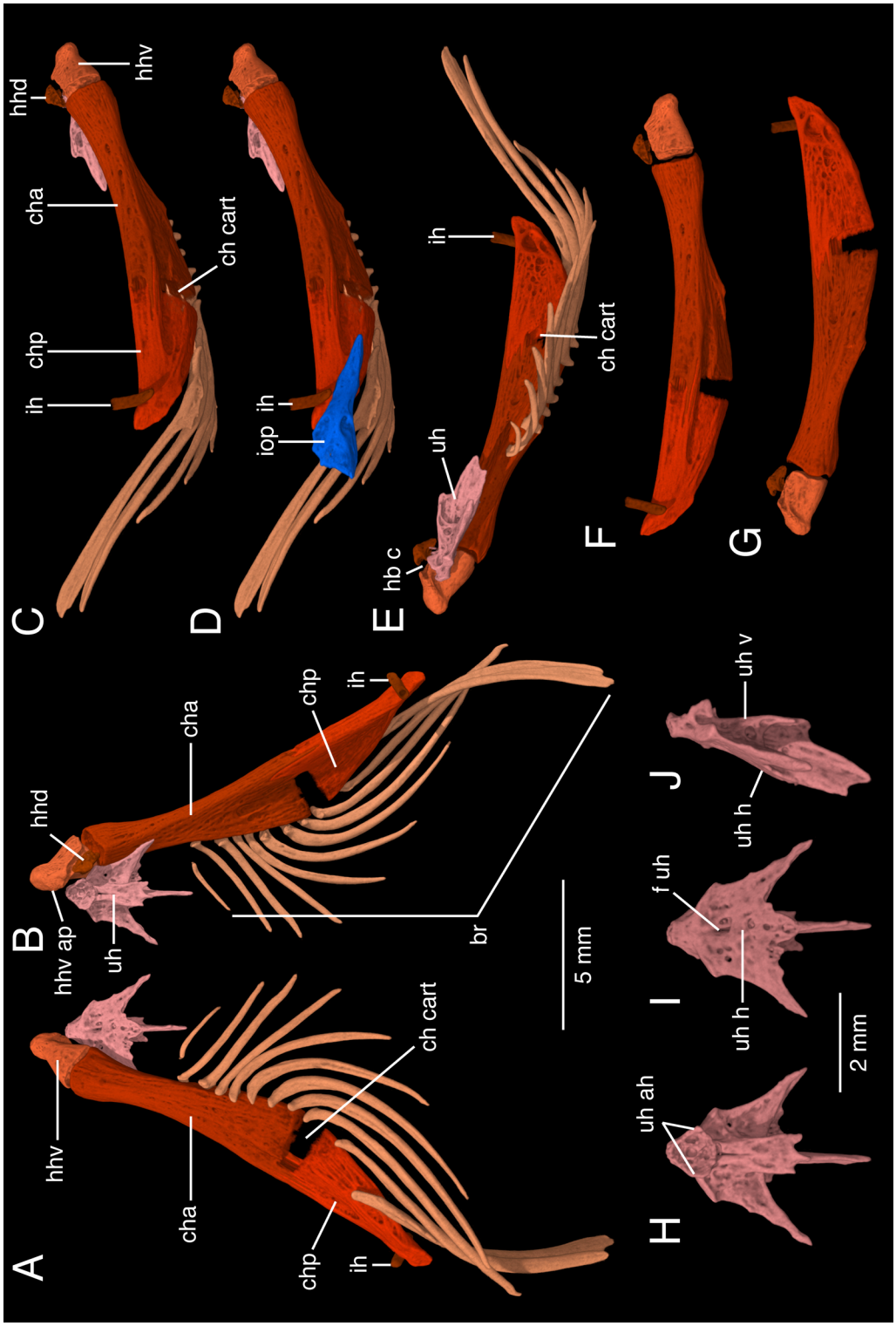

Fig. 17. *Satan eurystomus*, USNM 195930, 88.7 mm SL. 3-D HRXCT model of right-side lower bones of the hyoid arch. A. Ventral, B. Dorsal, C. Lateral, D. Lateral with interopercle included, E. Medial, F. Lateral without branchiostegal rays and urohyal, G. Medial without branchiostegal rays and urohyal. H-J Urohyal, H. Dorsal, I. Ventral, J. Lateral, left side. Abbreviations: br, branchiostegal rays; ch cart, ceratohyal cartilage; cha, anterior ceratohyal; chp, posterior ceratohyal; f uh, urohyal foramen; hb c, hypobranchial artery canal; hhd, dorsal hypohyal; hhv, ventral hypohyal; hhv ap, articular processes of ventral hypohyals; ih, interhyal; iop, interopercle; uh, urohyal; uh ah, urohyal articular head; uh h, urohyal horizontal lamina; uh v, urohyal vertical lamina.

The lower pharyngeal tooth patch (Fig. 18E) on fifth ceratobranchial has sparse and exceptionally weak teeth that are much smaller than the teeth on the upper pharyngeal tooth plate (Fig. 18D) and oral jaws.

The four paired epibranchial bones are well ossified and have the typical form found in most catfishes. The medial tips of the first and second epibranchials are close together above the third ceratobranchial. The first epibranchial bends posteriorly at its first third along its mediolateral length. It has an anterior crest at the bend and five gill rakers on its anterolateral margin, the lateralmost at its joint with first ceratobranchial. The second epibranchial similarly bends posteriorly and has a low anterior crest at the bend, and five gill rakers on the lateral half of its anterior margin. The medial tip of the third epibranchial is above the upper pharyngeal tooth plate and part of a three-way synchondral joint with the two pharyngobranchials. The third epibranchial has a large, flattened, hook-shaped and medially directed uncinate process off the posterior margin near its ceratobranchial joint. The third epibranchial has five anterior gill rakers. The medial tip of the fourth epibranchial is above the posterior margin of the upper pharyngeal tooth plate. The fourth epibranchial lacks an uncinate process but its posterior margin projects convexly backward. The fourth epibranchial has two gill rakers laterally on its anterior margin.

The two posterior pharyngobranchials, identified here as the third and fourth are ossified. The third pharyngobranchial is a short rod projecting anteriorly off the third epibranchial and fourth pharyngobranchial. The fourth pharyngobranchial is a small bony block situated over the upper pharyngeal tooth plate posterior to the third pharyngobranchial and between the tips of the third and fourth epibranchials.

The ovoid upper pharyngeal tooth plate (Fig. 18D) bears a cluster of large teeth that face the posterior end of the lower pharyngeal tooth plate.

Vertebral column.—The radiographs of five well ossified specimens of *Satan* show a range of 41-43 total vertebrae including the modified vertebrae of the Weberian apparatus and the PU1+U1 vertebra in the caudal skeleton. Precaudal and caudal vertebral counts determined from two lateral view radiographs are: UMMZ 190922 - 19 and 23, USNM 195830 - 18 (1 added to account for first centrum fusion with the basioccipital) and 25.

In Ictaluridae, the Weberian apparatus (Fig. 2, 3, 19, 20) normally includes parts of the anterior five vertebrae: unfused first, Weberian compound vertebra (fused second, third and fourth), and unfused fifth. This is the condition in *Satan* documented by TCWC 8279.01 (Fig. 20) and three other X-rayed specimens. As noted, however, the first centrum of USNM 195830 is fused with the basioccipital (Fig. 2, 3, 11, 13, 19) and has lost its anterior concave joint surface. In both scanned specimens, the first vertebra is represented by its centrum and separate neural arch modified as the second Weberian ossicle or scaphium. The first vertebra lacks parapophyses, zygapophyses and the neural spine. The scaphium has its normal position dorsally on the first centrum in the wall of the *sinus impar* and neural canal. This element has the typical ovoid plate or concha anterior to a short, vertical ascending process. The scaphium is the only Weberian ossicle that we find in *Satan*; the tripus and os suspensorium, intercalarium and claustrum are apparently absent.

In both TCWC 8279.01 and USNM 195830, the three centra of the Weberian compound vertebra are fused, and the anterior face of the compound centrum has a normal, sub-circular and concave intervertebral joint surface at its articulation with the first centrum. In TCWC 8279.01, the posterior end of the compound centrum is also a normal intervertebral joint surface articulated with the anterior face of the fifth vertebra. The fifth vertebra of TCWC 8279.01 is normally proportioned anteriorly and posteriorly, forming standard amphicoelous intervertebral joints with the compound and sixth centra. In this specimen, the ventral side of the compound centrum is a shallow, open aortic groove that continues a short distance onto the fifth centrum. The sidewalls of the aortic groove are low. In TCWC 8279.01 the compound centrum is 1.7 times longer than the fifth centrum, and together the compound plus fifth centra are 2.8 times longer than the sixth centrum.

In contrast, USNM 195830 (Fig. 19) has the compound and fifth centra closely articulated and shortened. The posterior end of the compound centrum is highly modified as a deeply interlocking bony joint with a distorted anterior end of the fifth centrum. The fifth vertebra is severely diminished in size anteriorly and is inserted into and surrounded by the posterior end of the compound centrum. We interpret this as another malformed intervertebral joint, unlike the simple joint as in TCWC 8279.01 (Fig. 20), or the deeply interdigitating compound centrum-fifth centrum joint characteristic of epigean ictalurids. The combined length of the compound and fifth centra in USNM 195830 is shortened, only 1.7 times longer than the sixth centrum. Also, in USNM 195830 the ventral side of the compound centrum has a scarcely developed shallow, open aortic groove that continues onto the fifth centrum

As in all other ictalurids, *Satan* has enlarged paired transverse processes on the Weberian compound vertebra; these are the parapophyses of the fourth vertebra. These processes are similarly shaped in both scanned specimens but in USNM 195830 they are distally narrower,

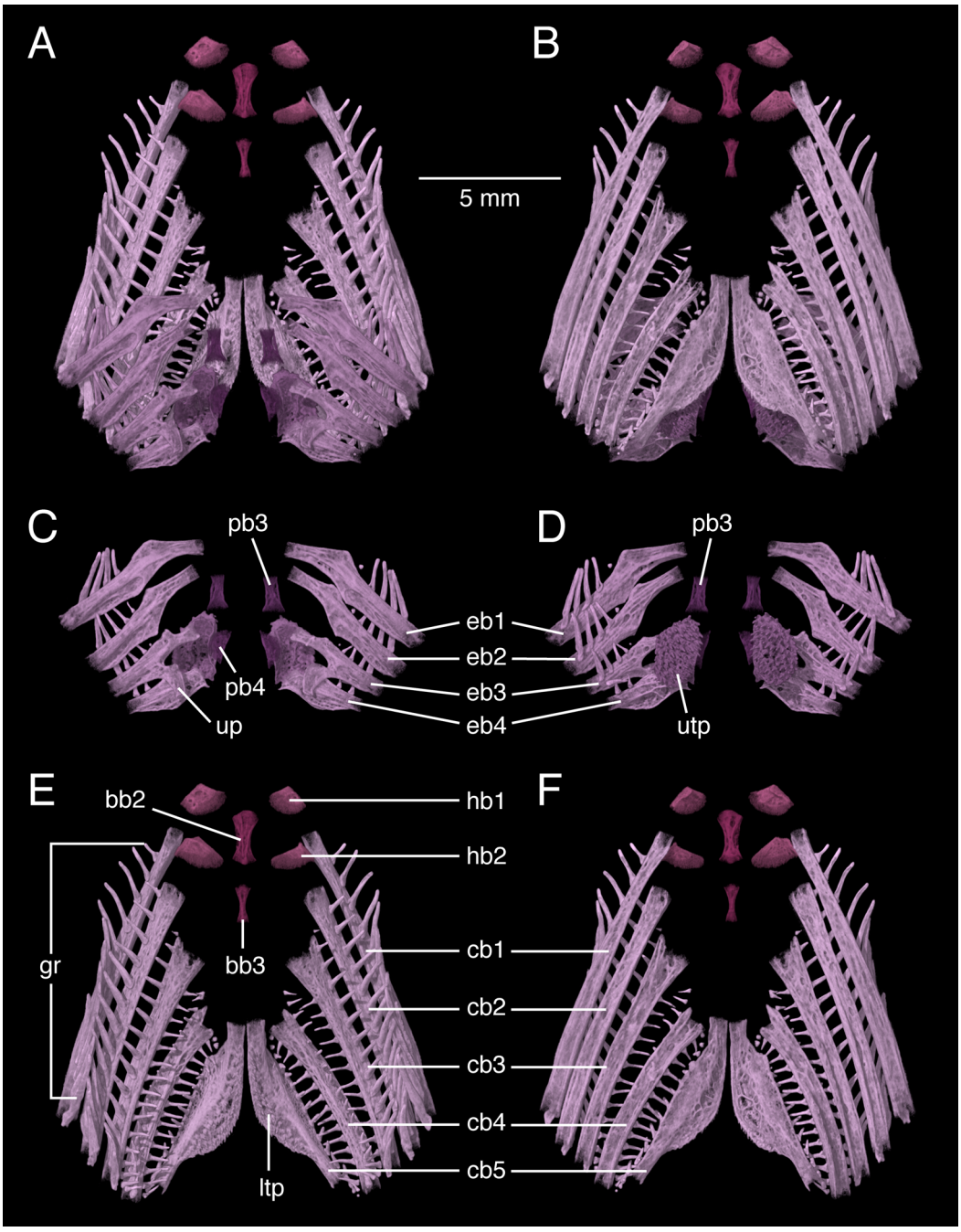

Fig. 18. *Satan eurystomus*, USNM 195930, 88.7 mm SL. 3-D HRXCT model of branchial arch skeleton, A-B. Entire branchial bony skeleton, A. Dorsal, B. Ventral; C-D. Upper branchial elements, C. Dorsal, D. Ventral; E-F. Lower branchial elements, E. Dorsal, F. Ventral. Abbreviations: bb2-bb3, basibranchials 2, 3; cb1-cb5, ceratobranchials 1, 2, 3, 4, 5; eb1-eb4, epibranchials 1, 2, 3, 4; gr, gill rakers; hb1-hb2, hypobranchials 1, 2; ltp, lower pharyngeal tooth plate; pb3-pb4, pharyngobranchials 3, 4; up, uncinate process; utp, upper pharyngeal tooth plate.

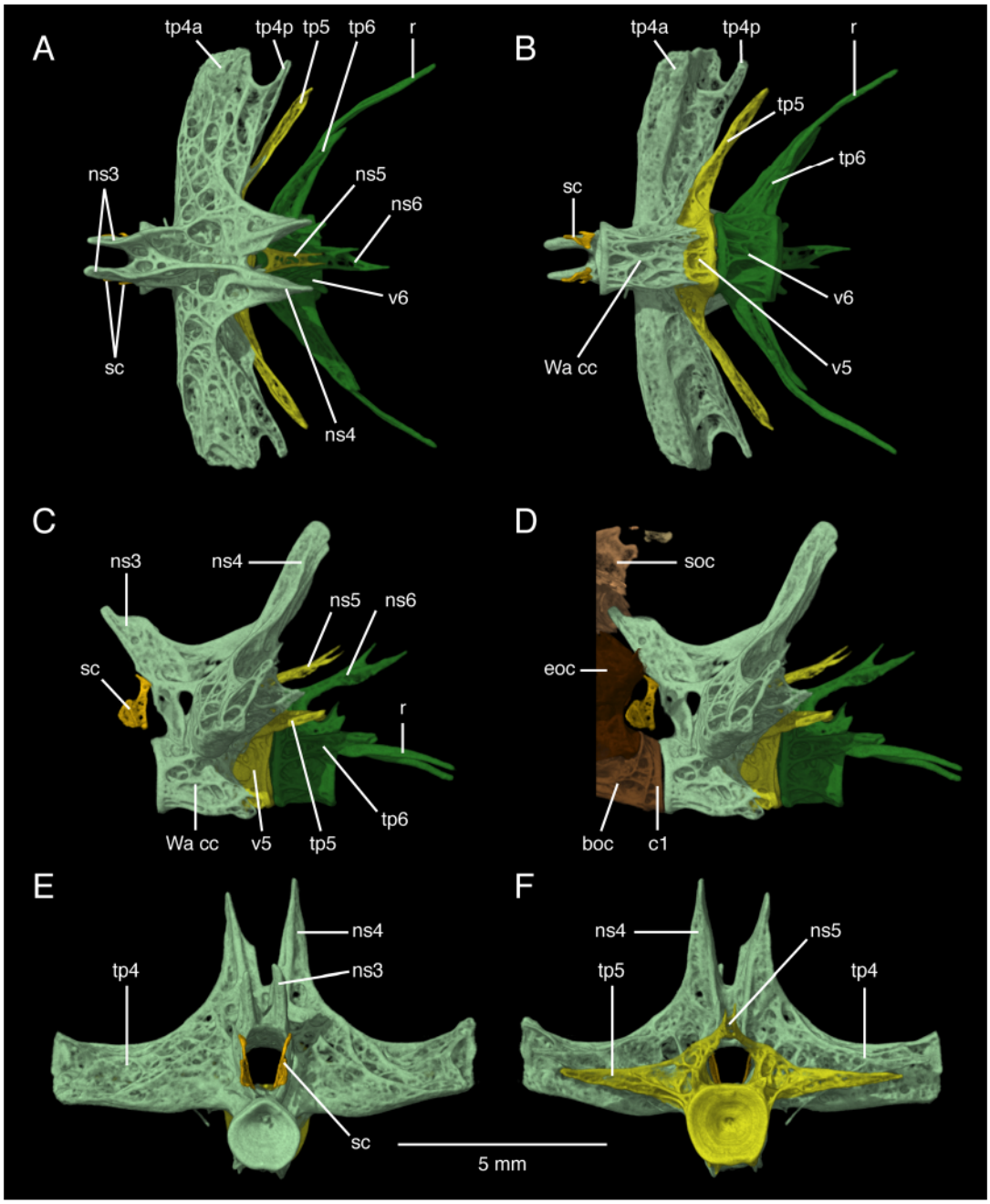

Fig. 19. *Satan eurystomus*, USNM 195930, 88.7 mm SL. 3-D HRXCT model of anterior vertebrae including Weberian apparatus, vertebra 6 and occipital bones. A. Dorsal, B. Ventral, C. Left-side lateral, D. Left-side lateral with occipital bones, E. Anterior of Weberian compound vertebra, F. Posterior of Weberian compound vertebra and vertebra 6. Abbreviations: boc, basioccipital; c1, first centrum; eoc, exoccipital; ns3-ns6, neural spines 3, 4, 5, 6; r, rib; sc, scaphium ossicle; soc, supraoccipital; tp5-tp6, transverse processes of vertebrae 5, 6; v5-v6, vertebrae 5, 6; Wa cc, Weberian compound vertebra; tp4a, Weberian apparatus anterior limb of fourth transverse process, tp4p, Weberian apparatus posterior limb of fourth transverse processes.

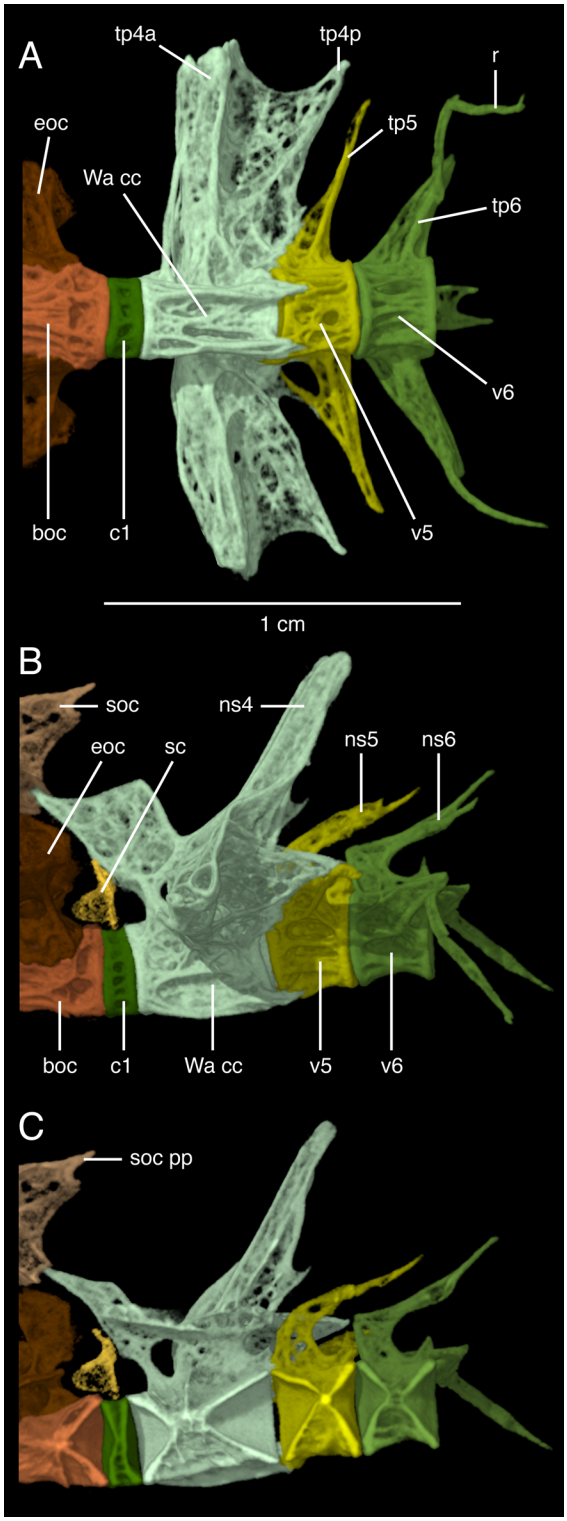

corresponding to the shorter compound vertebra, versus much more widely expanded in TCWC 8279.01. In both specimens, the fourth transverse processes reach the cleithrum and posttemporo-supracleithrum, and nearly reach the skin posterior to the pectoral girdle. The fourth parapophyses are also divided into a robust anterior limb and narrower posterior limb. These limbs are divided distally by a concave marginal notch that is incised to about 22% of the length of the anterior limb in the TCWC specimen, and about 18% in the USNM specimen. The distally thickened end of the anterior limb makes the joint with the vertebral process of the posttemporo-supracleithrum. The posterior limbs taper distally and are directed a little posterolaterally without peripheral bony contacts. Dorsally between the anterior and posterior limbs a curved ridge on the fourth parapophysis rises and is continuous with the lateral ridges that ascend the much enlarged fourth neural spine.

In both scanned specimens, the Weberian apparatus has an enlarged compound neural arch and spine structure that is formed from the third and fourth neural arches and spines. The neural spine of the third arch is directed anterodorsally behind the skull to about half the height of the occiput and its neural spine is bifid distally to receive the vertical lamina of the supraoccipital's posterior process. In USNM 195830 a broken terminal fragment of that supraoccipital process is suspended in the median septum (Figs. 3A, 20D). This fragment resembles in its position a third supraneural ("neural complex") but that element is absent in this species. The fourth neural arch and spine are tall and directed posterodorsally toward the dorsal fin. The fourth neural spine is also distally divided. Its thickened limbs run alongside the enlarged first and second dorsal-fin pterygiophores that form and support the articulation platform for the two dorsal-fin spines. Between the third and fourth neural spines the dorsal midline of the compound Weberian vertebra has an elevated, thin vertical lamina with a concave profile in lateral vie .

The anterior margins of the fifth neural arch and parapophysis are little expanded and are applied closely to the corresponding but larger fourth neural arch and fourth

Fig. 20. (left) *Satan eurystomus*, TCWC 8279.01, 180 mm SL. 3-D HRXCT model of anterior vertebrae including Weberian apparatus, vertebra 6 and occipital bones. A. Ventral, B. Left-side lateral, C. Medial view of right-side from near sagittal plane. Abbreviations: boc, basioccipital; c1, first centrum; eoc, exoccipital; ns4-ns6, neural spines 4, 5, 6; sc, scaphium ossicle; soc, supraoccipital; soc pp, supraoccipital posterior process; tp5-tp6, transverse processes of vertebrae 5, 6; v5-v6, vertebra 5, 6; Wa cc, Weberian compound centrum; tp4a, Weberian apparatus anterior limb of fourth transverse processes; tp4p, Weberian apparatus posterior limb of fourth transverse processes.

parapophysis. The fifth neural spine is much shorter than the fourth and is subequal in length and orientation to the sixth neural spine. The fifth and sixth neural spines are ventral and separate from the overlying proximal dorsal-fin radials. The thin fifth parapophysis diverges posteriorly from the expanded parapophysis of the fourth and runs parallel with the sixth parapophysis. The fifth vertebra also has a pair of short posterior zygapophyses that articulate with small anterior zygapophyses on the base of the neural arch of the sixth vertebra. There is no free rib on the fifth parapophysis. Ventrally the fifth centrum has no superficial ossificatio and very low crests flanking the midventral aortic groove

The Weberian apparatus of *Satan* has no detectable development of so-called superficial ossification (Bridge and Haddon, 1892; Chardon et al., 2003) that in epigean ictalurids and other catfishes covers the sides and venter of the compound and fifth centra and to which the swim bladder is closely applied. There is no thickened swim bladder wall in *Satan*, the space normally occupied by a swim bladder is filled with loosely organized adipose and connective tissue (Langecker and Longley, 1993; pers. obs.).

Post-Weberian vertebral structure of *Satan* is generally similar to that of the majority of siluriforms: amphicoelous centra, precaudal vertebrae with serially shortening parapophyses, ribs articulated with the ventral sides of the parapophyses of vertebrae six to about 12, anterior zygapophyses on the bases of their neural arches and paired posterior zygapophyses on the postero-dorsolateral corners of their centrua, short neural arches and spines below and just posterior to the dorsal-fin pterygiophores; and caudal vertebrae with fully developed hemal spines commencing at about vertebra 18.

The following description of the caudal skeleton of *Satan* is based on two lateral-view radiographs of the holotype UMMZ 190922 and USNM 195830 (Fig. 2), and the CT scan of TCWC 8279.01 (Fig. 21). The caudal-fin is weakly emarginate in form and supported by 17–18 principal caudal-fin rays plus 15-17 upper-procurrent and 13-14 lower-procurrent fin rays that extend anteriorly to the level of the fifth preural centrum. Lundberg and Baskin (1969), using a radiograph of the holotype, interpreted the hypural fusion pattern of *Satan* as PH; 1+2; 3+4+5+6 (i.e. parhypural separate from two fused lower hypurals, and four fused upper hypurals). In contrast, our images of both USNM 195830 and TCWC 8279.01 show that the hypural fan includes a separate parhypural, lower hypurals 1 and 2 that are at least partly separate and together more than twice as large as the parhypural. There is a distinct horizontal gap between the lower and upper hypurals, and the upper hypurals 3, 4, 5 and 6 are at least partly distinguishable by narrow gaps and thickened ridges that may be lines of fusion or abutting joints. Hypurals 3 and 4 together are much larger than hypural 5 and an uppermost, much smaller and separate hypural 6. The relative sizes of these hypural elements is similar those of other ictalurids with unconsolidated hypurals (e.g. Lundberg and Baskin, 1969, figs. 1, 2A, pp. 9, 10)

The caudal margin of the hypural fan is smoothly and rounded. The hypurapophysis on the hemal arch of PU1 is small and separate from a small secondary hypurapophysis on the base of hypural 1 posterodorsal to the caudal artery foramen. There is no autogenous U2 centrum. In addition, there is a single broad epural that lacks bony contact with adjacent bones; the uroneural is strongly developed, sharp-tipped, and distally separate from the adjacent upper hypural. The neural spine of the compound caudal centrum does not reach more than half the height of adjacent PU2 neural spine. The neural spines of PU2-4 or 5 are slightly thickened and with truncated tips. The hemal spines of PU2-3 are expanded and nearly as broad as the parhypural, whereas the hemal spines of PU4-5 are slightly broadened and with truncated tips.

Dorsal fin and skeleton.—In *Satan* the dorsal fin (Fig. 2, 3, 22, 23) is supported by two fin spines and seven or eight branched soft rays. The dorsal fin is internally supported by the fourth supraneural and seven to eight pterygiophores.

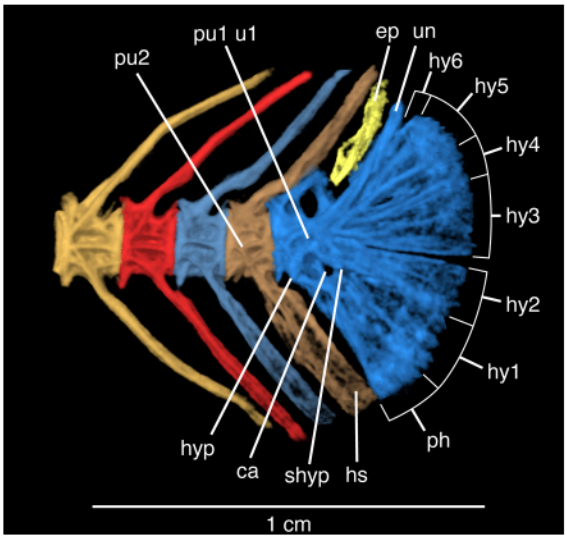

Fig. 21. *Satan eurystomus*, TCWC 8279.01, 180 mm SL. 3-D HRXCT model of caudal-fin skeleton and adjacent preural vertebrae in left-side lateral view. Segmented arc lines behind hypural fan estimate the distal limits of the parhypural and six hypurals. Abbreviations: ca, caudal artery and vein foramen; ep, epural; hs, haemal spine; hy1-hy6, hypurals 1, 2, 3, 4, 5, 6; hyp, hypurapophysis; ph, parhypural; pu1 u1, preural centrum 1 + ural centrum 1; pu2, preural centrum 2; shyp, secondary hypurapophysis; un, uroneural.

The first dorsal-fin spine is the short so-called spinelet that is present in most catfishes and involved in the dorsal-fin spine locking apparatus. The spinelet has the typical anatomical relationships with the fourth supraneural, fused proximal and middle radials of the first pterygiophore, long second dorsal-fin spine, and middle nuchal plate. In *Satan*, the spinelet has a unique shape (Fig. 23F-H): unusually wide and squat, with a distinctive dorso-median peak above broad, anteroventrally sloping limbs with sinusoidally-curved lateral margins, and strongly recurved ventrally with blunt tips.

The second dorsal-fin spine is the large defensive spine that moveably articulates with the nuchal plate on the second proximal radial. The spherical distal radial of the firs pterygiophore is ossified and fused medially to the spine base between the laterally expanded and rounded basal articular condyles. A basal foramen is present between the spine shaft, the median radial and the articular condyles. In *Satan*, lateral to the basal foramen, a pair of long posterior processes project prominently off the base of the spine. This spine is nearly straight and rounded in cross-section. The shaft has unornamented anterior and posterior margins without serrae or dentations. The first and tallest dorsal-fin soft ray is about 1.5 times longer than the adjacent dorsal-fin spine. The following six soft dorsal-fin rays are progressively shorter; the separate bases of the last two soft rays articulate together on the last pterygiophore.

At the base of the dorsal-fin insertion, the fourth supraneural is relatively small and remote from the posterior process of the supraoccipital. The supraneural

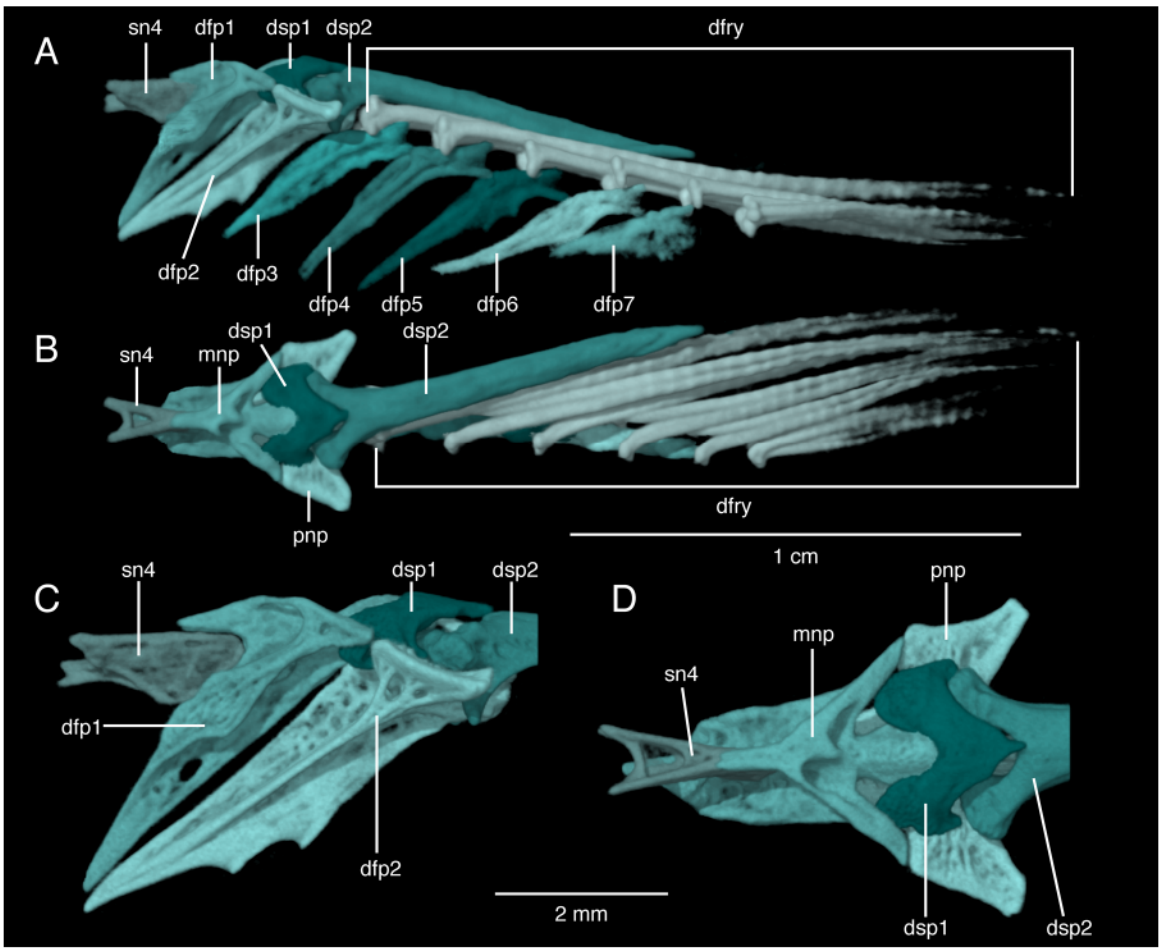

Fig. 22. *Satan eurystomus*, USNM 195930, 88.7 SL. 3-D HRXCT model of entire dorsal-fin and skeleton. A. Left-side lateral, B. Dorsal. C-D. Dorsal-spine bases and supporting skeleton. C. Left-side lateral, D. Anterodorsal. Abbreviations: dfp1-dfp7, dorsal-fin pterygiophores 1, 2, 3, 4, 5, 6, 7; dfry, branched dorsal-fin rays; dsp1, dorsal-fin spine 1 (spinelet); dsp2, dorsal-fin spine 2; ds, dorsal-fin spinelet; mnp, middle nuchal plate; pnp, posterior nuchal plate; sn4, supraneural 4.

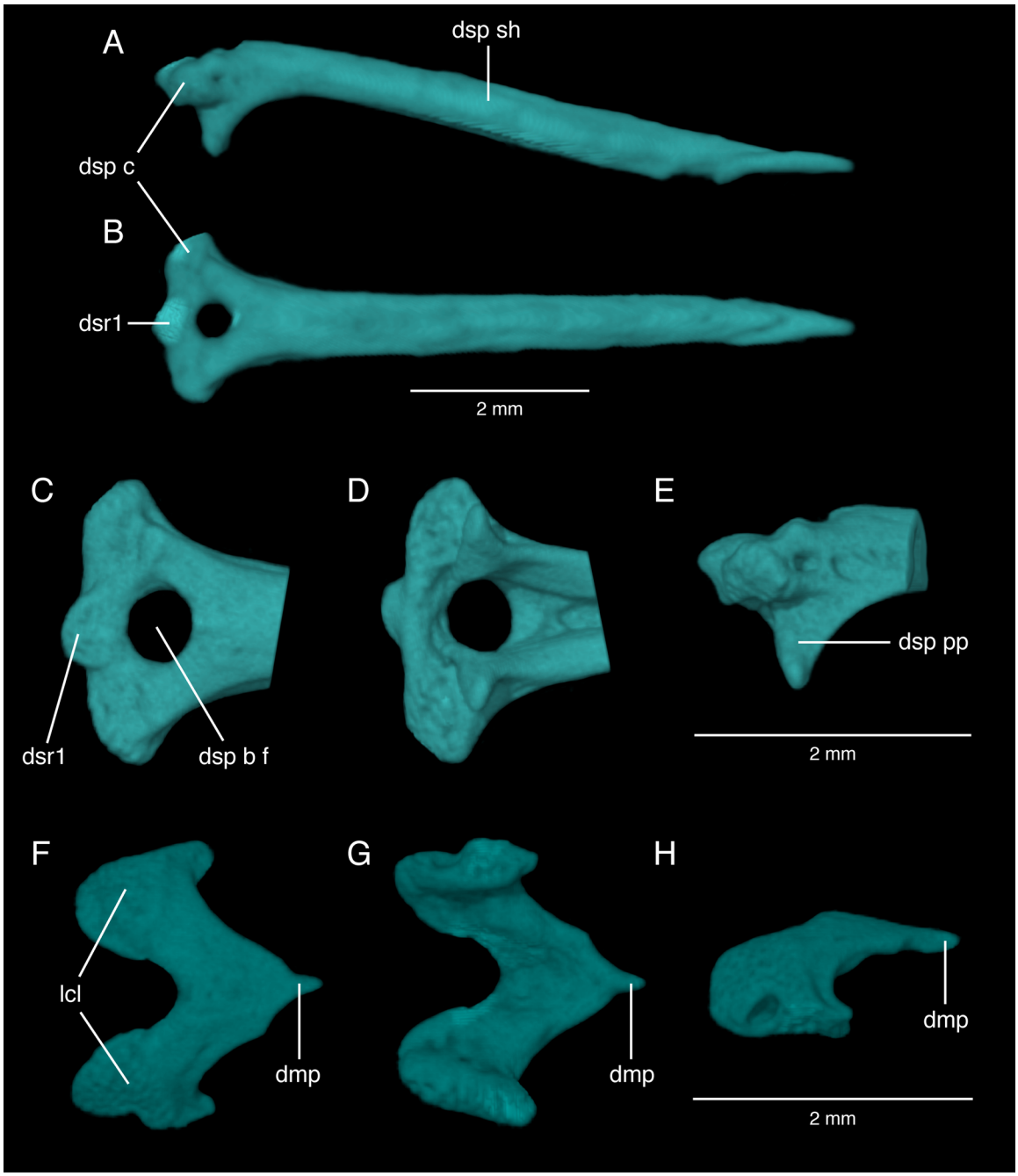

Fig. 23. *Satan eurystomus*, USNM 195930, 88.7 SL. 3-D HRXCT model of dorsal-fin spines. A-E. Second dorsal-fin spine. A. Left-side lateral, B. Anterior, C-E. Second dorsal-fin spine base. C. Anterior, D. Posterior, E. Lateral. F-H. First dorsal-fin spine (spinelet). F. Anterior, G. Posterior, H. Lateral. Abbreviations: dsp c, dorsal-spine 2 condyle; dsr1, dorsal spine 2 distal radial 1; dsp b f, dorsal spine 2 basal foramen; lcl, dorsal spine 1 (spinelet) lateral curved limb; dmp, dorsal spine 1 (spinelet) medial peak; dsp pp, dorsal spine 2 posterior process.

has an anteriorly bifid vertical plate that is only slightly expanded dorsally and it lacks a superficial nuchal plate in the skin. This supraneural articulates only with the distal third of the enlarged first proximal radial and ventral to the slightly expanded middle nuchal plate.

The first dorsal-fin pterygiophore is long and has prominent lateral ridges that are braced by the split neural spine of the fourth vertebra. The first proximal and middle radials are fused and distally expanded in the skin as the middle nuchal plate. This plate is pierced dorsally by a pair of foramina for the passage of arrector-muscle tendons that insert on the limbs of the spinelet. The middle nuchal plate also sends a median, beak-like process anteriorly over the fourth supraneural. Posteriorly the middle nuchal plate divides into paired horizontal limbs that articulate with the posterior nuchal plate on the second radial. The middle radial of the first pterygiophore is an enlarged, median peg-like process that sits behind the ventral limbs of the spinelet and sends its slender, curved distal end through the foramen in the spine base to contact a matching anteriorly-directed process off the second middle radial. These two midline processes of the first and second middle radials unite to form a bony ring through the median foramen in the base of the second dorsal-fin spine.

The second proximal radial is long, articulated to the first along the midline, and has prominent lateral struts that dorsally support its wing-like posterior nuchal plate, the articular facets for the second fin spine base, and the ring-forming median process of the middle radial.

Anal fin and skeleton.—The anal fin (Figs. 1, 2) is supported by 19-21 rays of which about six anterior rays are simple. The anal-fin pterygiophore counts are one or two less than the number of fin rays. The anal-fin proximal radials overlap and are not tightly joined to their adjacent hemal spines from about vertebra 18-30.

Pectoral fin and skeleton.—The pectoral fin (Figs. 2, 3, 24, 25) is supported by its leading fin spine plus 10-11 soft fin rays. There are two separate, ossified pectoral-fin radials. Cartilaginous pectoral radials are radiotransparent. The firs (lateralmost) pectoral-fin radial is the shorter and closest to the outer three soft-rays; the medial radial is closest to the inner soft-rays. Both radials are dorsoventrally flattened and club-shaped, gently curved posteriorly (laterally concave) and distally expanded near their moveable synchondral joints with the soft fin-rays. The pectoral-radial proximal joints with the scapulocoracoid are moveable and synchondral. The pectoral-fin rays gradually diminish in length along their scarcely convex fin margin from the longest and most lateral ray to the short medial ray that is one-third of the length of the longest ray.

The pectoral-fin spine (Fig. 25) is well ossified and has a typical base with three well-developed articular processes involved in the locking joint with the cleithrum and scapulocoracoid (Fine et al., 1997; Vanscoy et al., 2015). The flange-like and rounded dorsal process inserts into a matching deep articular groove on the medial face of the cleithrum. The beak-like anterior process of the spine base articulates with the dorsal surface of the abductor bridge of the scapulocoracoid anterior and ventral to the cleithral articular groove. The ventral process is club-shaped, distally rounded in outline and flattened below its articulation with the ventral surface of the abductor bridge of the scapulocoracoid.

The pectoral-spine shaft is stout, nearly straight along its middle and distal span, sharp-tipped with one developing distal unfused fin-spine segment on both the left and right spines. There are no distal serrae on the anterior side of the shaft, but a shallow anterodistal concavity proximal to the tip marks the limit of the latest fused fin-spine segment. Along the generally smooth anterior margin of the spine, the midline ridge and flanking grooves are scarcely developed and there are no anterior dentations. On its dorsal surface the spine shaft has a narrow sulcus that subtends the posterior dentations. There are five and seven posterior dentations along the middle third of the posterior margin of the shaft. The dentations are of moderate height, about half of the shaft width, and unicuspid, sharp to acutely rounded, and erect to antrorse. Most posterior dentation bases arise from dorsal half (hemitrichium) of the spine shaft.

Figures 3 and 24 illustrate the arrangement and shapes of the three bones comprising the pectoral girdle including the cleithrum, compound scapulocoracoid plus mesocoracoid and posttemporo-supracleithrum.

The dermal cleithrum has robust vertical and horizontal limbs that meet ventrolaterally along a 90° bend at the girdle's shoulder. The pectoral-fin spine articulates with the pectoral girdle on the medial face of the shoulder. In this joint the cleithrum provides the deep, curved articular groove that receives the dorsal process of the fin-spine base. The horizontal limbs of the cleithrum expand medially to meet on the midline in a broad, loosely abutting symphysis. Commencing at the shoulder, the anterior margin of the horizontal limb is downturned to form the anterior wall of a ventral side fossa occupied by spine-arrector (abductor) muscles. The muscle fossa and wall smoothly diminish medially and disappear before the midline symphysis. Near the symphysis this imparts a distinctive truncation to the anterior profile of the cleithral ma gin.

At the base of its vertical limb, and posterior to the shoulder and fin-spine joint, the cleithrum has a robust, triangular and sharply-tipped posterior (humeral) process

that extends to about the midpoint of the depressed pectoral-spine shaft. The exposed lateral surface of the cleithral posterior process is ornamented with horizontally-trending, subparallel ridges and grooves, but is without dermal tubercles or coarse rugosities. The vertical limb of the cleithrum is forked and articulates with the posttemporo-supracleithrum.

The scapula, scapulocoracoid and mesocoracoid arch are completely fused to form a scapulocoracoid complex that is tightly bound to the posterior, medial and ventral surfaces of the cleithrum. At the shoulder, medial to the cleithral articular groove for the fin spine, the scapulocoracoid carries the joint surfaces for the ventral and anterior articular processes of the fin spine, and pectoral-fin bony radials that, in turn, articulate with cartilaginous fin radials and the fin rays. A scapular foramen is present in the scapulocoracoid wall above these joints and the lower end of the mesocoracoid arch attaches to the scapulocoracoid below the scapular foramen. Also at the shoulder, but anterior to the cleithral articular groove, a stout abductor bridge of bone extends from the scapulocoracoid to the downturned anterior margin of the cleithrum. The scapulocoracoid and mesocoracoid arch extend dorsally on the medial face of the dorsal limb of the cleithrum.

Medial to the scapulocoracoid-pectoral radial joints, the contralateral horizontal limbs of the scapulocoracoids broaden greatly and meet in their symphysis with five to six coarsely interlocking sutural processes. The dorsal surfaces of the expanded horizontal limbs of the scapulocoracoids form the floor of a large triangular extensor fossa, which is a major site of origin of the *arrector dorsalis and abductor superficialis* muscles that insert on the pectoral-fin spine and rays respectively. The anterior edge of the extensor fossa is limited by a low crest along the posterior edge of the cleithrum. Laterally, the cleithrum with this crest turn posterodorsally to form a roof over the scapulocoracoid extensor fossa and become the anterior face of the dorsal limb of the cleithrum.

Immediately ventral to the joint surfaces for the pectoral spine and fin rays the scapulocoracoid has a sharply elevated and transversely oriented keel that extends medially along its border with the cleithrum. The scapulocoracoid keel is short, terminating less than one fourth of the distance to the scapulocoracoid symphysis. There is no development of a secondary keel on the rear edge of the scapulocoracoid just below the scapular foramen.

The posttemporo-supracleithrum (Figs. 3, 4, 10-12, 24) is well developed and has the characteristic 4-pronged shape and articulations with the cleithrum, the occipito-temporal region of the skull, the basicranial wall of the occiput, and the Weberian apparatus. First, the ventrolateral cleithral process of posttemporo-supracleithrum (Fig. 24C) reaches ventroposteriorly along the lateral side of the vertical limb of the cleithrum. Second, the pterotic or dorsal process of the posttemporo-supracleithrum extends dorsally to its ligamentous contact with the epioccipital and barely touches the supraoccipital, but in *Satan* this process passes well posterior to the pterotic bone. Third, the partially ossifie transcapular ligament is the medially directed limb of the posttemporo-supracleithrum that joins the pectoral girdle to the basicranium at a facet on the basioccipital–exoccipital joint lateral to the occipital condyle. The medial-most end of the transcapular ligament of *Satan* remains unossified. Fourth, the vertebral process of the posttemporo-supracleithrum extends ventrally along the medial side of the vertical limb of the cleithrum to a direct bony joint with the anterolateral tip of the fourth parapophysis of the compound Weberian vertebra.

The posttemporo-supracleithrum also provides the connection between the body lateralis sensory canal and the postotic part of the cephalic sensory canals. The main body canal enters the posttemporo-supracleithrum posteriorly from two tubular ossicles and the canal exits anteriorly to pass into the small tubular extrascapula. A short, tubular extension of the posttemporo-supracleithrum, comparable to the subpterotic process of other ictalurids, projects anteriorly toward but does not contact the extrascapular and pterotic.

Pelvic fin and girdle.—There are 9-10 pelvic fin rays; the lateral-most ray is unbranched, the second and third rays are the longest. The pelvic-fin margin is scarcely convex from the longest ray to the shorter, most medial rays (Fig. 26). There is no pelvic splint lateral to the outer pelvic-fin ra .

The basipterygia are broad plates that meet on the midline in a wide synchondral symphysis. Each basipterygium bears two short anterior processes separated by an anterior marginal notch. The outer anterior process is narrow, pointed and directed anteriorly. The inner anterior process is broad and meets its contralateral inner process on the midline. This process is posteriorly continuous via thin fenestrated bone to the medial margin of the basipterygial plate. The lateral edge of the basipterygial plate projects prominently outward anterior to the base of the outer pelvic-fin ray. This posterolateral process is not joined anteriorly by a bony membrane to the outer margin of the outer anterior process. The posterior margin of the basipterygium is smoothly rounded and there is no ossified posterior process mesial to the inner fin rays

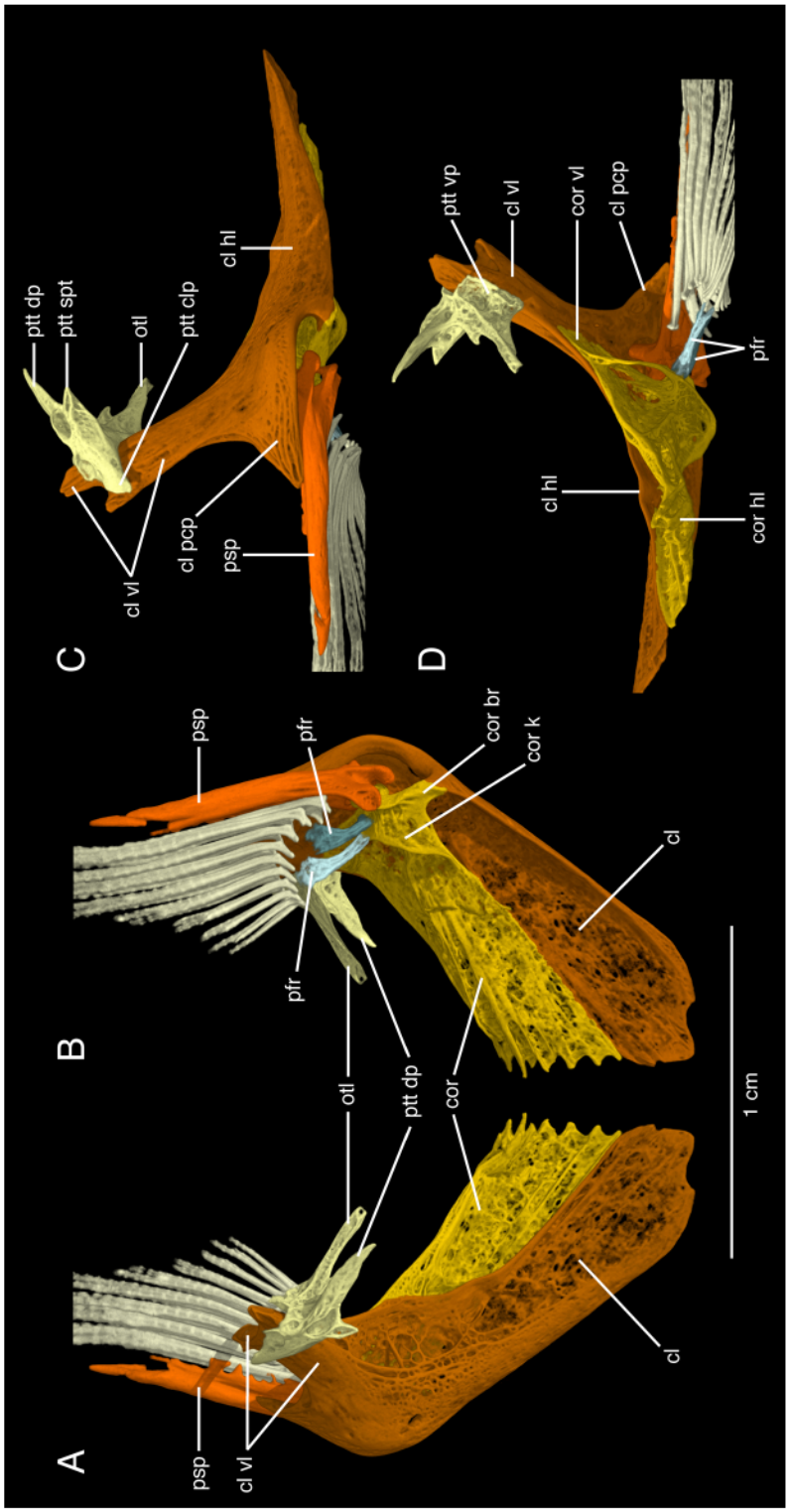

Fig. 24. *Satan eurystomus*, USNM 195930, 88.7 SL. 3-D HRXCT model of right-side pectoral girdle and fin. A. Dorsal, B. Ventral, C. Lateral, anterior to right, D. Medial, anterior to left. Abbreviations: cl, cleithrum; cl hl, cleithrum horizontal limb; cl pcp, cleithral posterior process; cl vl, cleithrum vertical limb; cor, scapulocoracoid; cor br, scapulocoracoid bridge to cleithrum; cor hl, scapulocoracoid horizontal limb; cor k, scapulocoracoid keel; otl, ossified transcapular ligament; pfr, pectoral-fin radials; psp, pectoral-fin spine; ptt clp, posttemporo-supracleithrum cleithral process; ptt dp, posttemporo-supracleithrum dorsal (pterotic) limb; ptt spt, posttemporo-supracleithrum subpterotic process; ptt vp, posttemporo-supracleithrum vertebral process.

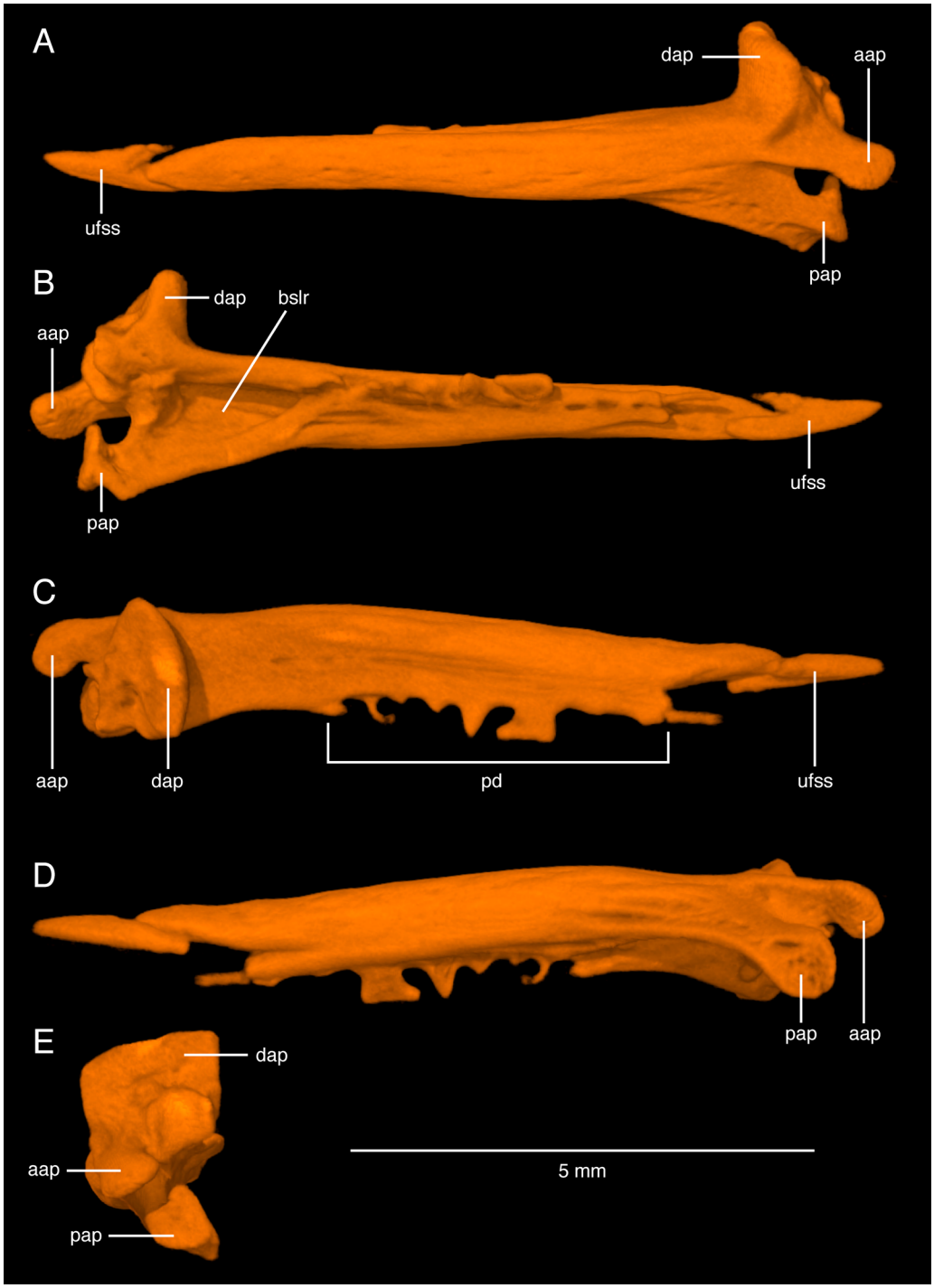

Fig. 25. *Satan eurystomus*, USNM 195930, 88.7 SL. 3-D HRXCT model of right-side pectoral-fin spine. A. Anterior, B. Posterior, C. Dorsal, D. Ventral, E. Medial. Abbreviations: aap, anterior articular process; bslr, basal recess; dap, dorsal articular process; pap, posterior articular process; pd, posterior dentations; ufss, unfused spine segment.

MORPHOLOGICAL RESULTS AND COMPARISONS

Here we list and review the morphological characters of *Satan* that we find to be unique among Ictaluridae or shared as potential synapomorphies with either *Pylodictis* (Hubbs and Bailey, 1947; Lundberg, 1970, 1975, 1982, 1992), or the other ictalurid stygobites (Arce-H. et al., 2016). Our phylogenetic framework for assessing the evolutionary significance of these features as apomorphies, plesiomorphies and homoplasies follows. *Satan* is a member of family Ictaluridae *sensu* Arce-H. et al. (2016) including the seven extant genera and without extinct †*Astephus*. As circumscribed, the key morphological synapomorphy uniting the Ictaluridae is the spread of jaw adductor muscle over the hyomandibular–cranial joint onto the skull roof and concomitant development of parasagittal and occipital crests of muscle origin on the supraoccipital and frontal bones (Figs. 3, 4, 27). Another correlate of cranial expansion of the jaw adductor muscles is the shift of the cranial exit of the infraorbital sensory canal from the sphenotic bone anteriorly into the frontal. Second, Asian *Cranoglanis* (Cranoglanididae) has been hypothesized to be the living sister lineage of Ictaluridae. This is based on nuclear and mitochondrial gene sequence evidence presented by Hardman (2005), Peng et al. (2005) and Sullivan et al. (2006). Sullivan et al., (2006) and Lundberg et al. (2007) placed these two families together in a putative monophyletic Superfamily Ictaluroidea. Diogo (2004) suggested morphological evidence that supports the ictalurid-cranoglanidid relationship but the limited comparative scope of that work suggests it needs verification. The combined molecular and morphological analyses of Arce H. et. (2016) did not resolve the position of Cranoglanididae relative to Ictaluridae. Third, the extinct North American genus †*Astephus* is possibly closely related to ictalurids and this fossil taxon is often compared to modern ictalurids (Lundberg, 1975, 1992; Grande and Lundberg, 1988; Arce-H. et al., 2016). Grande and Lundberg (1988) supported this relationship based on apomorphic but homoplasious features of the pelvic fin and girdle, and their endemism in North America. Fourth, Superfamily Ictaluroidea and †*Astephus* belong to the monophyletic Suborder Siluroidei (*sensu* Sullivan et al., 2006; Lundberg et al., 2007) within which their interrelationships to other families are currently unresolved.

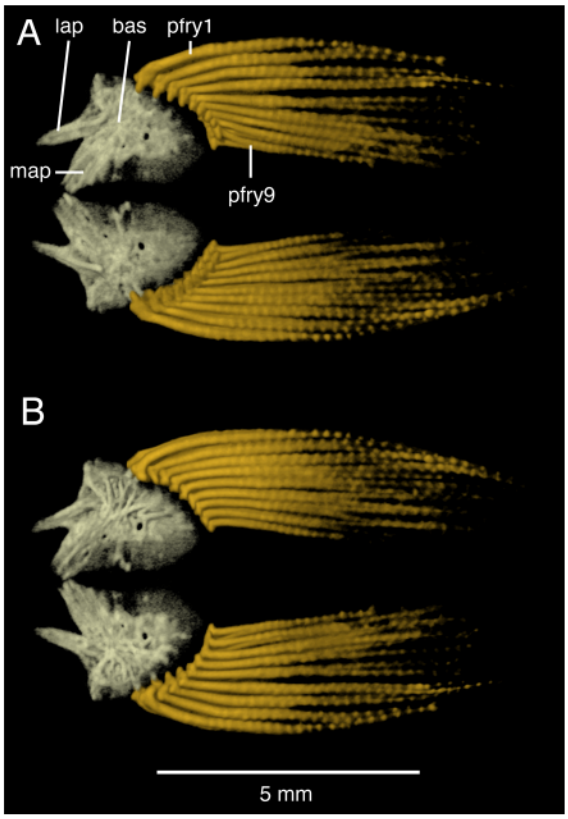

Fig. 26. *Satan eurystomus*, USNM 195930, 88.7 SL. 3-D HRXCT model of pelvic girdles and fins. A. Dorsal, B. Ventral. Abbreviations: bas, basipterigyum; lap, lateral anterior process of basipterygium; map, medial anterior process of basipterygium; pfry1, pelvic-fin ray 1; pfry9, pelvic-fin ray 9

Singular features of *Satan* among Ictaluridae

Here we note twelve salient features that uniquely characterize *Satan* among North American catfishes

1. Frontal-lateral ethmoid joint (Figs. 3-6). In *Satan*, the immobile bony joint between the frontal and lateral ethmoid on the dorsal surface of the skull roof is simple and overlapping, without multiple, interdigitating bony sutures. We interpret this feature to be an autapomorphy of *Satan*. In most other ictalurids, *Cranoglanis*, †*Astephus* and other siluroid families the frontal-lateral ethmoid articulation on the dorsal side of the skull roof is moderately to extensively interdigitating. *Trogloglanis* is exceptional in having no bony contact at all between the frontal and lateral ethmoid. Instead, a wide, band of the lateral ethmoid's antorbital process cartilage separates the bony elements (Lundberg, 1982, fig. 6, p. 23; Arce-H. et al., 2016, MorphoBank project 2100, media #M374321). This feature is an autapomorphy of *Trogloglanis* within Ictaluridae.

2. Posterior cranial fontanel (pcf) closure (Figs. 3, 4, 7, 8). In contrast to the many reductions of bony joints, *Satan* has an expanded and distinctive pattern of partial closure of the pcf formed by a novel series of three dorsal midline joints that together separate short anterior and posterior

remnants of the plesiomorphically open fontanel. The most anterior of the midline joints is between the frontals posterior to the small anterior fontanel remnant. In having a symphysis of interdigitating sutures this interfrontal joint is similar to the epiphyseal bar that lies in front of the anterior fontanel remnant. The second midline joint closes a section of the pcf immediately posterior to the first. This joint is also interfrontal but is a simple, straight, abutting midline contact without interdigitating edges or fusion. The third and most posterior pcf closure is within the supraoccipital immediately behind the second and it too is a straight abutting contact on the midline without apparent interlocking sutures or fusion. This developmentally complex complement of three midline joints and fontanel remnants is an autapomorphy of *Satan*.

A few ictalurid species retain a plesiomorphically open or slightly narrowed pcf. With growth and development, however, most species show more severe narrowing of the fontanel or its complete closure. Generally, these closures result from straight, abutting midline contacts between the somewhat elevated pair of parasagittal crests along the pcf margins on the frontal and/or supraoccipital. Remnant slit-like openings of the pcf may persist anteriorly and/or posteriorly, as for examples in *Pylodictis* (Fig. 27); *Trogloglanis* (Lundberg, 1982, fig. 6, p. 23); and *Prietella phreatophila* (MorphoBank project 2100, media #M374321 and Lundberg, 1982, fig. 7B, p. 34)

3. Supraoccipital median sulcus (Figs. 3, 4, 7, 8). In *Satan,* the posterior half of the supraoccipital has an elongate dorsomedian bony sulcus that includes the posterior pcf remnant. The sulcus is narrowly and sharply bounded by the raised parasagittal crests and posteriorly by the sharp margins of the supraoccipital posterior process. The sulcus autapomorphy is reductive in that bone is diminished immediately adjacent to the midline, but the bounding parasagittal crests remain well developed as sites of jaw adductor muscle attachment.

Among ictalurids there is a great variety of bony surface topographies and textures near the dorsal midline of the neurocranium. No other ictalurid has a median sulcus like that of *Satan*. Off the midline, however, the marginal outline of the parasagittal crests and supraoccipital posterior process of *Satan* is similar in the outline to *Pylodictis* (see below).

4. Temporal fossa wide and deep (Figs. 3, 4, 9-11). *Satan* has an extraordinarily wide and deep cavity within the temporal fossa. The temporal fossa and cavity are centered between the supraoccipital, epioccipital, pterotic and sphenotic. It remains to be determined if this cavity is filled with jaw muscle, as might be expected of an ictalurid, or with loose connective and adipose tissue that is generally present subcutaneously in *Satan*. Among other ictalurids, only *Pylodictis* (Fig. 27) and *Trogloglanis* (MorphoBank project 2100, media #M374321) show some excavation of the temporal region into a fossa of similar outline to that in *Satan,* but these are far less pronounced. We have not observed a comparable deep cavity of the temporal fossa on the otic capsule and occipital region roof in other living Ictaluridae, *Cranoglanis*, †*Astephus* or other siluroid families.

5. Position of the infraorbital sensory canal (Figs. 3, 4). Alone among living ictalurids, *Satan* has the junction of the infraorbital, supraorbital and otic sensory canals and the associated cranial exit of the infraorbital canal located in the sphenotic-frontal joint. The bony channels for these sensory canals and their foramina are enlarged in *Satan*. In contrast, other ictalurids (Fig. 27), including the other stygobitic species, have the junction of these three sensory canals and the infraorbital canal cranial exit located anteriorly, entirely within the frontal bone.

In Siluriformes, the infraorbital sensory canal plesiomorphically joins the supraorbital and otic canals within the sphenotic and the infraorbital canal directly enters the skull roof to the sphenotic (Lundberg, 1975, 1982, 1992; Grande and Lundberg, 1988). This condition of the infraorbital canal is retained in *Cranoglanis* and †*Astephus*. The condition in *Satan* is morphologically intermediate between the plesiomorphic sphenotic position of the infraorbital exit and the apomorphic frontal position. This might be viewed as a transitional condition between the sphenotic-only and frontal-only placements, or, alternatively, in *Satan* it may be stygomorphically related to enlargement of the sensory canals and foramina plus bone reduction in the sphenotic-frontal joint.

6. Infraorbital bone number (Figs. 3, 4). *Satan* has five tubular infraorbital bones, the lowest number of infraorbitals among ictalurids. Other species of the family have six to eight infraorbital bones. This feature is a presumed reductive autapomorphic bone loss in *Satan*.

7. Pterotic-posttemporo-supracleithrum articulation (Figs. 3, 4, 10, 11). The posttemporo-supracleithrum of *Satan* lacks direct bony articulations with the pterotic via its pterotic and subpterotic processes. This loose and likely entirely ligamentous articulation is interpreted as a reductive autapomorphy of *Satan*.

In other ictalurids the dorsal or pterotic limb and, in most species, the subpterotic process of the posttemporo-supracleithrum plesiomorphically make close and direct bony contact with the pterotic at the posterolateral corner of the skull. *Cranoglanis*, †*Astephus* and most other siluriforms have a tighter cranial joint of the pterotic limb.

8. Branchiostegal membranes (Fig. 3B, 30A). Hubbs and Bailey (1947) noted the widely overlapping branchiostegal membranes of *Satan*. Other ictalurids,

Cranoglanis and most other siluroid catfishe plesiomorphically have non-overlapping branchiostegal membranes. Hubbs and Bailey (1947) also stated that the overlapping condition is "often" present in *Pylodictis*. We observed the branchiostegal membranes to be scarcely overlapping in just four of 45 fluid preserved or cleared/stained specimens, the others having non-overlapping membranes (Fig. 30B). We suggest that the apparent consistently overlapping condition of the branchiostegal membrane is an autapomorphy of *Satan*. Functionally this may be related to the expansive bucco-pharyngeal space and a suction-feeding mechanism of *Satan*.

9. Interhyal (Figs. 3, 17). The interhyal of *Satan* is greatly elongated, roughly two to three times longer than the interhyals of other ictalurids and *Cranoglanis* at comparable body size. Also, in *Satan* the interhyal extends ventrally (Fig. 17C, D, F) from its upper end on the medial face of the preopercle to reach downward over the lateral face of the posterior ceratohyal near the interopercle. The autapomorphically elongated and large size of the interhyal of *Satan* is possibly related to its inferred suction feeding mechanism.

10. Interopercle-posterior ceratohyal joint (Figs. 3, 17). The interopercle of *Satan* lacks a well-defined, raised facet on its medial face at its articulation with the posterior ceratohyal. This reduced structure of the interopercle-posterior ceratohyal joint in *Satan* is an autapomorphy. This also may be related to its inferred suction feeding mechanism. The interopercles of other ictalurids, *Cranoglanis* and †*Astephus* plesiomorphically have a distinct concavity, often with a raised rim, at its joint the posterior ceratohyal.

11. Dorsal-fin spinelet (first dorsal spine) (Figs. 22, 23). *Satan* has a well-developed and distinctively shaped dorsal-fin spinelet. The spinelet has a sharp mid-dorsal peak and heavy, abruptly-recurved ventral limbs. This novel feature is a small-sized but non-reductive autapomorphy of *Satan*.

Well-developed dorsal-fin spinelets are present plesiomorphically in other ictalurids except for the two species of *Prietella* that lack the structure. The dorsal-fin spinelet is also present in *Cranoglanis*, †*Astephus* and most other siluriforms with a well-developed second dorsal-fin spine. Generally, the spinelet is stout, well ossified, a horseshoe-, V- or U-shaped with simple, nearly straight limbs.

12. Anterior margin of cleithrum (Figs. 3, 24). In *Satan,* the anterior margins of the cleithra are shallowly concave and transversely truncated across their ventral midline symphysis. In other ictalurids, *Cranoglanis*, †*Astephus* and most other siluriforms, the anterior margins of the cleithra are straight or smoothly convex anteriorly near and across their midline symphysis.

The foregoing list advances twelve autapomorphies that distinguish *Satan* within Ictaluridae and probably, at least in combination, from all other catfishes. Some of these are reductive loss or simplification features of skull bones (infraorbitals, pterotic) and joints (frontal-lateral ethmoid, interopercle-posterior ceratohyal). Some of the autapomorphies are anatomically and perhaps developmentally complex, such as the series of three midline joints closing the posterior cranial fontanel, the deeply excavated temporal fossa and interhyal enlargement. One, the dorsal-fin spinelet, is the novel shape of a tiny single bone that generally functions to lock the dorsal-fin spine when elevated.

Synapomorphies uniting *Satan* and *Pylodictis*

This section reviews ten synapomorphies of *Satan* and *Pylodictis* that were suggested in previous studies or discovered in the present work. Further, we raise questions about the polarities of paired-fin ray meristic characters in Ictaluridae and we correct five errors in the past literature dealing with misinterpreted characters in these catfishes. The primary literature includes: Hubbs and Bailey (1947), Suttkus (1961), Taylor (1969), Lundberg (1970, 1975, 1982, 1992), Langecker and Longley (1993), Walsh and Gilbert (1995) and Arce-H. et al. (2016).

1. Head shape and mouth position (Fig. 1, Plate I). Hubbs and Bailey (1947) pointed out the external resemblance between *Satan* and *Pylodictis* in their depressed, flattened heads and wide transverse mouths. This is a consistent and exclusive synapomorphy of *Satan* and *Pylodictis*. Other ictalurids (including the flat bullheads *Ameiurus platycephalus* and *A. brunneus*) and *Cranoglanis* have deeper and more arched heads and most ictalurids have notably narrower gapes than *Satan* and *Pylodictis*.

The flat-headed and wide-mouthed external form of *Satan* and *Pylodictis* is reflected in many aspects of their skull roofing bones and jaws (Figs. 3, 27). These features appear to be functionally associated with an enhanced mechanism for suction feeding in *Pylodictis* that can be extrapolated to *Satan* (discussed below).

2. Mesethmoid bone shape (Figs. 3, 5, 27, 28). Suttkus (1961) was the first investigator to examine aspects of the skeletal anatomy of *Satan*. Based on a radiograph of TU 10809, he called attention to the close similarity between *Satan* and *Pylodictis* in their broad and shallowly-forked mesethmoid cornua. *Trogloglanis* and *Prietella lundbergi* (unknown until 1995) also have divergent and shallowly forked mesethmoid cornua. As defined, we can interpret this form of the mesethmoid cornua as a consistent but non-exclusive synapomorphy of *Satan* and *Pylodictis*. However, the mesethmoid of *Trogloglanis* is highly divergent in its

gracile structure including the delicately slender cornua supported by an extremely narrow mesethmoid neck that is only about 7% of the width across the cornua tips. The mesethmoid neck of *P. lundbergi* is also narrow at about 16% of the width across the cornua tips. These more lightly built mesethmoids are distinct from the heavily built mesethmoid cornua and neck present in *Satan* and *Pylodictis*, about 30% of the width across the cornua tips.

In most ictalurids including *P. phreatophila* the mesethmoid cornua are narrowly forked and closely surround a deep, constricted median notch. *Cranoglanis* has widely forked cornua that flank a deep but unconstricted notch. The width of the mesethmoid neck is variable among the epigean ictalurids.

3. Lateral ethmoid posterior process (Figs. 6, 28). *Satan* and *Pylodictis* share a unique posterior process of the lateral ethmoid that arises from the dorsolateral margin of that bone and extends laterally along the frontal and then ventral to the frontal margin. Other ictalurids and *Cranoglanis* lack such a process. We interpret the posterior process of the lateral ethmoid as a consistent and exclusive synapomorphy of *Satan* and *Pylodictis*.

4. Supraoccipital posterior process (Figs. 3, 4, 8, 27). Taylor (1969) noted that the supraoccipital processes of *Satan* and *Pylodictis* are extremely narrow compared to most other ictalurids although these processes greatly differ in length between these species. In both, the width of supraoccipital posterior process abruptly diminishes behind the occiput to a thin, vertical blade completely lacking a superficial horizontal plate in the integument. We interpret the blade-like supraoccipital process as a consistent but not exclusive synapomorphy of *Satan* and *Pylodictis*. In *Pylodictis* the supraoccipital posterior process is long, reaching nearly half way across the nape to the dorsal-fin origin; in *Satan*, the process is much shorter but not rudimentary, a condition found also in *Noturus miurus*. The entire supraoccipital process is rudimentary in other *Noturus* and *Prietella*. The supraoccipital posterior processes of *Ictalurus*, *Ameiurus* and *Trogloglanis* are horizontally expanded in the skin of the nape to varying degrees and ornamented with pits or ridges and grooves.

5. Parasagittal and occipital crests (Figs. 3, 4, 8, 11A, 27). *Satan* and *Pylodictis* share a distinctive arrangement of the parasagittal and occipital muscle-attachment crests on the supraoccipital and along the occipital margin. This is a structurally complex, consistent and exclusive synapomorphy for these species. Different aspects of these same structures have been described and used in the phylogenetic analyses of Lundberg (1970, 1982, 1992) and Arce-H. et al. (2016). These may be summarized as follows. In *Satan* and *Pylodictis* the parasagittal crests have sharply angular margins. In *Satan*, these edges frame the midline sulcus, whereas in *Pylodictis* the crest's sharply angular edges flank paired, flat-topped and finely ridged plateaus that abut on the midline. Also in *Satan* and *Pylodictis*, the occipital crests are tilted obliquely forward (anterodorsally) and delimit, with their medially adjacent parasagittal crests, a paired posteriorly-open narrow notch on the supraoccipital occupied by an anterior lobe of epaxial muscle. Thus, the epaxial muscles are extended anteriorly onto the skull roof more so than in other ictalurids.

Other ictalurids manifest a variety of distinctly different arrangements of the parasagittal and occipital crests that reflect differences in the jaw and epaxial muscles on the skull (Lundberg, 1970, 1982, 1992; Arce-H. et al., 2016).

6. Opercular frame and panel (Figs. 3, 16, 29). An outstanding feature of the opercular bones of *Satan*, first observed in the CT image of USNM 195830, is the arrangement of the opercle, preopercle and an elongate interopercle. In this specimen, the three opercular bones frame the sides of a large, triangular area in the gill cover. This opercular frame is covered by a panel of integument and presumably filled with a thin layer of connective tissue and possibly some muscle. Initially we suspected the opercular frame and panel to be an artifact of preservation with the opercle and interopercle possibly fixed in a pose of pharyngobranchial expansion. However, the opercular frame and panel are also present in the second scanned specimen of *Satan* TCWC 8279.01. Furthermore, several specimens of *Pylodictis* including five articulated cleared/stained preparations, two dry skeletons and several alcohol-preserved specimens consistently show a comparable opercular frame and panel between similarly-shaped opercular bones and covered with the integument of the gill cover. The elongated shape of the interopercles in these two species is linked in the anatomical context of the opercular frame and panel as one side of the bony triangle connecting the widely divergent lower corners of the opercle and preopercle.

The recently-obtained CT scans of *P. lundbergi* show a gap between the opercle and preopercle, suggesting a comparable opercular frame and panel. However, in this species the interopercle is short and deeply triangular. By contrast, all other ictalurids examined, including cleared/stained and articulated dry skeletons, representing species of *Ictalurus*, *Ameiurus*, *Noturus*, *P. phreatophila* and *Trogloglanis*, have the opercular bones largely in contact and the interopercle is short and deep. In these species, there is no indication of a large triangular opercular frame, panel or long interopercle like that of *Satan* and *Pylodictis*. Nor have we seen a bony frame and panel in the operculum in a cursory survey of catfishes of other families. The ictalurid species without the opercular frame and panel, and as well *P. lundbergi*, have the interopercle tucked

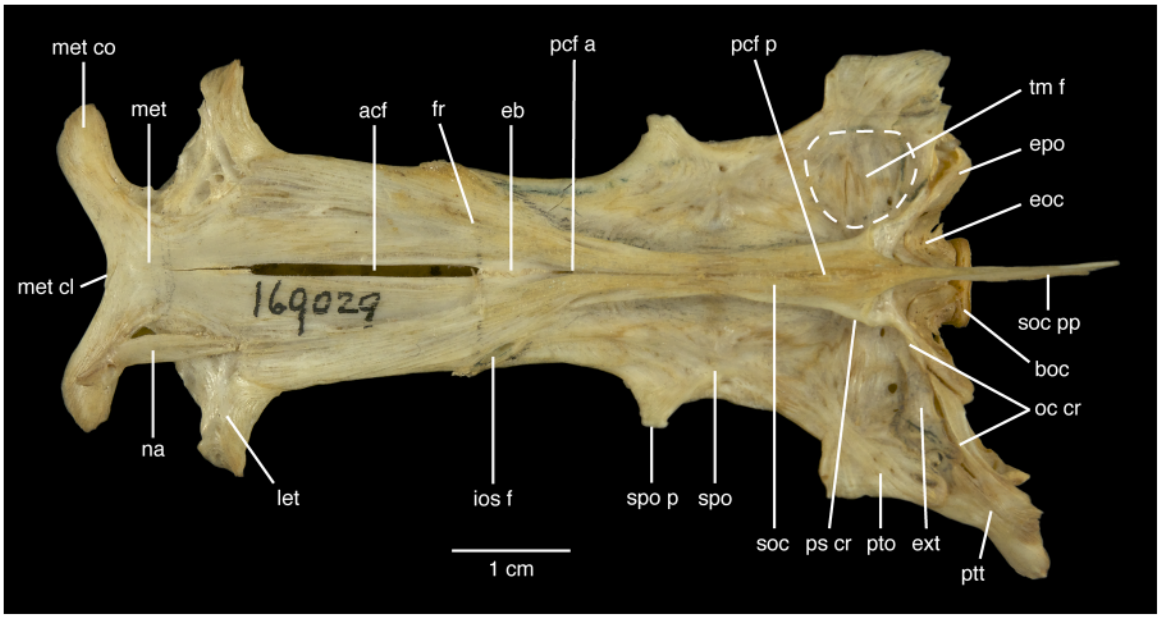

Fig. 27. *Pylodictis olivaris*, UMMZ 169029, 306 mm SL. Dry neurocranium, dorsal view, with dotted line indicating outline of right-side temporal fossa. Photograph by M. Arce-H. Abbreviations: acf, anterior cranial fontanel; boc, basioccipital; eb, epiphyseal bar; eoc, exoccipital; epo, epioccipital; ext, extrascapula; fr, frontal; ios f, foramen at union of infraorbital, supraorbital, otic canals; let, lateral ethmoid; met, mesethmoid; met cl, mesethmoid cleft; met co, mesethmoid cornu; na, nasal; oc cr, occipital crest; pcf a, posterior cranial fontanel, anterior subdivision; pcf p, posterior cranial fontanel, posterior subdivision; ps cr, parasagittal crest; pto, pterotic; ptt, posttemporo-supracleithrum; soc, supraoccipital; soc pp, supraoccipital posterior process; spo, sphenotic; spo p, sphenotic process; tm f, temporal fossa.

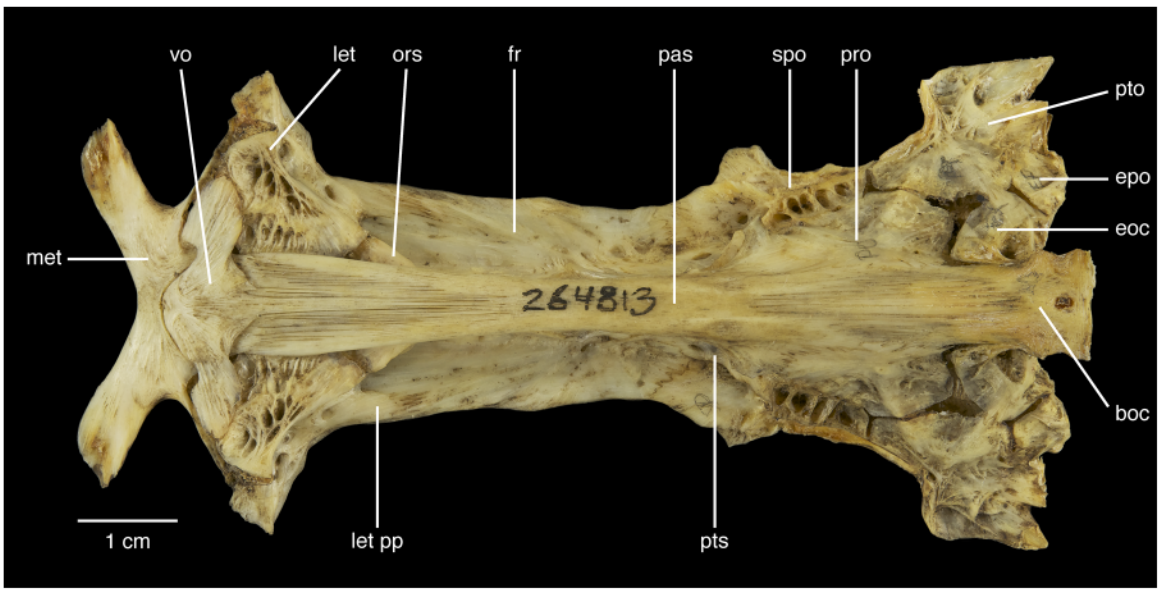

Fig. 28. *Pylodictis olivaris*, USNM 264813, 99 mm basicranial length. Dry neurocranium, ventral view. Photograph by M. Arce-H. Abbreviations: boc, basioccipital; eoc, exoccipital; epo, epioccipital; fr, frontal; let, lateral ethmoid; let pp, lateral ethmoid posterior process; met, mesethmoid; ors, orbitosphenoid; pas, parasphenoid; pro, prootic; pto, pterotic; pts, pterosphenoid; spo, sphenotic; vo, vomer.

below the adjacent opercle and preopercle. Therefore, the opercular panel and frame with a long interopercle appears to be a consistent and potentially exclusive synapomorphy of *Satan* and *Pylodictis*.

7. First mandibular sensory canal pore (Figs. 1 ventral view, 3, 15, 30). Hubbs and Bailey (1947) observed in *Satan* and *Pylodictis* that the paired first or symphyseal pores of the mandibular lateralis canal have a common opening in a median pit on the chin. Subsequent authors (Suttkus, 1961; Taylor, 1969; Lundberg, 1970, 1982) have verified in *Satan* and *Pylodictis* that the first mandibular sensory canal foramina, tubes and pores are close to the symphysis and the tubes open by a common median pore. This also is a consistent and exclusive synapomorphy for *Satan* and *Pylodictis* within Ictaluridae. In other ictalurids and siluriforms generally, the anteriormost mandibular canal pores are spaced apart posterolaterally away from the mandibular symphysis.

8. Preoperculo-mandibular sensory canal foramina and pores (Figs. 3, 15, 16, 30). Taylor (1969) reported that *Satan* and *Pylodictis* have 12 sensory pores associated with the preoperculo-mandibular canal. This is viewed as a synapomorphic increase of pores above the more general number of 10-11 pores in other ictalurids. The increase of pore numbers in the preoperculo-mandibular branch of the cephalic canal system has also been expressed as the count of bone foramina along the mandible. Lundberg (1992) and Arce-H. et al. (2016) observed eight mandibular foramina in *Satan* and *Pylodictis* (including the foramen of passage of the main canal between mandible and preopercle) vs. six or seven in other ictalurids. In either case *Satan* and *Pylodictis* show the increase in pores and associated foramina of the preoperculo-mandibular branch.

9. Posterior ceratohyal (Fig. 17). Both *Satan* and *Pylodictis* have similarly shaped, elongated posterior ceratohyal bones. This is a consistent and exclusive synapomorphy among ictalurids. Other ictalurids have shorter, triangular-shaped posterior ceratohyals as do *Cranoglanis* and †*Astephus*.

In *Pylodictis* the posteroventral corner of the posterior ceratohyal is also expanded, whereas in *Satan* the lower margin of posterior ceratohyal is smoothly curved and not ventrally expanded. The lack expansion may be a plesiomorphic condition and the expansion an autapomorphy of *Pylodictis*.

10. Fourth supraneural and anterior nuchal plate. (Figs. 3, 22, 31). The anterior nuchal plate is absent in *Noturus, Prietella, Pylodictis* and *Satan*. *Pylodictis* and *Satan* have well-developed fourth supraneural bones that articulate posteriorly with the first pterygiophore in a long vertical butt-joint and these species have a long median and narrowly-bifid anterior arm of the supraneural below the skin and between the epaxial muscle masses. This arrangement of the supraneural along with the loss of anterior nuchal plate is a consistent and exclusive synapomorphy of the fourth supraneural among ictalurids.

In species of *Noturus* and *Prietella* the fourth supraneurals are rudimentary and may fuse with the first pterygiophore or they are lost. Among ictalurids, all species of *Ictalurus, Ameiurus* and *Trogloglanis* plesiomorphically have well-expanded anterior nuchal plates and contact with the supraoccipital process is made in some species of *Ictalurus*.

Satan-Pylodictis *Synapomorphies Summary and Suction Feeding*.—The foregoing list advances ten synapomorphies supporting *Satan* and *Pylodictis* as sister lineages. These appear to be functionally related to feeding. Two of the synapomorphies of *Satan* and *Pylodictis* involve the anterior parts of the cephalic lateralis system that can play an important role in prey detection: medially united symphyseal mandibular canal pores and increase of preoperculo-mandibular canal pores. In the first comparison of *Satan* and *Pylodictis* Hubbs and Bailey (1947) called attention to their "greatly depressed" heads and "wide transverse" mouths (Figs. 1, 30; Plate 1). The head and mouth construction of these catfishes suggests that they feed on relatively large, whole prey. Indeed, the capacious gape and bucco-pharyngeal cavity and projecting lower jaw of large *Pylodictis* are well known to anglers and "noodling" hand fishers. Post-juvenile Flathead Catfish (>30cm TL) become large, voracious and dedicated piscivores (Jackson, 1999). Small, eyeless Widemouth Blindcat are known from their gut contents to feed on stygobitic crustaceans in the deep aquifer (Longley, 1981; Langecker and Longley, 1993). A foraging Flathead Catfish executes a rapid suction component in its attack on mobile, whole prey. Similar morphology implies the same for *Satan*.

It is likely that all ictalurids and most catfishes practice some degree of suction feeding. But, several features shared by *Pylodictis* and *Satan* suggest they have a heightened role for suction feeding compared to other ictalurids.

Anatomical and advanced biomechanical analyses of many actinopterygian fishes have identified the musculoskeletal components involved in producing fast-suction for prey capture (Lauder, 1985; Westneat, 2006). The relatively wide mouths and heads of these catfishes reflect the increased capacity of their bucco-pharyngeal space for taking in water and large prey. Epaxial muscles inserting high on the occiput and skull roof have been shown to rotate the neurocranium dorsally during the expansion phase of suction feeding. In *Pylodictis* and *Satan* the conformation of the parasagittal and occipital crests on the occipital region bones reflect an anterior

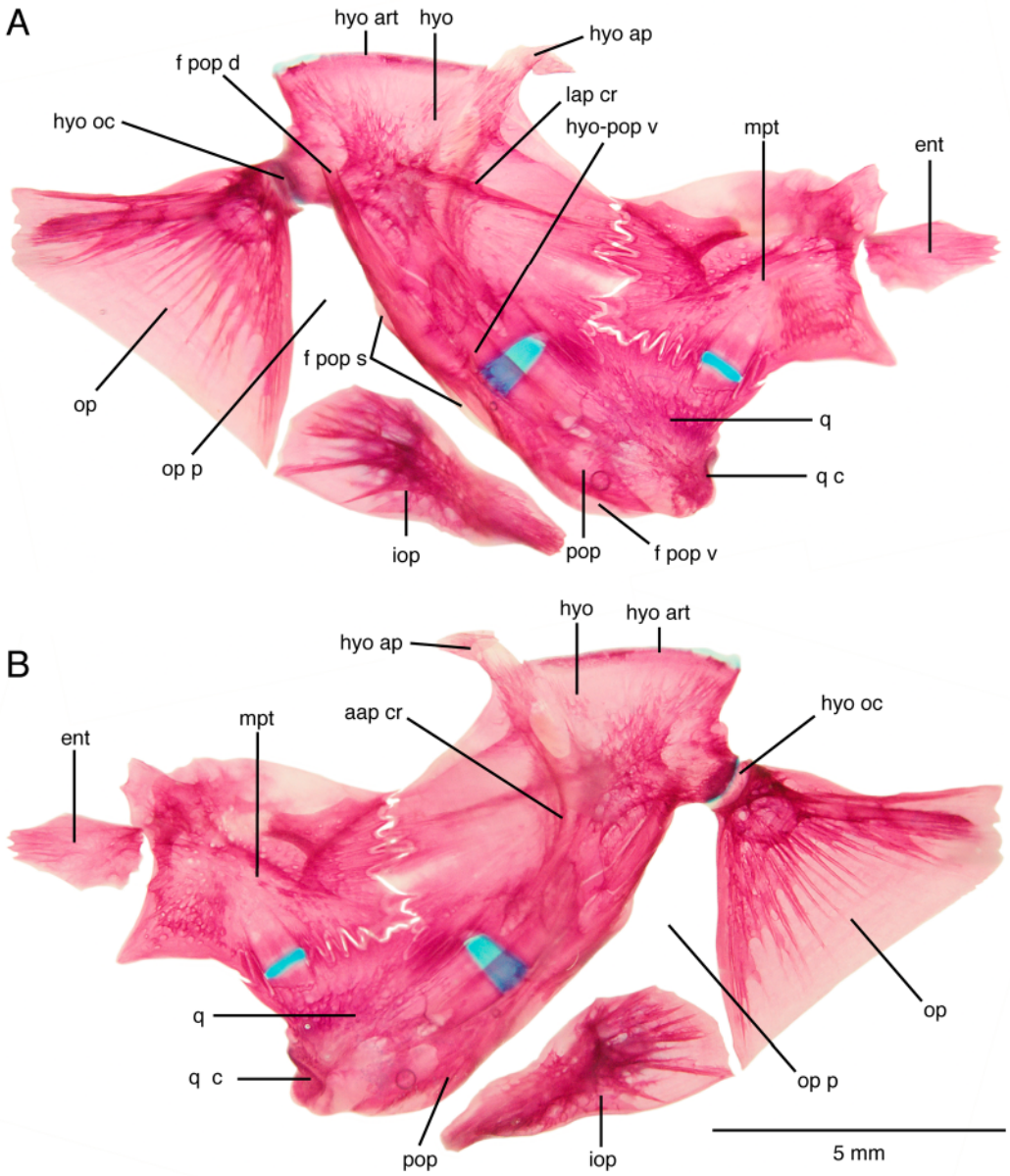

Fig. 29. *Pylodictis olivaris*, ANSP 150648, 83 mm SL. Cleared and double stained, right-side suspensorium and opercular bones. A. Lateral, B. Medial. Photograph by M. Arce-H. Abbreviations: aap cr, *adductor arcus palatini* crest; ent, endopterygoid; f pop d, preopercle main sensory canal dorsal foramen; f pop s, preopercle sensory canal side-branch foramina; f pop v, preopercle main sensory canal ventral foramen; hyo, hyomandibula; hyo ap, hyomandibular anterodorsal process; hyo art, hyomandibular articular head; hyo oc, hyomandibular-opercular condyle; hyo-pop v, hyomandibula-preopercle ventral articulation; iop, interopercle; lap cr, *levator arcus palatini* crest; mpt, metapterygoid; op, opercle; op p, opercular panel; pop, preopercle; q, quadrate; q c, quadrate articular condyle.

extension of epaxial muscle onto the skull roof table that other ictalurids do not have. Also, the vertical, bladelike supraoccipital posterior processes of *Pylodictis* and *Satan* may reflect an increase in epaxial muscle insertion just behind the occiput. The opercular frame and panel, the integument-covered triangular space between the divergent opercle and preopercle with an elongated interopercle, are found only in *Pylodictis* and *Satan* among ictalurids. The opercular frame and panel of *P. lundberg*i differs in having a short, deep interopercle as in other ictalurids. Therefore, the long interopercle in an opercular-panel frame appears to be a consistent and potentially exclusive synapomorphy of *Satan* and *Pylodictis*. The opercular frame and panel increases the surface area of the operculum and with that the volume of the pharyngeal space as the *levator arcus palatini* and *dilatator operculi* muscles lift the suspensorium and opercle. The posterior ceratohyals of *Pylodictis* and *Satan* are also elongated. Presumably, the resulting increased length of the hyoid bars should increase lateral and ventral expansion of the pharyngeal space during contraction of the sternohyoideus muscles.

There are also autapomorphic features of *Pylodictis* or *Satan* that relate to the mechanics of suction feeding. *Pylodictis* has a uniquely enlarged and elongated *levator arcus palatini* crest on the hyomandibula and metapterygoid. The *levator arcus palatini* muscle inserting on the crest lifts the suspensorium laterally causing pharyngeal expansion. *Satan* has enlarged, overlapping branchiostegal membranes that, like the opercular frame and panel, increase gill cover area and volume of the pharynx. *Satan* also has increased flexibility of two joints that are likely mobile during buccal expansion. The pterotic-posttemporo-supracleithrum articulation with the skull is ligamentous. This should permit a less constrained dorsal rotation of the skull upon epaxial contraction. Also, the interopercle-posterior ceratohyal joint of *Satan* is shallower by reduction of an interopercular articular crest. This more flexible joint could facilitate retraction of the longer hyoid bar during expansion. The interhyal of *Satan* is uniquely elongated compared to all other ictalurids. The exact role that a longer interhyal plays in the dynamics of hyoid bar movement during expansion or compression needs to be determined. Possibly its length is simply an accommodation to the expanded volume of the pharynx. Finally, in *Satan*, the uniquely truncated anterior margin of the cleithrum may be related to some modification of the sternohyoideus muscle in its role generating pharyngeal expansion. To date we have had no opportunity for direct study of the musculature or feeding behavior and mechanics of *Satan*.

Uncertainties.—*Satan* and *Pylodictis* have high numbers of paired-fin rays compared to other ictalurids: the pectoral lepidotrichia include a leading fin spine plus 10-11 soft rays (Fig. 30) and the pelvic fin ray counts are 9-10 soft fin rays. Other ictalurids have 8-9 soft pectoral-fin rays behind the leading spine (or in *Prietella* a leading simple lepidotrichium), and pelvic fin ray counts of 8-9. These higher counts of paired-fin rays shared by *Satan* and *Pylodictis* have been considered synapomorphies (Lundberg, 1970, 1975, 1982, 1992). However, the high pectoral- and pelvic-fin ray counts are apomorphic homoplasies under the alternative hypothesis that *Satan* is more closely related to *Trogloglanis* and *Prietella* than

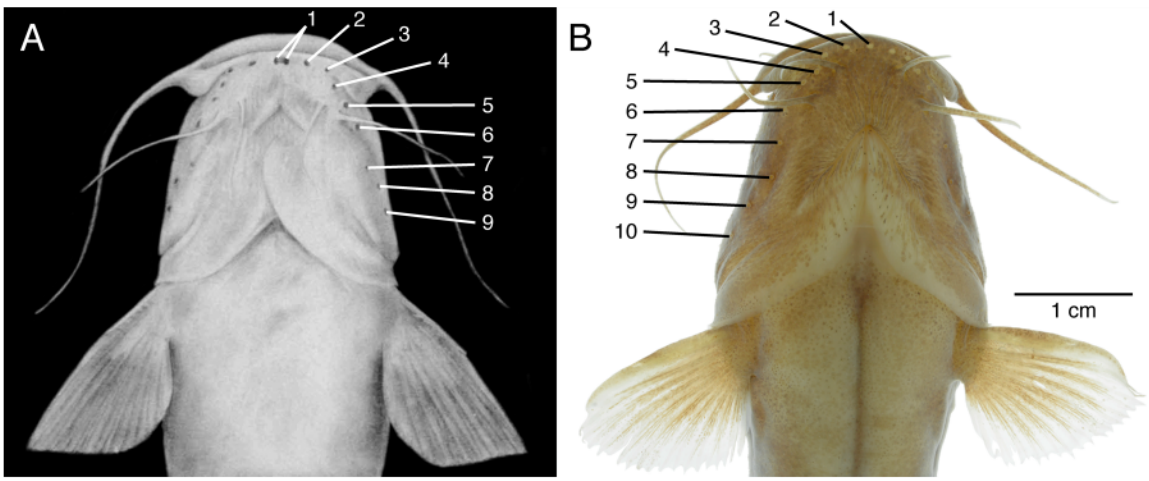

Fig. 30. Surface pores of the preoperculo-mandibular sensory canal in ventral view, numbered from 1 (first or symphyseal pores opening together in a median pit or common pore below the mandibular symphysis) to 9 or 10; A. *Satan eurystomus*, UMMZ 190922, 68.7 mm SL (see credit for Fig. 1); B. *Pylodictis olivaris*, ANSP 152383, 48.2 mm SL. Photograph by M. Arce-H.

to *Pylodictis* (Arce-H. et al., 2016). Within the broader context including Cranoglanididae as the possible sister lineage of Ictaluridae, the polarity of fin ray transformation within North American catfishes is reversed from previous hypotheses. Cranoglanidids have 9-11 soft pectoral rays following the fin spine and 11-14 pelvic-fin rays. Also, fossil †*Astephus* have 9-10 soft pectoral-fin rays, and ten soft pelvic-fin rays. A more fully resolved and well-supported tree for Ictaluridae is needed for ancestral state reconstruction of fin-ray transformation within the famil .

Corrections.—During the course of this closer examination of *Satan* we found five features that were incorrectly understood and published as potential synapomorphies of *Satan* and *Pylodictis*. These characters are no longer relevant to the hypothesis of relationship between *Satan* and *Pylodictis* and are corrected here.

Hubbs and Bailey (1947) suggested that the broadly overlapping branchiostegal membranes present in *Satan* is approached by *Pylodictis*. They state that *Pylodictis* often has overlapping branchiostegal membranes. We found only four specimens of *Pylodictis* with overlapping branchiostegal membranes among the 45 alcohol preserved individuals in the ANSP fish collection. Perhaps overlapping branchiostegal membranes occur in some specimens of the Flathead Catfish, but we suggest the character is rare or too variable to propose it as a strong cladistic character. We regard the overlapping branchiostegal membranes as a distinctive feature of *Satan* among ictalurids.

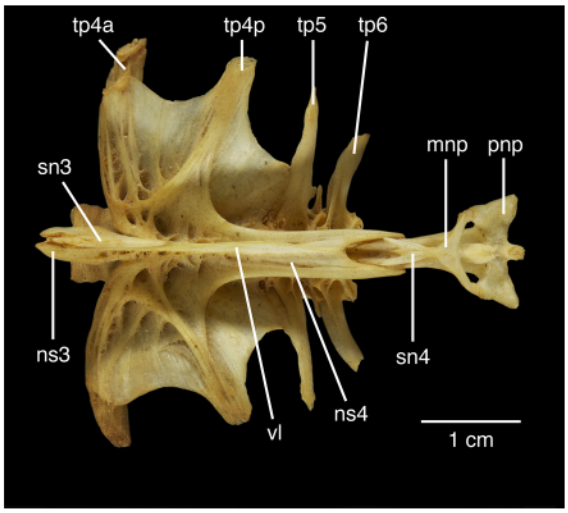

Fig. 31. *Pylodictis olivaris*, UMMZ 169029, 306 mm SL. Dry skeleton of Weberian apparatus, vertebra 6 and dorsal-fi pterygiophores (fin-spines removed) in dorsal view, anterior to left. Abbreviations: mnp, middle nuchal plate; ns3, neural spine 3; pnp, posterior nuchal plate; sn3-4, supraneurals 3, 4; tp5-6, transverse processes of vertebrae 5, 6; vl, vertical lamina; tp4a, Weberian apparatus anterior limb of fourth transverse processes; tp4p, Weberian apparatus posterior limb of fourth transverse processes. Photo by M. Arce. H.

Using dorsoventral and lateral view 2-D radiographs of the holotype of *Satan*, Lundberg (1970, 1982, 1992) suggested four synapomorphies for *Satan* and *Pylodictis* involving features of the nasal bone (broad and flattened), the coronoid process of the lower jaw (low), the articular bone (articular process enlarged) and scapulocoracoid symphysis (few, four to five midline sutures). Based on the greatly improved tomographic images now available, we see that the nasal bone of *Satan* is a wide tubular ossicle and not flattened with a rim of membrane bone as in *Pylodictis*. The coronoid process of the lower jaw of *Satan* is steep-sided and not low as in *Pylodictis*, and the articular bone process of *Satan* is moderately large but does not approach the more greatly projecting condition of *Pylodictis*. The scapulocoracoid symphysis of *Satan* is united by five to six coarsely interlocking sutures that is more than in *Pylodictis* and not as the earlier available data suggested. The number of midline sutures of the scapulocoracoid of *Satan* does not differ from or overlaps with several species of *Ictalurus*, *Ameiurus* and *Noturus*.

Synapomorphies uniting the Troglobites

This section reviews the fifteen morphological synapomorphies of the Troglobites, the clade of ictalurids recovered in the cladistic analysis of Arce-H. et al. (2016) containing the four stygobitic species: *Satan eurystomus, Trogloglanis pattersoni, Prietella phreatophila and P. lundbergi*. The study used TNT Parsimony Analysis (Goloboff et al., 2008) on a data set of 209 morphological characters for 64 ingroup terminals, including three species of †*Astephus*, and seven outgroup terminals sampling different siluroid families. Because *Satan* and *Trogloglanis* lack sequence data, no molecular synapomorphies are known for the Troglobites clade. Here we review the morphological characters, and their synapomorphic consistency and exclusivity for the Troglobites clade. The present study added information on many anatomical details of *Satan* but these have not changed the character states as scored by Arce-H. et al. (2016).

1. Eyes (Fig.1, Plate I). The four stygobites lack fully developed eyes. This stygomorphic feature is a consistent and exclusive synapomorphy for the Troglobites clade within Ictaluridae. All other ictalurids normally have fully developed eyes. Cases of eye absence, microphthalmia and polymorphic eye malformations are documented in natural populations of some ictalurid species but these are without systematic relevance (Weisel and McLaury, 1964).

It is noteworthy that *Satan* and *Trogloglanis* have not completely lost eyes. Langecker and Longley (1993) described the presence of eye rudiments in small individuals of these catfishes followed by regressive development. Developmental details of the eyes for the *Prietella* species are unknown.

2. Skin pigmentation (Fig. 1, Plate I). The four stygobite species lack skin pigmentation. This stygomorphic feature is a consistent and exclusive synapomorphy for the Troglobites clade within Ictaluridae. All other ictalurid species are normally pigmented. Cases of albinism and piebald coloration for several ictalurid species are reported in the popular press and online sport-fishing websites.

3. Fifth Vertebra (Figs. 3, 19, 20, 31). Complex overlapping and tightly sutural intervertebral joints between the Weberian and fifth vertebrae plesiomorphically characterize all epigean ictalurids and outgroup catfishes (Fig. 31; Lundberg, 1982; Chardon et al., 2003). In *Satan* (Fig. 20), *Trogloglanis* and the two-nominal species of *Prietella* the fifth vertebrae lack strongly overlapping sutural articulations with the posterior face of the Weberian compound centrum. These simplified fifth vertebrae resemble typical precaudal vertebrae. The reductive structure of the fifth vertebrae is a consistent and exclusive synapomorphy for the Troglobites clade within Ictaluridae.

4. Lateral line extent (Fig. 1). In *Satan, Trogloglanis* and both nominal *Prietella* species, the lateral line does not reach the caudal skeleton. This is reconstructed as a consistent but non-exclusive synapomorphy of Troglobites. In contrast, many *Ictalurus*, *Ameiurus, Pylodictis* and *Cranoglanis* plesiomorphically have complete lateral line body canals that reach the base of the caudal fin. All *Noturus* and some species of *Ameiurus* also have shortened lateral line canals that do not reach the caudal skeleton.

5. Mesethmoid cornua (Figs. 3, 5). The analysis of Arce-H. et al. (2106) recovered the widely-forked form of the mesethmoid cornua of *Satan, Trogloglanis and P. lundbergi* as a synapomorphy of Troglobites. *Prietella phreatophila* has narrowly divided mesethmoid cornua that surround a deep, narrow mesethmoid notch. The condition of *P. phreatophila* was reconstructed as a reversal within the Troglobites clade to the presumed plesiomorphic state retained by *Noturus*, most *Ameiurus* and *Ictalurus* species.

As described above (pp. 131-132) and noted by Suttkus (1961), *Pylodictis* also has widely forked mesethmoid cornua. Thus, reconstructions of mesethmoid character transformations conflict between the alternative hypotheses on the relationships of *Satan*.

6. Anterior cranial fontanel (Figs. 3, 4). In *Satan*, *Trogloglanis* and *P. phreatophila* the terminus of the anterior cranial fontanel falls posterior to a line across the lateral ethmoid wing tips. The state of this character was indeterminate for *P. lundbergi* in Arce-H. et al. (2016). This feature is reconstructed as a consistent but non-exclusive synapomorphy of Troglobites among ictalurids. The anterior extension of the anterior cranial fontanel varies in state within *Ictalurus*, *Ameiurus* and *Noturus*. *Pylodictis* and *Cranoglanis* have the presumed plesiomorphic more anterior limit of the anterior cranial fontanel.

7. Descending wing of frontal (Figs. 3D, 5). *Satan, Trogloglanis* (MorphobBank media # M374323) and *P. phreatophila* have shallow descending wings of the frontals between the ventral surfaces of the frontals and vertical walls of the orbitosphenoid, but the state of this character was indeterminate for *P. lundbergi* in Arce-H. et al. (2016). In the blind ictalurids the depth of the descending frontal wing is less than one third of the skull depth at that level. This feature was recovered as a consistent but non-exclusive synapomorphy of a monophyletic Troglobites clade. *Pylodictis* and *Noturus* have similarly shallow descending wings of the frontal bone and this was recovered as a homoplasious similarity by Arce-H. et al. (2016). All species of *Ictalurus* and *Ameiurus* have plesiomorphically tall frontal wings.

8. Supraoccipital posterior process (Figs. 3, 4). Arce-H. et al. (2016) scored the posterior process of the supraoccipital bone of *Satan, Trogloglanis* and the two species of *Prietella* as short, i.e. much shorter than length of the supraoccipital bone without the process. In contrast, many species of *Ictalurus*, *Ameiurus*, *Pylodictis* and *Cranoglanis* have moderately to very long supraoccipital processes. The supraoccipital process is rudimentary or very short in *Noturus*. Based on length only, the supraoccipital process is reconstructed as a consistent but non-exclusive synapomorphy of Troglobites clade (Arce et al., 2016). As noted above (p. 64), the supraoccipital posterior processes of *Satan* and *Pylodictis*, although differing in length, can be treated alternatively as synapomorphically similar in being vertically blade-like.

9. Pterotic wing (Figs. 3, 4, 10, 11). In *Satan, Trogloglanis* and both species of *Prietella* the posterolateral wing or corner of the pterotic is rounded (Arce-H. et al., 2016). In contrast, many ictalurids, *Cranoglanis* and several other siluroids plesiomorphically have a sharply-cornered or projecting pterotic wing. The shared rounded pterotic wing is recovered as consistent but not exclusive synapomorphy of a monophyletic Troglobites clade. At least one *Ameiurus* species and most or all species of *Noturus* have a similarly rounded pterotic wing. These were recovered as homoplasious features within the family Arce-H. et al. (2016).

10. Parasphenoid and orbitosphenoid (Figs. 4, 13). In *Satan, Trogloglanis* and *Prietella phreatophila* the orbitosphenoid has about the same width as the underlying

parasphenoid stem, but this feature was indeterminate for *P. lundbergi* in Arce-H. et al. (2016). This condition was reconstructed as a consistent although non-exclusive synapomorphy for the Troglobites. Many ictalurids and *Cranoglanis* plesiomorphically have an orbitosphenoid that is much wider than the parasphenoid stem. Some species of *Noturus* have orbitosphenoid widths similar to those of the stygomorphs and some species of *Noturus* show other states of orbitosphenoid width (Arce-H. et al., 2016). Generally, there appears to be a high level of homoplasy among ictalurids in orbitosphenoid width.

11. *Adductor arcus palatini* scar (Figs. 4, 13). In *Satan, Trogloglanis and P. phreatophila* the adductor arcus palatini scar of muscle origin is continuous with the ventral edge of the parasphenoid, but the state of this character was indeterminate for *P. lundbergi* in Arce-H. et al. (2016). This similarity is reconstructed as a consistent but non-exclusive synapomorphy of Troglobites. *Noturus* also has the muscle scar continuous with the ventral edge of the parasphenoid. In contrast, in *Ictalurus*, *Ameiurus*, *Pylodictis* and *Cranoglanis* the muscle scar on the parasphenoid plesiomorphically is turned dorsally, away from the ventral edge of the bone.

12. Anterior ceratohyal-ventral hypohyal joint. In *Satan, Trogloglanis* and *P. phreatophila* the anterior ceratohyal-ventral hypohyal joint is entirely synchondral but the state of this character was indeterminate for *P. lundbergi* in Arce-H. et al. (2016). This was reconstructed as a consistent but non-exclusive synapomorphy of Troglobites. This joint is variably synchondral or bony among species of *Ictalurus* and *Noturus*. In contrast, all species of *Ameiurus*, *Pylodictis* and *Cranoglanis* plesiomorphically have direct bony joints between the anterior ceratohyal-ventral hypohyal.

13. Dorsal hypohyal (Fig. 17). *Satan, Trogloglanis* and *P. phreatophila* have reduced, small dorsal hypohyals, but state of this character was indeterminate for *P. lundbergi* in Arce-H. et al. (2016). This condition is reconstructed as a consistent but non-exclusive synapomorphy of Troglobites among ictalurids. There is interspecific size variation of the dorsal hypohyal in *Noturus*. In contrast, species of *Ictalurus*, *Ameiurus*, *Pylodictis* and *Cranoglanis* plesiomorphically have unreduced dorsal hypohyals.

14. Upper hypurals. (Figs. 2, 21). In the upper half of the caudal skeletons of *Trogloglanis* (MorphoBank project 2100, media #M374312) and *P. phreatophila* (MorphoBank project 2100, media #M366791) there is a single, large upper hypural plate assumed to be the fused hypurals 3, 4, 5 and possibly 6, unless that element and perhaps others are lost. This same condition has been reported for *Satan* by Lundberg and Baskin (1969), Lundberg (1970, 1982) and Arce-H. et al. (2016). As originally coded and analyzed, fusion of these three or four hypurals is a consistent but non-exclusive synapomorphy of a monophyletic Troglobites clade. Similar fusions of the upper hypurals found in some species of *Noturus* are recovered as homoplasious features within Ictaluridae (Arce-H. et al., 2016).

Plesiomorphically, most ictalurids, *Cranoglanis* and many other siluroids have the upper four hypural elements as separate, unfused bones. However, in the X-ray and tomographic images of the caudal skeleton of *Satan* (USNM 195830, TCWC 8279.01) there are features such as notches, grooves and ridges that appear to correspond with the relative sizes, narrow gaps and/or boundary lines between hypural elements 3, 4, 5 and 6 (Figs. 2, 21), suggesting that the hypurals are partly separate and not as completely consolidated as the compactly-fused upper hypural plates of *Trogloglanis* and *P. phreatophila*. These observations raise a question about the primary homology of the upper hypural elements in the caudal skeleton of subterranean ictalurids.

15. Transcapular ligament ossification (Figs. 3, 4, 11). In *Satan, Trogloglanis* and the two *Prietella* species ossification of the transcapular ligament is incomplete medially near and at its basi-/exo-occipital facet. In most other ictalurids and siluroids in general ossification of the transcapular ligament is plesiomorphically complete with a direct bony joint on the occipital facet. Reduced ossification of the ligament is consistent but non-exclusive as a synapomorphy of a monophyletic Troglobites clade. *Pylodictis* and *Noturus* also have an incompletely ossified transcapular ligament and these features were recovered as homoplasious by Arce-H. et al. (2016).

Troglobites Synapomorphies Summary.—The foregoing list reviews the fifteen synapomorphies recovered by Arce-H. et al. (2016) that support monophyly of the four ictalurid Troglobites. Three of the fifteen synapomorphies are consistent and exclusive synapomorphies for the Troglobites: eye loss, pigment loss and simplification of the plesiomorphically complex intervertebral joint between the Weberian compound vertebra and fifth vertebra. The loss of eye structure, vision function and pigmentation are common convergent or parallel features of fishes and other animal inhabitants of hypogean habitats. Such features are often excluded from phylogenetic analyses including most previous phylogenetic treatments of Ictaluridae. Nevertheless, Arce-H. et al. (2016) argued that hypothesized adaptive scenarios should follow from phylogenetic work, rather than precede it, and all characters can be considered independent (e.g. Wheeler, 2012). There was no a priori reason to consider putative adaptive characters to be less independent than any other characters in our combined data context. Reduction of the complex anterior vertebral

joints also occurs in non-ictalurid stygomorphic and epigean catfishes (Lundberg et al., 2014). The Troglobites hypothesis posits that the co-occurrence of these features in the four subterranean ictalurids is due to descent from a common stygobitic ancestor. The remaining 12 synapomorphies of the Troglobites are non-exclusive within Ictaluridae. In listing these characters, we identify the other ictalurid taxa that share similar homoplasious features with the Troglobites. Reductive characters among these are the shortened lateral line canal, loss of an infraorbital bone and underdeveloped or incomplete ossifications of the pterotic, supraoccipital, hyoid arch bones and transcapular ligament.

Langecker and Longley (1993) list additional apomorphic and mostly reductive features present among the ictalurid stygobites. The optic lobes and pineal organs of *Satan* and *Trogloglanis* are reduced, but they have an enlarged cerebellum and *saccus vasculosus*. Of interest, is the recent demonstration that the *saccus vasculosus* of salmonids is responsive to seasonal day-length change and participates in regulating the photoperiodic activity of gonads (Nakane et al., 2013). If this function of the *saccus vasculosus* is general for teleosts, we speculate that for stygobites living in permanent darkness there could be a selective advantage to abandon light-mediated or any seasonal cycling of reproduction in favor of a more opportunistic strategy based on food or mate availability. The enlarged *saccus vasculosus* of *Satan* and *Trogloglanis* may be an expression of transformed control of gonad development and reproductive timing.

Walsh and Gilbert (1995) noted additional characteristics of the ictalurid stygomorphs. All four species have adnate adipose-caudal-fin folds (also characteristic of all *Noturus*). *Satan* and *Trogloglanis* have well-ossified and denticulated pectoral- and dorsal-fin spines. In contrast, the two species of *Prietella* have reduced the spinous structure of the first pectoral-fin ray and second dorsal-fin ray that remain segmented and flexible. Also, the dorsal-fin spinelet is lost in both *Prietella* species. *Satan*, *Trogloglanis* and *P. lundbergi* have lost the swim bladder and its space in the visceral cavity is filled with adipose deposits

DISCUSSION AND CONCLUSIONS

This work is the first detailed description and analysis of the bony skeleton of the Widemouth Blindcat, *Satan eurystomus*. In addition to this published text and illustrations, we created an online archive of still and animated tomographic images of the skeletal anatomy of this little-known species. These new research resources will allow *Satan* to be more fully incorporated into integrative and comparative phenomics, systematics and evolutionary biology of siluriform and stygobitic fishes

We found that missing morphological character data remains to be assembled for *P. lundbergi* and *P. phreatophila*. This information is needed to augment character data for more robust phylogenetic analyses. Preparation and analysis of additional CT scans and revision of the taxonomy of *Prietella* in progress by Hendrickson, Lundberg, Luckenbill and Arce.

In this paper, we used new and previously published character data to identify the distinctive and shared features of *Satan*. The characters supporting the *Satan-Pylodictis* relationship involve many structures that function in prey detection and suction feeding on relatively large prey. Under the *Satan-Pylodictis* hypothesis, the apomorphic similarities shared among *Satan* and the other stygobitic taxa *Trogloglanis*, *P. phreatophila* and *P. lundbergi* are reconstructed as stygomorphic convergences. Conversely, the characters that support monophyly of the Troglobites are the stygomorphisms and a mix of mostly reductive homoplasious features found in some other ictalurids. Under the Troglobites hypothesis, the apomorphic similarities shared by *Satan* and the epigean *Pylodictis* are reconstructed as convergent homoplasies related to feeding mechanisms.

Sorting out the competing hypotheses on the relationships of *Satan* will require additional character evidence that improves resolution and nodal support throughout the phylogenetic tree of Ictaluridae. *Ictalurus*, *Ameiurus* and *Noturus*, the three large epigean genera, are well-supported monophyletic groups (Lundberg, 1970, 1982, 1992; Hardman and Page, 2003; Hardman, 2004; Hardman and Hardman, 2008; Egge and Simons, 2009; Arce-H. et al., 2016). However, among these studies there are many conflicts on generic inter- and intra-relationships. Without a more complete and well supported resolution of ictalurid phylogeny constraints on subtrees including the stygomorphic species are weak. Additional morphological data for the rare blindcats can be obtained if some existing or newly collected specimens are better prepared and imaged. Molecular data are difficult to obtain due mainly to lack of appropriately preserved specimens of *Satan* and *Trogloglanis*.

Scenarios for Satan*'s origin*.—It is generally assumed that the evolutionary pathways leading to highly specialized, obligate cave dwelling species trace back out of their dark waters to typical, surface water ancestors. Armbruster et al. (2016, p. 775) described the transition as "a progression from epigean, to stygophile, to stygobiont." Regarding *Satan's* origin, the two hypotheses offer distinctly different views of the evolution of this small, blind catfish in the deep Edwards Aquifer.

If epigean *Pylodictis* and hypogean *Satan* are sister lineages, their exclusive synapomorphic characteristics are inferred to have originated in their common epigean

ancestor. As found herein, these are largely features related to feeding and finding prey. During the transition from surface to deep subterranean waters *Satan*'s lineage evolved the typical stygomorphic characteristics including a reduced body size, but retained its original functional morphology for suction feeding on whole prey. A few novelties were added, such as the much enlarged interhyal bone and further enlargement of cephalic laterosensory mechanoreceptors (Langecker and Langley, 1993). Despite their predatory sophistication, neither the *Satan* nor *Pylodictis* lineage is known to have diversified beyond their single modern species.

The Troglobites hypothesis of Arce-H. et al. (2016) posits a monophyletic group of all four extant stygobitic ictalurids. The interrelationships recovered in that study are: (*Trogloglanis* (*Satan* (*P. phreatophila*, *P. lundbergi*))). The proximate relatives of the Troglobites within Ictaluridae were unresolved among results of different analytical protocols, i.e. the closest epigean relatives are unknown. Nevertheless, the straightforward reconstruction for the Troglobites is a hypogean most recent common ancestor with synapomorphies such as loss of eyes and pigmentation, and simplification of the fifth vertebra. Cladogenesis and divergence within the Troglobites would have produced the four, extant species with distinctive specializations: swim bladder loss in *Trogloglanis*, *Satan* and *P. lundbergi*, reduction of fin spines in both *Prietella* species, development of the gaping, suctorial mouth and toothless jaws in *Trogloglanis*.

If the Texas-Mexican Troglobites are a clade united by continuity of descent and permanently confined to underground desert streams and deep aquifers, there are some intriguing puzzles in their subterranean history of speciation and biogeography. *Trogloglanis* and *Satan* are sympatric and narrowly endemic in the deep Edwards Aquifer below the city of San Antonio, Texas. Given the tree topology of the Troglobites, the Edwards Aquifer, or whatever hypogean waterways preceded it, would be part of the clade's ancestral distribution. Today, the deep pool of the Edwards aquifer that is home to *Satan* and *Trogloglanis* is known to be fed by runoff from the Edwards Plateau to the north and west, via its Trinity Aquifer (Gary et al. 2011). The southwestern parts of the Edwards Plateau recharge the Edwards-Trinity Aquifer (Boghici, 2004) where *Prietella phreatophila* is found. These aquifers all share the same limestone formations and tectonic histories, and, as their names indicate, they today are recognized to be hydrologically connected to at least some degree. The extent of those connections has surely varied over the history of both the aquifers and their styobitic biota. *Prietella lundbergi*, the most southern species, though sharing a home in related limestones of the same age, seems less likely to have had subterranean aquifer connections to the other species. Interestingly, *P. lundbergi* occurs literally in the heart of the distribution of another blind cavefish, the widely ranging and extensively studied *Astyanax mexicanus*, the Blind Mexican Tetra (Keene et al. 2016, and including a chapter on geological history and hydrology – Espinasa and Espinasa 2016).

The very existence of stygobitic species seems unlikely and it may be even more remarkable that some might have produced multispecies stygobitic clades such as the Troglobites. Two recent studies of small clades of stygobitic fishes suggest quite unexpected evolutionary histories. First, Armbruster et al. (2016) conducted a species-complete morphology-based phylogenetic analysis of North American freshwater Amblyopsidae (Cave-, Spring-, and Swampfishes). Their immediate results suggested the straightforward transition noted earlier from epigean species, to stygophile, to stygobiont species. The authors found, however, that support for some nodes was weak. Further, recent molecular-based studies of amblyopsids recover epigean and stygophilic species nested among the obligate stygobionts in phylogenetic reconstructions (Dillman et al., 2011; Gross, 2012; Grande et al., 2013; Niemiller et al., 2013a, b). The results imply multiple colonizations of cave waters, convergent evolution of stygomorphic features in subterranean waters, plus some reversals from hypogean to epigean species, even including a possible reversal from degenerate to functional eyes (Niemiller et al., 2013a).

Second, in a molecular phylogenetic study of Indo-Australian region gobiiform fishes, Chakrabarty et al. (2012) discovered a well-supported trans-oceanic sister-group pair of obligate stygobites. These are narrowly-endemic *Typhleotris* from karst cave habitats in Madagascar, and *Milyeringa* that is from similar habitats in northwestern Australia. These related freshwater species are now living several thousands of kilometers apart on opposite sides of the Indian Ocean. As estimated by molecular time-tree analyses their vicariant origins were about 120 Mya in the late Cretaceous during the break up of Gondwana.

The biology and diversity of *Satan* and its subterranean brethren are fascinating to behold and contemplate, however devilishly puzzling and difficult they are to understand

ACKNOWLEDGMENTS

We gratefully acknowledge J. Maisano and M. Colbert of the High-Resolution X-ray CT Facility, Department of Geological Sciences, The University of Texas, for their expert production of the CTscan data for *Satan eurystomus* USNM 195830. Similarly, we thank K. Conway of Texas A and M University and A. Summers of the University of Washington, Friday Harbor Laboratories for sharing CT data they produced for *Satan eurystomus* TCWC 8279.01. H.

Prestridge at TAMU generously shared measurement data and information on blindcat specimens. We thank K. McDermid, J. Krejca, P. Sprouse and B. Larsen of Zara Environmental LLC, Manchaca, TX for continuing interest in our work on Texas blindcats and for keeping us abreast of their studies on the Deep Aquifer Biota of the Edwards Aquifer. We also give special thanks to T. Carvalho, M. Sabaj, K. W. Conway, J. J. D. Egge, S. J. Walsh and J. W. Armbruster for careful and generous attention to drafts of the long manuscript and their many helpful comments. K. R. Luckenbill supported in part by oVert Thematic Collection Network (NSF DBI-1701943). The authors are responsible for all remaining errors and welcome feedback and suggestions from readers.

LITERATURE CITED

Arce-H, M., J.G. Lundberg and M.A. O'Leary. 2016. Phylogeny of the North American catfish family Ictaluridae (Teleostei: Siluriformes) combining morphology, genes and fossils. Cladistics (2016): 1–23.

Armbruster, J.W., M.L. Niemiller and P.B. Hart. 2016. Morphological Evolution of the Cave-, Spring-, and Swampfishes of the Amblyopsidae (Percopsiformes). Copeia 104(3):763-777.

Arratia, G. 2003. The catfish head skeleton – an overview. pp. 3-48 In: G. Arratia, B.G. Kapoor, M. Chardon and R. Diogo (eds.), Catfishes. Science Publishers, Enfield, N.H.

Boghici, R. 2004. Hydrogeology of Edwards and Trinity Aquifer of Texas and Coahuila in the Border Region. In Aquifers of the Edwards Plateau: Texas Water Development Board, Report 360, edited by Robert E. Mace, Edward S. Angle, and William F. Mullican III, 360:91–114. San Angelo, Texas, U.S.A.: Texas Water Development Board, Austin, Texas. http://www.twdb.texas.gov/publications/reports/numbered_reports/doc/R360/Ch04.pdf.

Bridge, T.W. and A.C. Haddon. 1892. Contributions to the Anatomy of Fishes. II. The Air-Bladder and Weberian Ossicles in the Siluroid Fishes. Proceedings of the Royal Society of London. 52:139–157.

Carranza, J. 1954. Descripción del primer bagre anoftalmo y depigmentado encontrado en aguas mexicanas. Ciencia (Mexico City) 14(7-8): 129-136, Pl. 1.

Chakrabarty, P., M.P. Davis, and J.S. Sparks. 2012. The first record of a trans-oceanic sister-group relationship between obligate vertebrate troglobites. PLoS One 7(8): e44083. [doi:10.1371/journal.pone.0044083]

Chardon, M., E. Parmentier, and P. Vandewalle. 2003. Morphology, development and evolution of the Weberian apparatus in catfish, p. 71–120. In: Catfishes G. Arratia, B. G. Kapoor, M. Chardon, and R. Diogo (eds.). Science Publishers, Enfield, New Hampshire

Dahdul, W. M., P. M. Mabee, J. G. Lundberg, P. E. Midford, J. P. Balhoff, H. Lapp, T. Vision, M. A. Haendel, and M. Westerfield. 2010. The teleost anatomy ontology: anatomical representation for the genomics age. Systematic Biology 50:369-683.

Datovo A, Vari RP. 2014. The adductor mandibular muscle complex in lower teleostean fishes (Osteichthyes: Actinopterygii): comparative anatomy, synonymy, and phylogenetic implications. Zoological Journal of the Linnaea Society, 171, 554-622

Dillman, C.B., D.E. Bergstrom, D.B. Noltie, T.P. Holtsford, and R.L. Mayden. 2011. Regressive progression, progressive regression or neither? Phylogeny and evolution of the Percopsiformes (Teleostei, Paracanthopterygii). Zoologica Scripta 40:45–60.

Diogo, R., 2004. Morphological Evolution, Aptations, Homoplasies, Constraints, and Evoutionary Trends: Catfishes as a Case of Study on Genera Phylogeny and Macroevolution. Science Publishers, Enfield, NH

Egge J.J.D. 2007. The osteology of the stonecat, *Noturus flavus* (Siluriformes: Ictaluridae), with comparisons to other siluriforms. Alabama Museum of Natural History Bulletin 25:71-89.

Egge, J.J.D. and A.M. Simons. 2009. Molecules, morphology, missing data and the phylogenetic position of a recently extinct madtom catfish (Actinopterygii: Ictaluridae). Zoological Journal of the Linnean Society 155: 60–75.

Eigenmann, C.H. 1919. *Trogloglanis pattersoni* a new blind fish from San Antonio, Texas. Proceedings of the American Philosophical Society 58 (6): 397-400.

Espinasa, L. and M. Espinasa. 2016. "Chapter 2 - Hydrogeology of Caves in the Sierra de El Abra Region." In Biology and Evolution of the Mexican Cavefish, edited by A.C. Keene, M. Yoshizawa and S.E. McGaugh, 41–58. Academic Press. doi:10.1016/B978-0-12-802148-4.00002-5.

Fine, M.L., J. P. Friel, D. McElroy, C. B. King, K. E. Loesser and S. Newton. 1997. Pectoral Spine Locking and Sound Production in the Channel Catfish *Ictalurus punctatus*. *Copeia* 4:777-790.

Gary, M.O., R.H. Gary, and Hunt, eds. 2011. Interconnection of the Trinity (Glen Rose) and Edwards Aquifers along the Balcones Fault Zone and Related Topics. Austin, Texas, U.S.A.: Barton Springs Edwards Aquifer Conservation District. http://bseacd.org/uploads/Proceedings_Edwards_Trinity_final.pdf.

Goloboff, P.A., J.S. Farris and K.C.Nixon. 2008. TNT, a free program for phylogenetic analysis. Cladistics 24: 774–786.

Grande, L. and Lundberg, J.G., 1988. Revision and redescription of the genus †*Astephus* (Siluriformes: Ictaluridae) with a discussion of its phylogentic relationships. Journal of Vertebrate Paleontology 8: 139–171.

Grande, T., W.C. Borden and W.L. Smith. 2013. Limits and relationships of Paracanthopterygii: a molecular framework for evaluating past morphological hypotheses, p. 385–418. In: Mesozoic Fishes 5—Global Diversity and Evolution. G. Arratia, H.-P. Schultze, and M.V. H. Wilson (eds.). Verlag Dr. Friedrich Pfeil, Munich, Germany.

Gross, J.B. 2012. The complex origin of *Astyanax* cavefish. BMC Evolutionary Biology 12:105.

Hardman M. 2004. The phylogenetic relationships among *Noturus* catfishes (Siluriformes: Ictaluridae) as inferred from mitochondrial gene cytochrome *b* and nuclear recombination activating gene 2. Molecular Phylogenetics and Evolution 30: 395–408.

Hardman, M. 2005. The phylogenetic relationships among non-diplomystid catfishes as inferred from mitochondrial cytochrome b sequences; the search for the ictalurid sister taxon (Otophysi: Siluriformes). Molecular Phylogenetics and Evolution, 37: 700–720.

Hardman M. and L.M. Hardman. 2008. The relative importance of body size and paleoclimatic change as explanatory variables influencing lineage diversification rate: an evolutionary analysis of bullhead catfishes (Siluriformes: Ictaluridae). Systematic Biology 58: 116–130.

Hardman M. and L.M. Page. 2003. Phylogenetic relationships among bullhead catfishes of the genus *Ameiurus* (Siluriformes: Ictaluridae). Copeia 2003(1): 20–33.

Hendrickson, D.A., J. Johnson, P. Sprouse, S. Howard, G.P. Garrett, J.K. Krejca and A. Gluesenkamp, et al. 2017. Discovery of the Mexican Blindcat, *Prietella phreatophila*, in the U.S., and an Update on Its Rangewide Conservation Status. doi:10.15781/T2FF3M51W.

Hendrickson, D.A., J.K. Krejca and J.M. Rodriguez. 2001. Mexican blindcats, genus *Prietella* (Ictaluridae): review and status based on recent explorations. Environ. Biol. Fishes 62, 315–337.

Hubbs, C. 1971. Fishes of Texas caves. pp. 91-93. In: Natural history of Texas caves. Lundelius, E. L. and B. H. Slaughter (eds.). Gulf Natural History, Dallas, 174 pp.

Hubbs, C.L and R.M. Bailey. 1947. Blind catfishes from artesian waters of Texas. Occasional Papers of the Museum of Zoology, University of Michigan. 499:1-17.

Jackson, D.C. 1999. Flathead Catfish: Biology, Fisheries, and Management. P. 23-35. in Catfish 2000: Proceedings of the International Ictalurid Symposium. Sympoisum 24. E. R. Irwin (eds). American Fisheries Society, Bethesda, MD.

Keene, A.C., M. Yoshizawa and S.E. McGaugh, eds. 2016. Biology and Evolution of the Mexican Cavefish. Academic Press. doi:10.1016/B978-0-12-802148-4.09999-0.

Kindred, J. E. 1919. The skull of *Amiurus*. Illinois Biol , Monogr.,5:1-120.

Langecker, T.G. and G. Longley. 1993. Morphological adaptations of the Texas Blind Catfishes *Trogloglanis pattersoni* and *Satan eurystomus* (Siluriformes: Ictaluridae) to Their Underground Environment. Copeia 1993(4):976-986.

Lauder, G.V. 1985. Aquatic feeding in lower vertebrates. In: Hildebrand M., Bramble D.M., Liem K.F., Wake D., eds. Functional vertebrate morphology. Cambridge, MA: Harvard University Press. p 210-229.

Longley, G. 1981. "The Edwards Aquifer: Earth's Most Diverse Groundwater Ecosystem?" International Journal of Speleology 11: 123–28.

Longley, G. and Karnei Jr., H.S., 1979a. Status of *Satan eurystomus* Hubbs and Bailey, the Widemouth Blindcat. U.S. Fish and Wildlife Service Endangered Species Report 5(1): 1–48.

Longley, G. and Karnei Jr., H.S., 1979b. Status of *Trogloglanis pattersoni* Eigenmann, the toothless blindcat. U.S. Fish and Wildlife Service Endangered Species Report 5(2): 1–54.

Lundberg, J.G., 1970. The evolutionary history of North American catfishes, family Ictaluridae. Unpublished PhD dissertation, The University of Michigan, Ann Arbor, Michigan. 524 p.

Lundberg, J.G. 1975. The fossil catfishes of North America. Papers in Paleontology, 11, University of Michigan Museum of Paleontology, 51 p.

Lundberg, J.G. 1982. The comparative anatomy of the toothless blindcat, *Trogloglanis pattersoni* Eigenmann, with a phylogenetic analysis of the ictalurid catfishes Miscellaneous Publications of the Museum of Zoology, University of Michigan, 163, 85 p.

Lundberg, J.G., 1992. The phylogeny of ictalurid catfishes: a synthesis of recent work. *In*: Mayden, R.L. (Ed.), Systematics, Historical Ecology, and North American Freshwater Fishes, Stanford University Press, Stanford, pp. 392–420.

Lundberg, J.G. and J.N. Baskin. 1969. The caudal skeleton of the catfishes, order Siluriformes. American Museum Novitates, 2398:1-49.

Lundberg, J.G., Sullivan, J.P., Rodiles-Hernandez, R., Hendrickson, D.A., 2007. Discovery of African roots for the Mesoamerican Chiapas catfish, *Lacantunia enigmatica*, requires an ancient intercontinental passage. Proceedings of the Academy of Natural Sciences of Philadelphia, 156, 39–53.

Lundberg, J.G., K. Luckenbill, K.K. Subhash Babu and H.H. Ng. 2014. A tomographic osteology of the taxonomically puzzling catfis *Kryptoglanis shajii* (Siluriformes, Siluroidei, *incertae sedis*): description and a first phylogenetic interpretation. Proceedings of the Academy of Natural Sciences. 163:1-41.

McMurrich, J.P. 1884. The osteology of *Amiurus catus*. Proceedings of the Canadian Institute, Toronto, new series, 2(3):270-310.

Mungall, C.J., C. Torniai, G. V. Gkoutos, S. E. Lewis, and M. A. Haendel. 2012. Uberon, an integrative multispecies anatomy ontology. Genome Biology 13:R5.

Nakane, Y. and 20 others. 2013. The *saccus vasculosus* of fish is a sensor of seasonal changes in day length. Nature Communications 4:2108 doi: 10.1038/ncomms3108

Niemiller, M.L., B. Fitzpatrick, P. Shah, L. Schmitz and T.J. Near. 2013a. Evidence for repeated loss of selective constraint in rhodopsin of amblyopsid cavefishes (Teleostei: Amblyopsidae). Evolution 67:732–748.

Niemiller, M.L., J.R. McCandless, R.G. Reynolds, J. Caddle, C.R. Tillquist, T.J. Near, W.D. Pearson, and B.M. Fitzpatrick. 2013b. Effects of climatic and geological processes during the Pleistocene on the evolutionary history of the northern cavefish, *Amblyopsis spelaea* Teleostei: Amblyopsidae). Evolution 67:1011–1025.

Page, L.M., H. Espinosa-Pérez, L.T. Findley, C.R. Gilbert, R.N. Lea, N.E. Mandrak, R.L. Mayden and J.S. Nelson. 2013. Common and Scientific Names of Fishes from the United States, Canada, and Mexico, 7th edition. American Fisheries Society, Special Publication 34, 243 pp.

Peng, Z., Zhang, Y.G., He, S.P., Chen, Y.Y., 2005. Phylogeny of Chinese catfishes inferred from mitochondrial cytochrome b sequences. Yi Chuan Xue Bao 32: 145–154.

Sabaj, M.H. 2016. Standard symbolic codes for institutional resource collections in herpetology and ichthyology: an Online Reference. Version 6.5 (16 August 2016). Electronically accessible at http://www.asih.org/, American Society of Ichthyologists and Herpetologists, Washington DC.

Sullivan, J.P., J.G. Lundberg, and M. Hardman. 2006. A phylo-genetic analysis of the major groups of catfishes (Teleostei: Siluriformes) using rag1 and rag2 nuclear gene sequences. Molecular Phylogenetics and Evolution 41: 636–662.

Suttkus, R.D. 1961. Additional information about blind catfishes from Texas. Southwestern Naturalist 6:55-64.

Taylor, W.R. 1969. A revision of the catfish genus *Noturus* Rafinesque with an analysis of higher groups in the Ictaluridae. Bulletin of the United States National Museum 282: 1–315.

Vanscoy, T., J.G. Lundberg and K.R. Luckenbill. 2015. Bony ornamentation of the catfish pectoral-fin spine: comparative and developmental anatomy, with an example of fin-spine diversity using the Tribe Brachyplatystomini (Siluriformes, Pimelodidae). Proceedings of the Academy of Natural Sciences of Philadelphia 164(1):177-212.

Walsh, S.J. and Gilbert, C.R. 1995. New species of troglobitic catfish of the genus *Prietella* (Siluriformes: Ictaluridae) from northeastern México. Copeia 1995(4): 850-861.

Weisel, G.F. and E.L. McLaury. 1964. Blind Catfis (*Ictalurus nebulosus*) from Dog Lake, Oregon. Copeia 1964(4):687-690.

Westneat, M.W. 2006. Skull Biomechanics and Suction Feeding in Fishes. Chapter 2 in G.V. Lauder and R.E. Shadwick. 2006. Fish Biomechanics. Fish Physiology Series, Vol. 23: 29-75.

Wheeler, W.C., 2012. Systematics: A Course of Lectures. Wiley-Blackwell, Oxford.

Winterbottom, R. 1974. A descriptive synonymy of the striated muscles of the Teleostei. Proceedings of the Academy of Natural Sciences of Philadelphia, 125(12): 225-317.

Wilcox, T.P., F.J. García de Leon, D.A. Hendrickson, D.M. Hillis, 2004. Convergence among cave catfshes: long branch attraction and a Bayesian relative rates test. Molecular Phylogenetics and Evolution 31: 1101–1113.

Zara Enviromental LLC. 2010. Final Report for Deep Aquifer Biota Study of the Edwards Aquifer. Edwards Aquifer Authority, San Antonio, Texas. http://www.edwardsaquifer.org/documents/library/document_image_display.php?dID=271

Zara Environmental LLC. 2014. Fauna of Wells Near the Saline Water Line of the Edwards Aquifer. Edwards Aquifer Authority, San Antonio, Texas. http://www.edwardsaquifer.org/documents/FAUNA%20OF%20WELLS%20NEAR%20THE%20SALINE%20WATER%20LINE%20OF%20THE%20EDWARDS%20AQUIFER,%20TEXAS.pdf

List of Abbreviations

A3 cr, deep *adductor mandibulae* (A3) crest;
aan, angulo-articular-retroarticular;
aap, anterior articular process;
aap cr, *adductor arcus palatini* crest;
acf, anterior cranial fontanel;
ad cr, main *adductor mandibulae* crest;
ah p, *adductor hyomandibularis* process;
anf, anal fin
asc, anterior semicircular canal;
bas, basipterigyum;
bb2-bb3, basibranchials 2, 3;
boc, basioccipital;
boc/c1, basioccipital and fused first centrum
br, branchiostegal rays;
bslr, basal recess;
c1, first centrum
ca, caudal artery and vein foramen;
car f, carotid foramen;
cb1-cb5, ceratobranchials 1, 2, 3, 4, 5;
ch cart, ceratohyal cartilage;
cha, anterior ceratohyal;
chp, posterior ceratohyal;
cl hl, cleithrum horizontal limb;
cl pcp, cleithral posterior process;
cl, cleithrum;
cl vl, cleithrum vertical limb;
cmb, coronomeckelian;
cor, scapulocoracoid;
cor aan, coronoid process of anguloarticular;
cor br, scapulocoracoid bridge to cleithrum;
cor den, coronoid process of dentary;
cor hl, scapulocoracoid horizontal limb;
cor k, scapulocoracoid keel;
cor s, scapulocoracoid symphysis;
csk, caudal skeleton;
cv1, first caudal vertebra
dap, dorsal articular process;
den pp, dentary postsymphyseal processes;
den, dentary;
df s, dorsal-fin skeleton
dfp1-dfp7, dorsal-fin pterygiophores 1, 2, 3, 4, 5, 6, 7
dfry, branched dorsal-fin rays
dmp, dorsal spine 1 (spinelet) medial peak;
dsp1, dorsal-fin spine 1 (spinelet)
dsp2, dorsal-fin spine 2
dsp b f, dorsal spine 2 basal foramen;
dsp c, dorsal-spine 2 condyle;
dsp pp, dorsal spine 2 posterior process;
dsr1, dorsal spine 2 distal radial 1;
eb, epiphyseal bar;
eb1-eb4, epibranchials 1, 2, 3, 4;
ent, endopterygoid;
eoc, exoccipital;
eoc mp, exoccipital medial processes;
ep, epural;
epo, epioccipital;
ext, extrascapula;
f m1-8, foramina for mandibular sensory canal and side branches;
f mag, foramen magnum;
f pop d, preopercle main sensory canal dorsal foramen;
f pop s, preopercle sensory canal side-branch foramina;
f pop v, preopercle main sensory canal ventral foramen;
f uh, urohyal foramen;
fb j, frontal abutting joint;
fc lh, facial canal lower foramen for hyoidean branch;
fc lm, facial canal lower foramen for mandibular branch;
fc u, facial canal upper foramen;
fm 7, fm 8, mandibular sensory canal foramina;
fr, frontal;
fs j, frontal sutural joint;
gr, gill rakers;
hb c, hypobranchial artery canal;
hb1-hb2, hypobranchials 1, 2;
hhd, dorsal hypohyal;
hhv, ventral hypohyal;
hhv ap, articular processes of ventral hypohyals;
hor sc, horizontal semicircular canal;
hs, haemal spine;
hy b, hyoid bar;
hy1-hy6, hypurals 1, 2, 3, 4, 5, 6;
hyo, hyomandibula;
hyo ap, hyomandibular anterodorsal process;
hyo art, hyomandibular articular head;
hyo oc, hyomandibular-opercular condyle;
hyo-pop v, hyomandibula-preopercle ventral articulation;
hyo-sk, hyomandibula-cranial joint;
hyp, hypurapophysis;
ih, interhyal;
io1-5, infrorbitals 1-5;
iop, interopercle;
ios f, foramen at union of infraorbital, supraorbital, otic canals;
la, lagenar chamber;
la o, lagenar otolith;
lap cr, *levator arcus palatini* crest;
lap, lateral anterior process of basipterygium;
lcl, dorsal spine 1 (spinelet) lateral curved limb;
let, lateral ethmoid;
let ap, antorbital process;
let pp, lateral ethmoid posterior process;
let-pal con, lateral ethmoid palatine condyle;
lop f, left optic nerve foramen;
ltf t, left trigemino-facial nerve foramen;
ltp, lower pharyngeal tooth plate;
map, medial anterior process of basipterygium;
mco p, coronoid process of mandible;
met, mesethmoid;
met cl, mesethmoid cleft;
met co, mesethmoid cornu;

met nk, mesethmoid neck;
mn s, mandibular (dentary) symphysis;
mnp, middle nuchal plate;
mpt, metapterygoid;
mx, maxilla;
mx-pal j, maxillary-autopalatine joint;
na, nasal;
ns3-ns6, neural spines 3, 4, 5, 6;
oc cr, occipital crest;
olf n f, olfactory nerve foramen;
olf, olfactory organ fossa;
op, opercle;
op f, optic nerve foramen;
op p, opercular panel;
ors, orbitosphenoid;
ors w, orbitosphenoid;
otl, ossified transcapular ligament
pal, autopalatine;
pal-let j, autopalatine-lateral ethmoid joint;
pap, posterior articular process;
pas, parasphenoid;
pas s, parasphenoid stem;
pas w, parasphenoid wing;
pb3-pb4, pharyngobranchials 3, 4;
pcf a, posterior cranial fontanel, anterior subdivision;
pcf p, posterior cranial fontanel, posterior subdivision;
pd, posterior dentations;
pf, pectoral fin
pfr, pectoral-fin radials
pfry1, pelvic-fin ray 1
pfry9, pelvic-fin ray 9
ph, parhypural;
plvf, pelvic fin
plvg, pelvic girdle (basipterygium);
pm f, preopercular-mandibular sensory canal foramina;
pmx, premaxilla;
pmx s, premaxillary symphysis;
pnp, posterior nuchal plate;
po f, post-otic sensory canal foramina;
po f1, pterotic foramen for passage of preopercular-mandibular sensory canal;
po f2, posterior foramen in pterotic for postotic canal;
pop, preopercle;
pro, prootic;
ps cr, parasagittal crest;
psc, posterior semicircular canal;
psp, pectoral-fin spine;
psp lj, pectoral spine locking joint;
ptg, pectoral girdle;
pto, pterotic;
pto w, pterotic wing;
pto-hyo soc, pterotic sulcus at hyomandibula joint;
pts, pterosphenoid;
ptt, posttemporo-supracleithrum;
ptt clp, posttemporo-supracleithrum cleithral process;
ptt dp, posttemporo-supracleithrum dorsal (pterotic) limb;
ptt spt, posttemporo-supracleithrum subpterotic process;
ptt vp, posttemporo-supracleithrum vertebral process;
pu1 u1, preural centrum 1 + ural centrum 1;
pu2, preural centrum 2;
q c, quadrate articular condyle;
q, quadrate;
q-ar j, quadrate-articular jaw joint;
r, rib;
rar p, retroarticular posterior process;
rop f, right optic nerve foramen;
rtf f, right trigemino-facial nerve foramen;
s oph f, superficial ophthalmic nerve foramen
sa, saccular chamber;
sa o, saccular otolith;
sb j, supraoccipital abutting joint;
sc, scaphium ossicle;
shyp, secondary hypurapophysis;
si, sinus impar;
sn3-sn4, supraneurals 3, 4;
so f par, parietal branch of supraorbital sensory canal;
so f, supraorbital sensory canal foramina;
soc, supraoccipital;
soc pp, supraoccipital posterior process;
spo, sphenotic;
spo p, sphenotic process;
spo-hyo soc, sphenotic sulcus at hyomandibula joint;
sym c, preopercle symplectic canal;
tf f, trigeminofacial foramen;
tl a, transcapular ligament attachment site;
tm f, temporal fossa;
tp4, Weberian apparatus transverse processes;
tp4a, Weberian apparatus anterior limb of fourth transverse processes,
tp4p, Weberian apparatus posterior limb of fourth transverse processes;
tp5-tp6, transverse processes of vertebrae 5, 6;
ufss, unfused spine segment;
uh ah, urohyal articular head;
uh h, urohyal horizontal lamina;
uh v, urohyal vertical lamina;
uh, urohyal;
un, uroneural;
up, uncinate process;
ut o, utricular otolith;
ut, utricular chamber;
utp, upper pharyngeal tooth plate;
v5-v6, vertebra 5, 6;
vl, vertical lamina;
vo, vomer;
Wa cc, Weberian compound centrum;
Wa, Weberian apparatus;

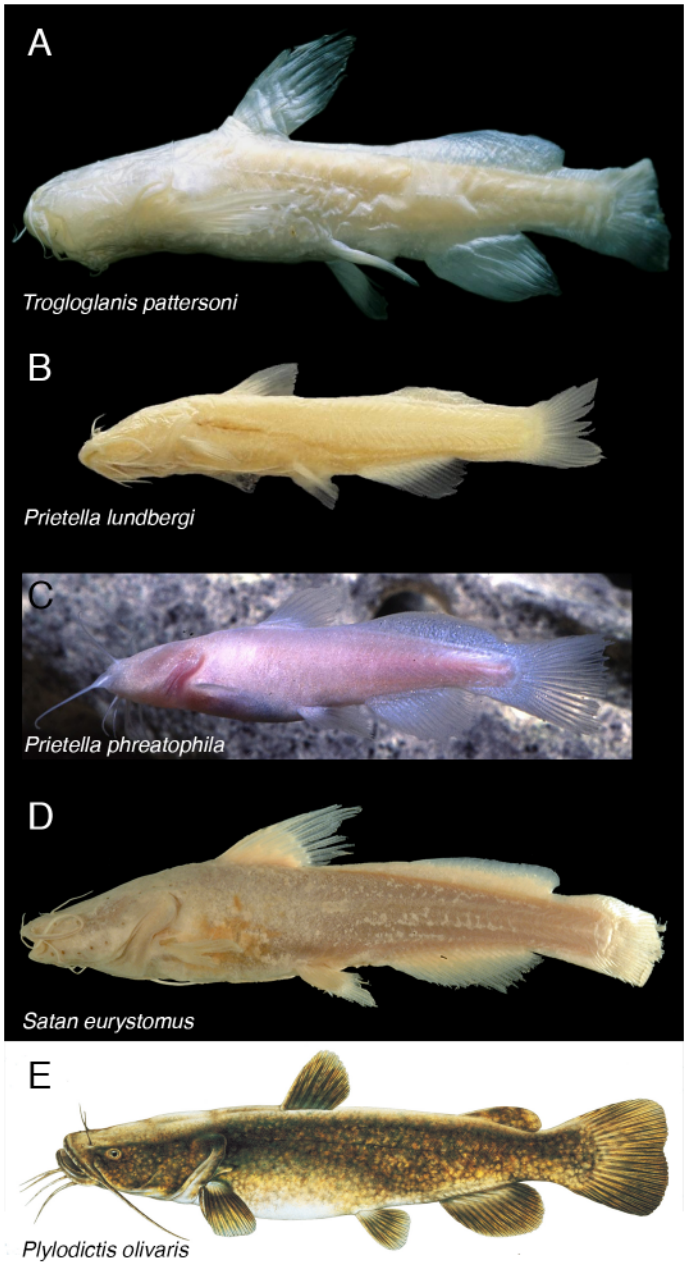

PLATE I. Fish photo images A. *Trogloglanis pattersoni*, photo courtesy of G. Sneegas, B. *Prietella lundbergi*, photo courtesy of Dean A. Hendrickson, C. *Prietella phreatophila*, photo courtesy of Dean A. Hendrickson, D. *Satan eurystomus*, Holotype UMMZ 190922, © University of Michigan Museum of Zoology, used with permission, E. *Pylodictis olivaris*, illustration courtesy of J. Tomelleri.